# HISTIDINE-METHIONINE CONTRIBUTIONS TO FUNCTION

# IN COPPER PROTEINS

By

Chelsey Dawn Kline

A DISSERTATION

Presented to the Institute of Environmental Health

and Oregon Health & Science University School of Medicine

In partial fulfillment of the requirements for the degree of

Doctor of Philosophy

In

Biochemistry and Molecular Biology

May 2015

School of Medicine

Oregon Health & Science University

CERTIFICATE OF APPROVAL

_____

The dissertation "Histidine-Methionine Contributions to Function in Copper

Proteins" by Chelsey Dawn Kline has been examined and approved by the following

examination committee:

_____
Ninian J. Blackburn, Research Advisor
Professor

_____
Pierre Moënne Loccoz
Professor

_____
Paul Tratnyek
Professor

_____
Ujwal Shinde
Professor

# TABLE OF CONTENTS

# LIST OF FIGURES

# LIST OF TABLES

# ACKNOWLEDGMENTS

I would like to begin by thanking my research advisor, Dr. Ninian J. Blackburn for the constant support, advice, and opportunities made available during my graduate studies. He provided me with the necessary tools and helped me advance my abilities as a research scientist, independently exploring scientific projects and collaborations. I would like to thank Mary Mayfield for the mentoring relationship that was fostered; I truly appreciate all of the love and support, as it was more than I could have ever expected. I also wish to thank Dr. Pierre Moënne-Loccoz for his insightful discussions and guidance throughout my studies.

Kelly Chacón and Shefali Chauhan have been amazing lab mates and have become more like family during my graduate studies. I would like to thank both of them for their friendship and endless support. I am also grateful to Professors Peter Zuber, James Whittaker, Pierre Moënne-Loccoz and Ninian Blackburn as well as the entire faculty of the Institute of Environmental Health (IEH) for their education and knowledge in biochemistry and molecular biology. I wish to also thank my committee members Professors Ujwal Shinde, Pierre Moënne-Loccoz, Paul Tratnyek, and Ninian Blackburn for carefully reviewing my dissertation. I wish to also thank the administrative staff of IEH especially Nancy Christie, Bonnie Gibbs, Jim Mohan, Karen Sears, Michele Webber, and Amy Johnson for helping me with the challenges of being a graduate student. Nancy Christie has been a big part of my doctoral journey since day one, and I would like to express just how grateful I am for all of the assistance along the way. Thank you.

**ABBREVIATIONS:** MES, 2-(N-morpholino)ethanesulfonic acid; HEPES, 4-(2-hydroxyethyl)-1-piperazineethanesulfonic acid;  CHES, N-cyclohexyl-2-aminoethanesulfonic acid; dansyl- YVG, dansyl- Tyr-Val-Gly; PHMcc, Peptidylglycine-hydroxylating monooxygenase catalytic core; EXAFS, extended X-ray absorption fine structure; XAS, X-ray absorption spectroscopy; XANES, X-ray absorption near-edge spectroscopy; HPLC, high pressure liquid chromatography; ICP-OES, inductively coupled plasma- optical emissions spectrum; DBM, TBM, Tyramine $\beta$-Monooxygenase; TFA, trifluoroacetic acid; TCA, trichloroacetate; WT, wild-type; ; Dhfr-, dyhydrofolate reductase deficient; CHO DG44, Chinese hamster ovary; DMEM F-12, Dulbecco's modified Eagle's medium; FBS FCII, fetal bovine serum fetal clone II; SDS-PAGE, sodium dodecyl sulfate polyacrylamide gel electrophoresis; PBS, phosphate buffer saline; ECS, extra capillary space; MWCO, molecular weight cut off; Ac- YVG, Ac- Tyr-Val-Gly; PAM, peptidylglycine $\alpha$-amidating monooxygenase; CO, carbon monoxide; Hc, hemocyanin; Hc-CO, carboxyhemocyanin; HA, Hippuric Acid; FTIR, Fourier transform infrared; KIE, kinetic isotope effect; DFT, density functional theory; HM, histidine-methionine; HMBD, heavy metal binding domain; TS, transition state

# ABSTRACT

**Histidine-Methionine Contributions to Function in Copper Proteins**

Chelsey Dawn Kline

Thesis Advisor: Dr. Ninian J. Blackburn

The goal of this research is to characterize the contribution of histidine and methionine to function in copper proteins. The emergence of His and Met residues in copper proteins is not new, but the flexible dynamic provided is novel and has been shown to alter function. We have characterized the pH-dependent coordination chemistry involving His-Met residues in cuproproteins peptidylglycine hydroxylating monooxygenase (PHM) and the HM Loop of ATP7A, which is involved in copper translocation.

PHM is a member of the unique class of dicopper monooxygenase enzymes that play essential roles in biological processes. Proteins, such as PHM, traverse the secretory pathway where changes in vesicle pH are employed for sorting and post-translational processing. PHM contains two distinct copper centers, termed CuM and CuH. Despite being separated by an 11 Å solvent filled cavity, the His and Met ligands are essential at each copper center for controlling the catalytic activity. Here, we use spectroscopic techniques such as FTIR and XAS in addition to Michaelis-Menten kinetics of PHM WT and several variants in order to relate copper coordination to activity. PHM WT was found to have optimal catalytic activity at pH 5.8, which is meticulously controlled by the Cu-S(Met) interactions occurring at the catalytic CuM center. An additional Cu-S(Met) interaction was found to bind to the CuH center when the pH decreases below 5 and results in deactivation of the

enzyme. Altogether our results demonstrate how one copper center can greatly influence the other's coordination chemistry, which can largely impact the substrate triggering mechanism. Therefore the coordination of His and Met residues to both centers is critical in controlling the catalytic activity in PHM and may be further regulated by the pH of each individual vesicle.

Copper transporter ATPase, ATP7A transports copper from the cytosol into the lumen of vesicles. However, copper release from ATP7A to copper proteins such as PHM, is unknown. Previously, Blackburn and co-workers suggested that copper release involved the HM Loop between TM1 and TM2 on the lumenal side since mutations impacted dephosphorylation, a catalytic step associated with release of the metal ion(s). The transfer of copper is generally mediated by chaperones, but interestingly chaperones do not occur in this system. We have found that factors such as copper loading, redox, and pH contribute to the coordination chemistry and may thus alter function. In addition to the previous HM Loop studies, here we show via XAS spectroscopy that reduced copper is indeed coordinated by a combination of His and Met residues, with a higher degree of Cu-S(Met) coordination at lower pHs. Seleno-methionine labeling for Se K-edge XAS was employed which confirmed and further illustrated the results at the Cu K-edge. Double and triple Met mutants with and without SeM labeling XAS data failed to implicate a specific methionine as critical to the copper coordination, rather they suggested that at least two Met residues acted in concert to control the reactivity. We hypothesize that the His and Met residues in the HM Loop act as a copper chaperone to PHM, both capable of responding to the pH environments encountered.

# CHAPTER 1

# INTRODUCTION

## 1.1 OVERVIEW

This thesis describes the spectroscopic characterization of histidine-methionine

coordination believed to be important for regulating, structure and thus function, in

copper transporting ATP7A's "HM Loop" and target copper enzyme, peptidylglycine

hydroxylating monooxygenase (PHM). Copper transporting ATPases are required to

metallate cuproproteins (Steveson et al. 2003) and are co-located with the enzymes

in the lumen of vesicles within the trans-Golgi network (TGN) where they are

subject to pH gradient environments (Paroutis, Touret, and Grinstein 2004) that

may effect copper coordination. Comparing WT protein to histidine and methionine

mutants at various pHs will enable us to gain valuable information on the ligands

that bind copper and allow unique, flexible coordination that could alter function.

The knowledge derived from this study will be beneficial in designing future

transport experiments in order to better understand the pathophysiology of copper

related diseases such as Alzheimer's, Menke's and Wilson's disease.

Chapter 1 introduces copper in biology, including a discussion of copper

transport inside the cell involving copper membrane proteins, chaperones,

transporting ATPases, and finally the target copper enzymes. The binding sites of

various copper proteins are discussed. Typically a combination of histidine,

methionine, and cysteine residues coordinate copper, with some exceptions. Our

current goal for this study is to investigate the novel pH-dependent coordination of His-Met residues at copper active sites. Chapter 2 describes the materials and methods used in this thesis.

In Chapter 3, Fourier Transform infrared (FTIR) spectroscopy is used to investigate carbon monoxide (CO, an oxygen analog) binding in PHM and discusses how substrate induces a change detectable only by FTIR. This study demonstrates that the presence of substrate amplifies an additional CO stretching frequency believed to be a second, activated conformation of the enzyme. Hypotheses for the activated CO complex are discussed in more detail in Chapter 3, and include how copper coordination to the His and Met residues provide the proper protein scaffold required for substrate activation.

Chapter 4 uses a combination of spectroscopic and biochemical techniques to demonstrate that a Cu-S(Met) coordination in PHM terminates activity at low pHs. FTIR and X-ray absorption spectroscopy (XAS) of site-directed mutants provided unambiguous assignment that the Cu-S(Met) interaction arises from an additional Met residue (Met109), part of a conserved HHM motif at the CuH center otherwise not known to coordinate. This work provides insight into protonation/ deprotonation events that toggle active and inactive states in PHM.

The His/Met (HM) chemistry observed for PHM has intriguing similarities to that emerging from studies of the HM Loop of ATP7A. In Chapter 5, XAS is used to study the Cu (I) coordination chemistry of the HM Loop of ATP7A and Met variants with and without selenium labeling in order to assign the Cu-S(Met) ligand. The 3-

coordinate His-Met mixed environment was found to be pH-dependent, swapping His residues for Met at low pH.

Chapter 6 provides the final conclusions of the thesis, including future studies to probe the IR absorption of CO in PHM WT in the presence and absence of deuterated substrate and solvent, as well as an additional study characterizing the pH-dependent coordination of single Met mutations in the HM Loop of ATP7A.

## 1.2    COPPER IN BIOLOGY

Copper is a redox-active metal used as an essential cofactor in metabolic enzymes involved in respiration, neurotransmitter biosynthesis, stress response, and iron metabolism, among others. Defects in copper homeostasis are directly responsible for human diseases such as Menke's and Wilson's disease (Lutsenko 2010; Lutsenko, Bhattacharjee, and Hubbard 2010; Gupta and Lutsenko 2009; Kaplan and Lutsenko 2009; Lutsenko et al. 2008; Lutsenko, LeShane, and Shinde 2007). Due to the deleterious redox effects of copper, the metal ion requires tight homeostatic regulation that is provided by cuproteins with limited sets of metal binding residues. Histidine, methionine and/or cysteine residues are predominately found binding copper in copper proteins and can provide exquisite control. External factors such as oxidation state, stoichiometry, and pH have been suggested to govern the various ligands that bind copper, and are discussed in more detail below.

The metal binding sites of cuproteins are governed by the Hard Soft Acid Base (HSAB) theory, which states that Cu (I) (a soft Lewis acid) forms strong bonds with soft bases, like sulfur, while Cu (II) (an intermediate Lewis acid) prefers

3

nitrogen, hydroxyl, carboxyl or primary amine side chains (Bertini et al. 2007). Histidine has two nitrogen atoms capable of protonation at $pK_A$ of 6 and 14 in the free amino acid, but in metal proteins the metal coordination and environment can highly impact the $pK_A$ *(vide infra)*. Cysteine's thiol side chain has a $pK_A$ of approximately 8.5, and is additionally sensitive to oxidation, forming disulfide cross-links. On the other hand, methionine residues do not contain a protonatable side group, nor do they cross-link. The thioether side group therefore does not contain the same pH-dependence as the other two residues, and is also not as sensitive to oxidative environments as cysteine residues. Although there are some exceptions, the types of coordination environments found in copper binding sites of proteins tend to be a combination of His/Cys or His/Met ligand sets, which provide critical structure-function relationships capable of responding to the various extracellular environments.

**1.3 COPPER TRANSPORT INSIDE THE CELL**

Copper is necessary for many essential biological functions inside the cell, requiring careful maintenance to protect the cell from toxic side reactions, like Fenton chemistry shown in Equation 1.1 (Urbañski and Berêsewicz 2000). Cu (I) can be oxidized to Cu (II), generating radicals that

$$H_2O_2 + Cu\ (I) \rightleftharpoons Cu\ (II) + OH + OH^- \qquad \text{(Equation 1.1)}$$
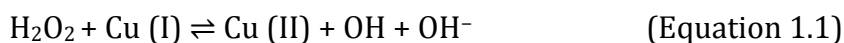
wreak havoc inside the cell. Therefore, copper dependent proteins, like importer

proteins, chaperones, and membrane translocating ATPases are involved in

selectively binding copper, while additionally being capable of handing it off to

cognate proteins using similar ligand sets (Pufahl et al. 1997; Field, Luk, and Culotta

2002; Harrison, Jones, and Dmeron 1999; Lin and Culotta 1995). Historically, the

baker's yeast, *Saccharomyces cerevisiae* has been used as a model system to study

copper transport through the cell. Copper can be imported into the cell by copper

transport proteins providing copper availability to a variety of chaperone proteins

once inside the cell (Figure 1.1). The chaperone proteins shuttle copper to

compartment specific organelles like the mitochondria, nucleus, trans-Golgi

network (TGN), and to specific enzymes, preventing free copper and deleterious

reactions from occurring. Insight into the novel coordination chemistry at the

copper active sites may shed some light on various factors such as pH and redox

environments that could potentially influence structure and therefore function and

disease.

One of the first well characterized high affinity copper transport proteins,

Ctr1, uses a combination of His, Met, and Cys residues to drive transport of copper

into the cell (Rubino et al. 2011). Ctr1 is an integral membrane protein ubiquitously

expressed in eukaryotes. Ctr1 consists of three 190-amino acid monomers forming a

cone shaped pore through the plasma membrane. Each monomer has an

extracellular N-terminal domain, three transmembrane (TM) helices and a short

intracellular C-terminal domain (De Feo et al. 2009; Aller and Unger 2006; Klomp et

al. 2003). Franz and colleagues noted that the N-terminal domain in yeast Ctr1
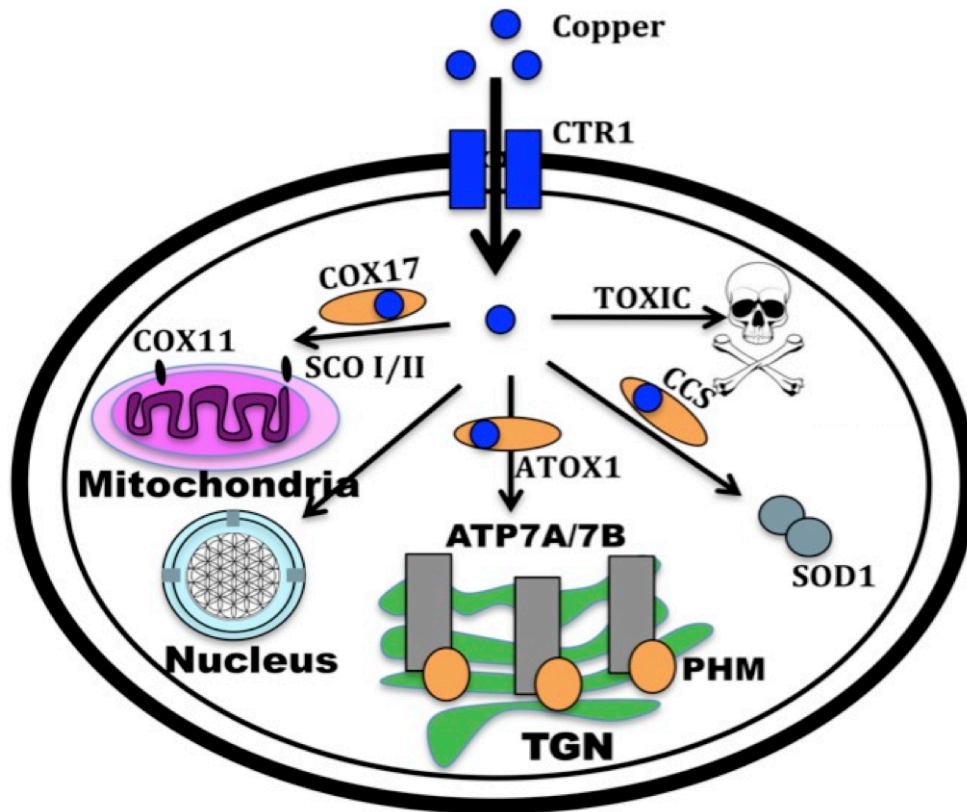
***Figure 1.1.*** *Copper transport protein (Ctr1) accepts copper from the extracellular environment for use inside the cell. Copper can be distributed to a variety of chaperones for compartment specific delivery, preventing unwanted, toxic side reactions. COX17 shuttles copper to the mitochondria with an ensemble of other proteins for use in electron transport reactions, whereas CCS targets SOD to use as an antioxidant, Atox1 transports copper to the trans-Golgi network (TGN) necessary for metallating cuproenzymes, and further incorporation into the nucleus.*

contains of 30 methionine residues, while the mammalian N-terminal contains a combination of His and Met residues to recruit Cu into the cell (Dancis et al. 1994; Rubino et al. 2011). In order to understand the preference for the amino acid composition found in the different organisms, model peptides were used. Franz and

co-workers designed heptapeptides, $MG_2XG_2M$, replacing X with Met, His or Cys and measured the relative Cu (I) binding affinities. They then used mass spectroscopy (MS) and X-ray absorption spectroscopy (XAS) studies to investigate copper coordination and the preference for ligand sets at varying pHs (Rubino et al. 2011). The competitive binding studies indicated that the cysteine heptapeptide complex dominated with a higher affinity for copper over the His and Met complexes, and yet copper preferred His coordination to Met at physiological pH. Haas *et al.*, 2011 rationally explained that the preference for Met over His coordination at the N-terminal domain would therefore be effective at acidic pHs and employed where the extracellular milieu is below pH 6, like in yeast. The use of His/Met copper coordination environments in the mammalian Ctr1 N-terminal domain was again used as a model peptide and found to contain high affinity Cu (I) and Cu (II) binding sites at neutral pH (Haas et al. 2011). The cupric binding site was thought to facilitate reduction and delivery into the cell, which could be monitored by the decrease of the Cu (II) signal at 525 nm. Reduction occurred within one hour after ascorbate was added to the model peptide (Perrone et al. 2010; Haas et al. 2011). His mutations could not reduce Cu (II) alone, and in live cell studies, histidine mutants generated copper-deficient phenotypes, providing a critical role for these residues in mammalian Ctr1 proteins.

Although conflicting conclusions still exist regarding the essential roles for each of the individual His and Met residues in acquiring copper at the N-terminal domain of Ctr1, the consensus is that Met motifs lining the pore act as a selectivity filter, helping to drive transport of copper inside the cell (Figure 1.2)
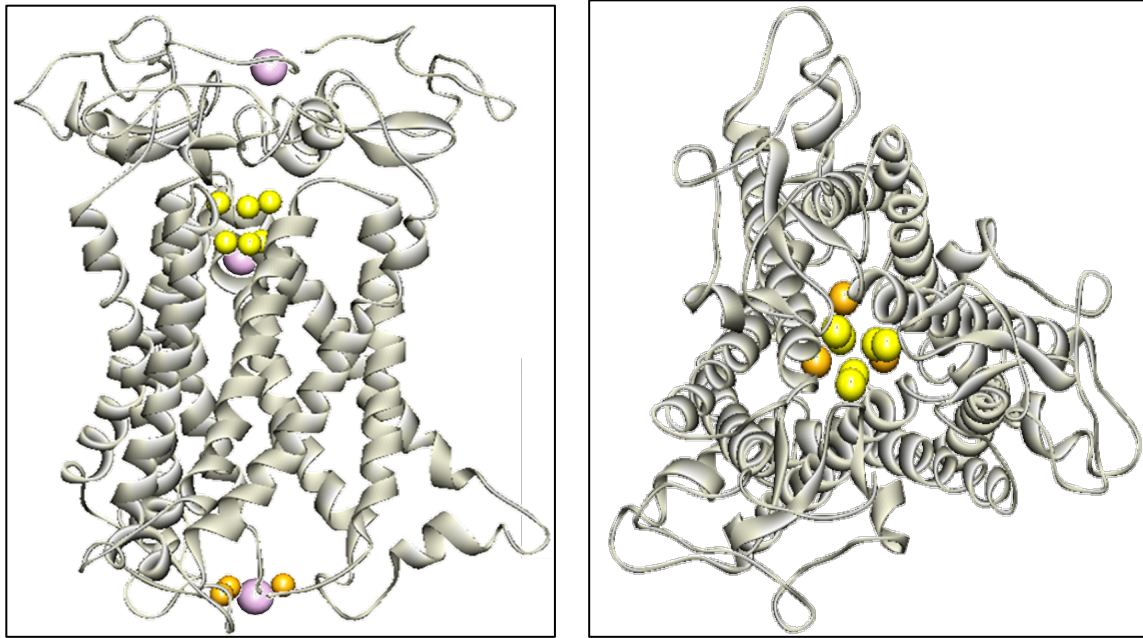
***Figure 1.2.*** *Visual representation of the suggested copper transport mechanism through the CTR1 transporter from reference (Blackburn, Yan, and Lutsenko 2014). Cu(I) enters the pore through the N-terminal funnel and is drawn downwards to the double triad of Met residues (shown in pale yellow). This is followed by a conformational change coupled to organization of the Cys triad (orange) on the cytoplasmic side so as to provide a driving force for transport through the pore. The figure at the right is a top view of the proposed CTR1 structure. The image is a view looking down the N-terminal funnel towards the vestibular Met triads (yellow) and the C-terminal HCH motifs (orange).*

(Maryon et al. 2013). XAS data exposed two copper binding sites per trimer of Ctr1, both existing in a three-coordinate Cu-S environment. The electron crystallography structures along with other previous site-directed mutagenesis studies revealed the second TM helix as having Met components responsible for coordinating one of the

copper binding sites, (De Feo et al. 2009; Puig et al. 2002; Maryon et al. 2013) while

the other binding site was dominated by the cysteines in the HCH motif at the C-

terminus (De Feo et al. 2009). However, truncating the C-terminal domain did not

abolish transport of $^{64}$Cu inside the cell, and yet kinetic data supports the notion that

the C-terminus motif may help regulate the rate of copper entry (Maryon et al. 2013;

De Feo et al. 2009; Aller and Unger 2006; Puig et al. 2002). The elegant molecular-

recognition system involving His and Met residues for Ctr1 provides both high

affinity and labile copper binding sites, essential for acquiring and distributing

copper to other proteins inside the cell.


## 1.4 COPPER CHAPERONES

Copper ions are transported across the cell membrane via Ctr1 proteins and then

further trafficked to metallo-chaperones within the cell. Chaperones have the dual

function of protecting and transferring Cu (I) to specialized compartments where

the selectivity arises from the protein's ligand set at the metal active site. Several

well-known cytoplasmic copper chaperones, CCS and Atx1, use fundamental

features of chaperone-partner interactions for compartment specific delivery. These

chaperones are proposed to have similar interactions for acquiring copper from

cognate proteins utilizing Cys residues for metal ligand exchange reactions

(Prohaska and Gybina 2004; Field, Luk, and Culotta 2002; Lutsenko 2010). CCS and

Atx1 use a conserved MXCXXC metal-binding motif, where X represents other amino

acids in the sequence that are not conserved (Rubino and Franz 2012). CCS was

discovered as the second and true copper chaperone for Cu/Zn superoxide

dismutase (SOD) when cells lacking CCS were shown to express and accumulate apo

SOD (Culotta et al. 1997). Interestingly, *sod1Δ* null mutants were auxotrophic for

methionine and lysine (Field, Luk, and Culotta 2002). Atx1 was also discovered in

baker's yeast, *S. cerevisiae* containing *sod1Δ* null mutations (Lin and Culotta 1995;

Culotta et al. 1997). Over expression of Atx1 appeared to suppress the affects of the

SOD null mutants, functioning as an antioxidant.

Human Atx1 ortholog, Atox1 is a small, soluble protein with a ferredoxin-like

(βαββαβ) fold structure containing a linear two-coordinate Cu (I)–S geometry

(Ralle, Lutsenko, and Blackburn 2003). Comparison of XAS spectra of Atox1 with

spectra of 2- and 3-coordinate models confirmed a linear 2-coordinate Cu (I)

binding site. The short Cu-S distance of 2.16 Å is suggested to arise from the two-

cysteinyl thiolates in the MXCXXC motif. At physiological levels, Atx1 was actually

found to shuttle copper to ATPase proteins in the TGN, (Pufahl et al. 1997) not to

SOD as originally proposed (Lin and Culotta 1995).

The metal binding domains (MBD) of copper transporting ATPases, ATP7A

and ATP7B, responsible for Menke's and Wilson's disease, respectively, contain the

same CXXC motifs observed for Atox1. Numerous XAS and NMR studies have

confirmed a single Cu (I) ion is capable of binding to each of the six MBD's with a

similar two coordinate Cu (I)-S geometry observed for Atox1 (Ralle et al. 1998;

Pufahl et al. 1997; DiDonato et al. 2000; Banci et al. 2009; Banci et al. 2008). β-

galactosidase (β-Gal) activity was measured in yeast hybrid experiments to indicate

a direct interaction between Atx1 and Ccc2-a (yeast homologue to Menke's and

Wilson's protein) required for metal transport. The β-Gal activity was enhanced in

the presence of copper (indicative of copper transport), and diminished when Cu-chelator bathocuproine disulfonic acid (BCS) was added, which prevented copper transport (Pufahl et al. 1997). A chemical ligand exchange mechanism was proposed by which two and three-coordinate Cu-S bridged-intermediates could occur between the two proteins metal active sites. Further NMR and mutagenic studies also suggest a 3-coordinate intermediate facilitates copper exchange between the cognate chaperone proteins (Banci et al. 2009; Walker, Tsivkovskii, and Lutsenko 2002; Banci et al. 2008). The specific role in trafficking copper to each of the MBD's of the ATPases has not been resolved, and the mechanism of copper transport throughout the rest of the protein for incorporation into further cuproteins is less clear.

## 1.5 COPPER TRANSPORTING ATPASES

Copper transporting ATPases are integral membrane proteins part of the P1B family of heavy metal transporters required for transporting copper out of the cell and into specialized vesicles via the TGN. Genetic defects in Cu ATPase, ATP7A causes Menke's disease, which is a lethal disorder resulting from inadequate delivery of copper to a number of copper-dependent enzymes. Mutations in Cu ATPase, ATP7B, result in Wilson's disease causing a severe hepato-neurological disorder. The two Cu- ATPases are highly homologous and share general mechanisms of copper transport, but are not well understood.

Translocation of copper ions is derived by ATP hydrolysis and is proposed to have similar catalytic mechanism as first described by the Albers-Post model, with

well-known examples in the sodium/potassium ($Na^+/K^+$) and calcium ($Ca^{2+}$) ATPase pumps (Barry et al. 2011). The Albers-Post model describes E1 and E2 states, which are interconverted from one high affinity, conformationally stable state, E1 into a low affinity conformation, E2. Based on a combination of the Albers-Post model and inference from the CopA crystal structure, (Gourdon et al. 2011; Andersson et al. 2014) a speculative copper translocation pathway was proposed and can be assumed to be similar for ATP7A and ATP7B homologues.

In 2011, the first complete structure of a copper transport protein in *Legionella pneumophila*, CopA, was reported at 3.2 Å (Gourdon et al. 2011) and at 2.8 Å resolution in 2014,(Andersson et al. 2014) revealing class-specific details in addition to the well-known canonical ATPase features (Figure 1.3). The P1B type ATPases have significant sequence and structural identity containing six MBD's (mentioned previously with the CXXC motifs at the N-terminus) and the characteristic ATP-binding domains that include the actuator domain (A-domain), phosphorylation domain (P-domain) and nucleotide-binding domain (N-domain), accessible from the cytosol. In addition, there are 8 TM helical domains proposed to contain two unusually coordinated copper binding sites that coincidentally overlap with the coordinating residues in the $Ca^{2+}$ ATPase. The CopA crystal structure was determined in a Cu-free transition state and was assigned to the occluded E2 transition state (Andersson et al. 2014).

The MBD is unable to be modeled in the crystal structure of CopA due to weak or absent electron density, but is located in the periphery of the A-domain and consistent with the suggested position from other experimental data

12
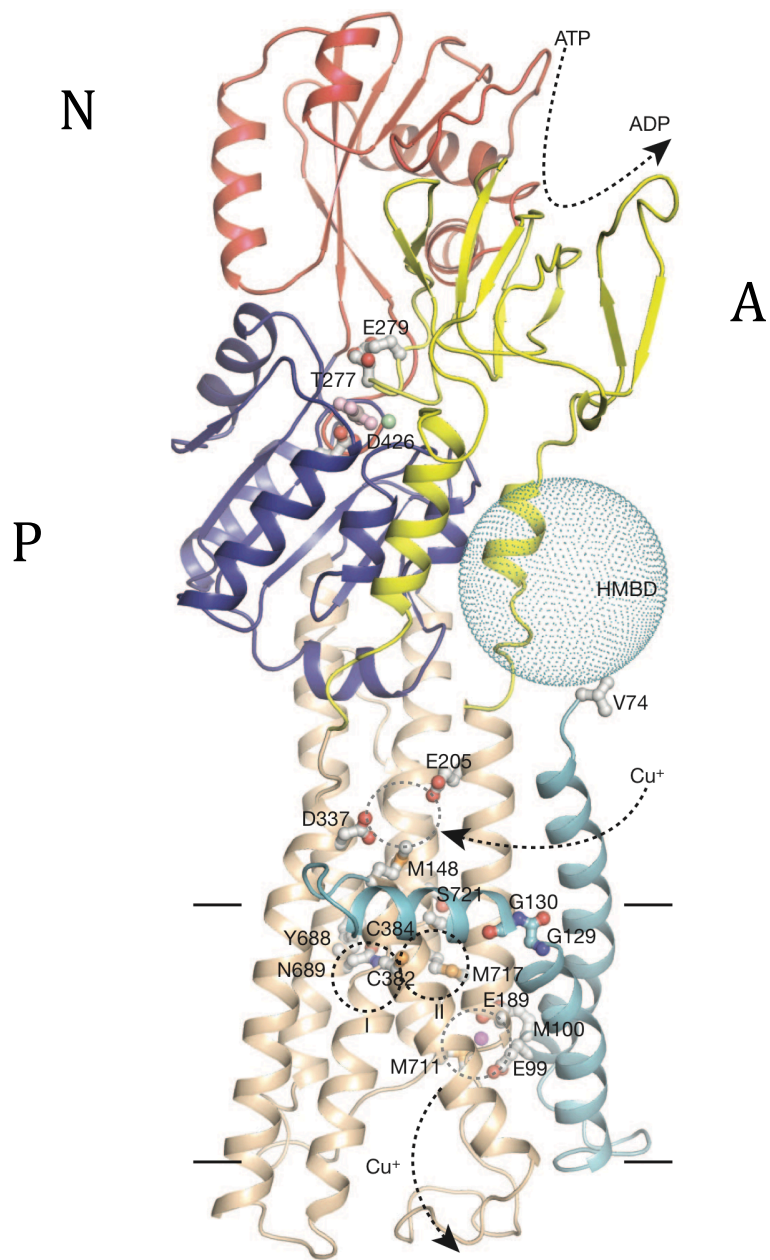
**Figure 1.3.** *Structure of L. pneumophila Cu ATPase, CopA. The A-, N-, and P- domains are in yellow, red, and blue respectively, with the TM helices in cyan and wheat. The dotted sphere is the heavy metal binding domain (HMBD). Arrows indicate the suggested Cu transport pathway, whereas circles depict the putative Cu binding sites (Gourdon et al. 2011).*

(Hatori et al. 2007). The MBD position next to the A- domain revealed a putative entry-binding site. The crystal structure exposed available Met, Glu, and Asp residues as potential ligands for copper to bind, with subsequent data providing a role for these residues in translocating copper across the membrane (Padilla-Benavides, McCann, and Arguello 2013). Mutations to Ala for each of these residues did not affect the ATPase activity when free copper was added, and the metal ion could still access the TM binding sites. However, when the copper chaperone, CopZ for this pathway, was loaded with copper prior to incubation with CopA, the ATPase activity was severely diminished. This result confirms a direct role for the entrance site residues in accepting copper from chaperones and may further promote movement of copper to the high affinity TM sites upon phosphorylation of the canonical aspartic residue in the P-domain. The TM binding sites are composed of tyrosine, asparagine, and serine, as well as the commonly used methionine and cysteine residues for coordinating two high affinity copper binding sites. Subsequent copper release is coupled to the dephosphorylation reaction, represented in the E2-like transition state of the crystal structure, but no clear path is present.

Further investigations comparing the structural differences of copper ATPases ATP7A and ATP7B led to the discovery of a unique loop between transmembrane 1 and 2 on the lumenal side of ATP7A, not found in ATP7B (Barry et al. 2011). This loop contains a characteristic histidine methionine (HM) rich segment that has been found to play a role in the binding and subsequent release of copper to target proteins (Figure 1.4) (Barnes et al. 2005). The ATP7A lumenal loop,

14

**A**

Lumen

1 2 3 4 5 6 7 8

Acceptor protein

Cu

CxxC
CxxC
CxxC
CxxC
CxxC
A
P
N
C
N

Cytosol

**B** "HM Loop" H₅M₄

M2 (M687)
M3 (M692)
H4 (H683)
H5 (H696)
H3 (H682)
M4 (M699)
H2 (H677)
H1 (H676)
M1 (M674)

**C**

```
LVSLFFCIPVMGLMIYMMVMDHHLATLNHNQNMSNEEMINMHSSMFLERQILPGLSIMNLLSLLLCLPVQF ATP7A_RAT
LVSLFFCTPVMGLMMYMMAMEHHFATIHHNQSMSNEEMINMHSAMFLERQILPGLSIMNLLSLLLCLPVQF ATP7A_MOUSE
LVSLFFCIPVMGLMIYMMVMDHHFATLHHNQNMSKEEMINLHSSMFLERQILPGLSVMNLLSFLLCVPVQF ATP7A_HUMAN
LVSLFFCIPVMGLMIYMMVMDHHLATLHHNQNMSQEEMINSHSSMFLERQILPGLSIMNLLSFLLCIPVQF A5A788_PIG
LCSLVFGIPVMGLMIYMLVPS---------------STPHESMVLDHNVIPGLSILNLIFFILCTFVQL BOEVF7_CANFA
LCSLVFGIPVMGLMIYMLVPS---------------NEPHESMVLDHNIIPGLSILNLIFFILCTFVQL D2H7F9_AILME
LCSLVFGIPVMALMIYMLIPS---------------NEPHQSMVLDHNIIPGLSILNLIFFILCTFVQL ATP7B_HUMAN
LCSLVFGIPVMGLMVYMLIPS---------------STPQETMVLDHNIIPGLSVLNLIFFILCTFVQF ATP7B_MOUSE
LCSLVFGIPVMGLMIYMLIPS---------------HEP-QSSVLDHNVIPGLSILNLIFFILCTFVQF ATP7B_SHEEP
```

*Figure 1.4.* ATP7A uses ATP hydrolysis to transport copper ions across the membrane and into target proteins (Barry et al. 2011). A, graphic structure of ATP7A depicts the N-terminus with the six MBD containing the CXXC copper binding motifs, the ATP-binding domains consisting of the A-, P- and N- domains, and a characteristic His Met sequence between TM1/TM2. Transport of copper requires copper binding to the TM domains, while copper release at the luminal side is suggested to bind to the HM Loop sequence, which accompanies dephosphorylation. B, Rosetta ab initio model of the HM Loop. C, sequence alignment of the TM1,2 hairpin of ATP7A and ATP7B. The shaded sequence indicates residues present in the TM; Met and His residues are in bold (Barry et al. 2011).

or HM Loop contains five histidines and four methionines as potential copper ligands. Mutations in the HM loop of full length ATP7A caused a decrease in the rate of dephosphorylation, a process associated with copper release (Barry et al. 2011). However, the direct role of the HM Loop is difficult to investigate in the full-length protein, because as previously mentioned the N-terminal domain can bind up to six Cu (I) ions with two additional copper binding sites in the TM. Therefore, to further explore the role of the HM Loop a model peptide was designed.

The copper-binding properties of the ATP7A HM loop were investigated previously using a model construct in which the TM1/TM2 loop sequence ([674]MDHHFATLHHNQNMSKEEMINLHSSM[699]) replaced the CXXXC motif of the *B. subtilis* Sco protein (Barry et al. 2011; Otoikhian et al. 2012). All other His and Met residues were mutated to Ala, preventing additional unwanted copper binding sites. The HM Loop was shown via X-ray absorption spectroscopy (XAS) and electron paramagnetic resonance (EPR) to have various coordination sites dependent on the oxidation state and amount of copper loaded.(Barry et al. 2011) XAS demonstrates that at Cu: protein ratios close to 1, a combination of His and Met residues bind copper. As the copper to protein ratio increases to 2:1, the coordination changes to all His. Cu (II) data fits four histidine residues, substituting two non-His as the copper to protein ratios increase.

The mechanism of copper binding and subsequent transfer from the HM Loop to acceptor protein, peptidylglycine hydroxylating monooxygenase (PHM), was previously explored (Otoikhian et al. 2012). The Cu (I) and Cu (II) fully loaded HM Loop forms were further shown to transfer copper to PHM in the presence of

16

chelex resin, suggesting a reaction mechanism that involves protein-protein interactions for copper exchange (Otoikhian et al. 2012). PHM was not only fully loaded with copper after the transfer experiment, but also catalytically active, providing a direct role for the HM Loop of ATP7A in trafficking copper. The cytosolic N-terminal domains of ATP7A are believed to mediate transfer of copper into the transmembrane sites, whereas copper release may be controlled by structural elements at the lumen.

## 1.6 COPPER ENZYMES IN THE SECRETORY PATHWAY

PHM, dopamine $\beta$-monooxygenase (D$\beta$M), and tyrosinase (TYR) acquire copper within specialized vesicles of the TGN via copper transporting ATPases that traverse a pH-gradient secretory pathway (Figure 1.5) (Paroutis, Touret, and Grinstein 2004). These enzymes are necessary to catalyze physiological reactions such as neurotransmitter biosynthesis, stress response, embryonic development, and metabolic processes. PHM is part of a bifunctional enzyme called peptidylglycine amidating monooxygenase (PAM) that catalyzes the carboxy-terminal amidation of glycine-extended peptides using a two-step process (Eipper et al. 1993; Kolhekar, Keutmann, et al. 1997). PHM catalyzes the alpha hydroxylation reaction, whereas dealkylation is catalyzed by the zinc dependent enzyme peptidyl hydroxyglycine amidating lyase (PAL)(Atkinson et al. 2010). Tissue specific and developmental regulation of PAM can cause alternative splicing and yield several isoforms including a soluble PHM domain and a membrane associated or soluble PAL domain.
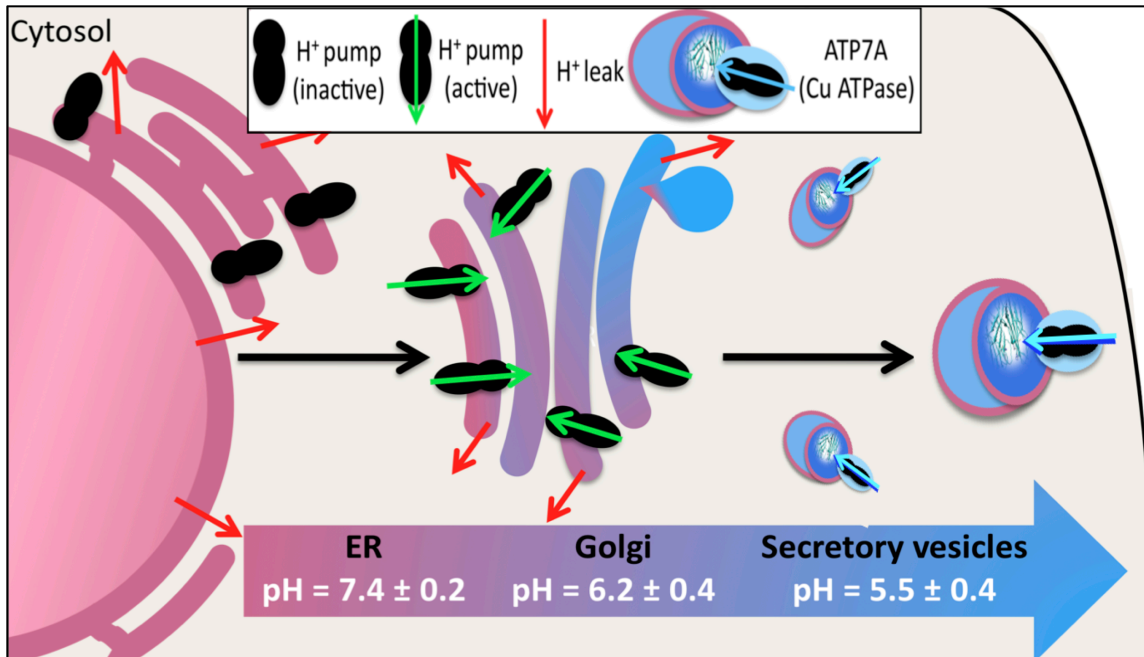
*Figure 1.5.* *Model of the pH-gradient secretory pathway. Acidification progresses from the endoplasmic reticulum (ER) to Golgi to the specialized vesicles where PHM will be metallated by a Cu ATPase, like ATP7A (Figure adapted from Paroutis, Touret, and Grinstein 2004).*

However, deletion of the PHM gene in *Drosophila* is lethal (Kolhekar, Roberts, et al. 1997).

PHM and DβM have a pair of uncoupled mononuclear centers with a catalytic pH optimum of about 5.5,(Klinman 2006a; Prigge et al. 2000) while TYR has a binuclear dicopper site with the catalysis optimum at pH 7 (Matoba et al. 2006b; Sendovski et al. 2011). PHM and DβM are homologous cuproproteins, which have been extensively investigated (Evans, Ahn, and Klinman 2003; Hess, McGuirl, and Klinman 2008; Kunishita et al. 2012; Eipper et al. 1995; Klinman 2006a). PHM, and therefore DβM, has two mononuclear copper sites that are structurally and

catalytically distinct from one another, yet function cohesively over an 11 Å wide

solvent filled cavity (Figure 1.6). PHM is a 35- kDa protein that catalyzes the

hydroxylation reaction of glycine extended substrates, the first step of the peptide

amidation reaction, while DβM converts dopamine into norepinephrine (Figure 1.7).

In PHM, one of the copper sites, termed CuM is coordinated by Met314,

His242, and His244 residues, while the other site termed CuH is bound by His107,

108, and 172. Reaction mechanisms have been proposed to be similar between the

homologous proteins involving the redox cycling of the two copper centers in which

oxygen is activated and induces hydroxylation of substrate at the CuM-site, via a

long-range electron transfer pathway from the CuH center (Bauman et al. 2011;

Klinman 2006a; Bauman, Jaron, et al. 2006; Prigge et al. 2000; Francisco et al.

2002a; Chufa´n et al. 2010). The mechanism of copper delivery to each of the copper

centers is unknown and the nature of the reactive oxygen intermediate, its mode of

activation, and the various pathways of electron transfer are all highly controversial

topics. However, Figure 1.8 shows a general overview of the PHM mechanism that is

based on theoretical calculations, which agree pretty well with experimental results

(Abad, Rommel, and Kaestner 2014). In the resting state of PHM, both copper

centers are in the oxidized state prior to being reduced by an external reductant,

such as ascorbate. Substrate binding then triggers oxygen activation, which Abad *et

al.,* 2014 indicates is most likely a Cu-$[O_2]^+$ species. The Cu-$[O_2]^+$ species becomes

protonated leading to Cu-$[OOH]^+$ species, which has a smaller energy barrier than

the Cu-superoxo species. Hydrogen from the substrate has been shown to be partly

transferred by quantum tunneling, and is again suggested in this mechanism.
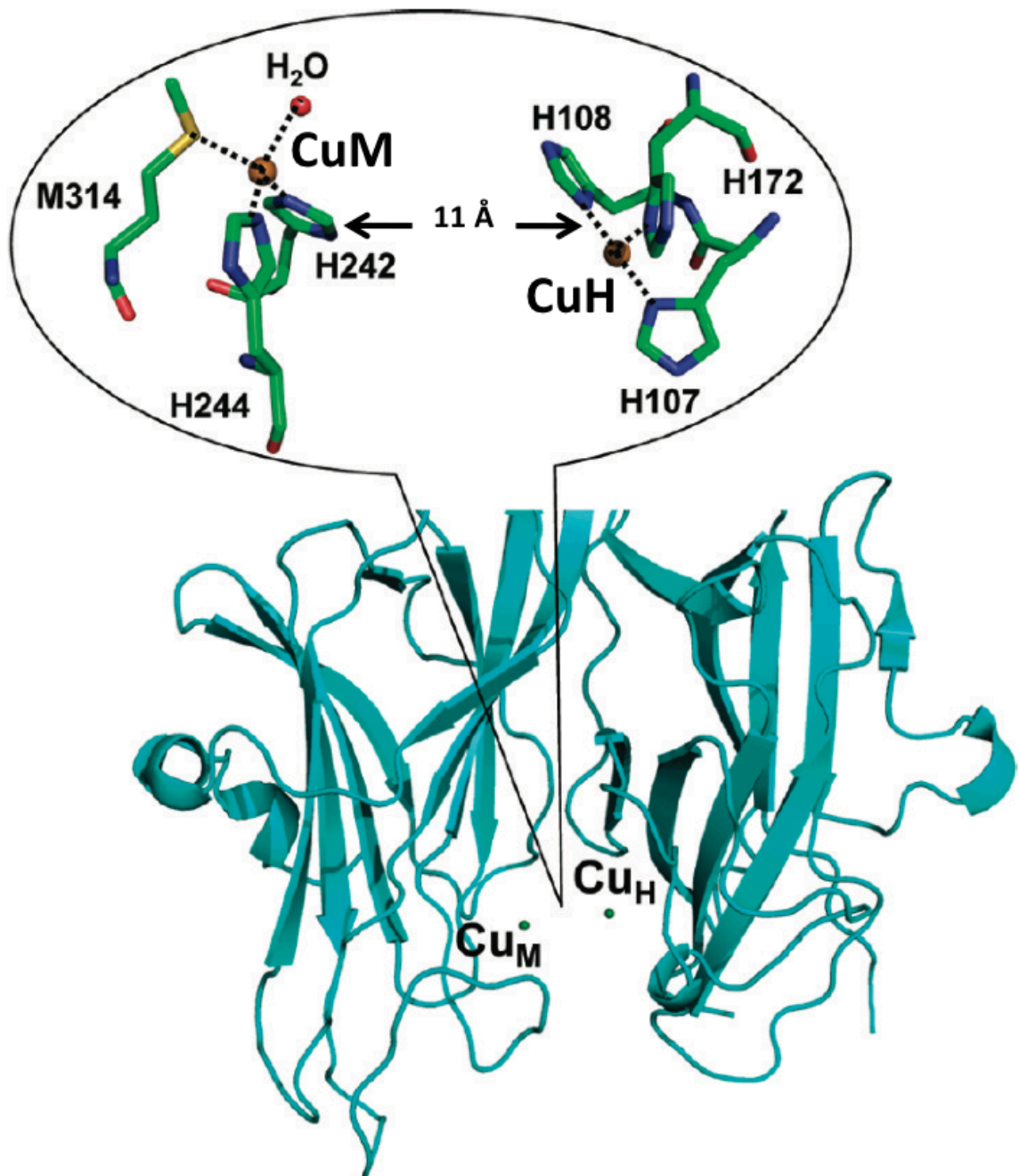
**Figure 1.6.** *Structure of PHM CuM and CuH centers. CuM is the catalytic site and CuH is the electron-transfer site, which are separated by 11 Å (Chufa'n et al. 2010).*

*Figure 1.7.* *Reactions catalyzed by PHM and DβM. A, PHM catalyzes the oxygen- and ascorbate-dependent hydroxylation of glycine extended peptides, while the PAL domain cleaves the intermediate, prior to peptide amidation (Prigge et al. 2000). B, DβM catalyzes the hydroxylation of dopamine at the β- carbon position (Hess, McGuirl, and Klinman 2008).*

Additionally, protonation and an electron transfer occur (most likely in a spontaneous fashion), which allow OH rebinding. A slight energy barrier is observed for cleaving the double protonated transition state (TS) 2, which leads to the final product. Recent studies from the Blackburn lab investigated the kinetic and structural components important for substrate activation in PHM, and suggest that the His and Met residues at both copper centers are equally important for catalytic activity. The specific aspects of PHM structure and function will be described in further detail in the introduction of Chapters 3 through 5.

*Figure 1.8.* *Reaction mechanism proposed for PHM with details found in the text (Abad, Rommel, and Kaestner 2014).*

Overall, the His-Met residues are critical for function in copper proteins and the fact that copper loading into PHM has been shown to bypass the use of chaperones is very interesting. The role of chaperones is suggested to take place via the His & Met motifs in the HM Loop of ATP7A, which coincidentally mimic the coordination chemistry of their target proteins. We hypothesize that the His and Met residues in the HM Loop can accommodate the different active site structural elements and pH environments encountered acting as a copper chaperone to PHM and/or DβM.

# CHAPTER 2

# MATERIAL AND METHODS

## 2.1    BIOLOGICAL METHODS

### 2.1.1   CLONING, EXPRESSION, AND PURIFICATION OF PEPTIDYLYGLYCINE HYDROXYLATING MONOOXYGENASE WT AND VARIANTS

PHM WT and variants were constructed using the PHM catalytic core (PHMcc) sequence comprised of residues 42–356. For the first time, Mary Mayfied-Gambill and I constructed PHMcc variants in house. PHM variants H108A, H107108A, and M109I were individually introduced into the pBS.ΔProPHM382s vector (obtained from Betty A. Eipper and Richard E. Mains) using Splicing by Overlap Extension (SOEing) (Eipper et al. 1995; Kolhekar, Keutmann, et al. 1997; Horton et al. 1990). Sense and antisense oligonucleotide primers encoding about 15 bases downstream and upstream of the mutation were used for site-directed mutagenesis and paired with primers upstream and downstream of two restriction enzyme sites, ClaI & XbaI (Table 2.1).  PCR products were purified on agarose gels. Final PCR products were phenol-chloroform extracted, digested using restriction enzymes (NEB), fractionated on agarose gels, purified via Qiagen PCR kit, and then ligated into the pCIS.2CXXNH expression vector (also acquired from Betty A. Eipper and Richard E. Mains). Sequence analysis was performed on mutant clones, and Qiagen midi prep was used to ensure 20 $u$g/ 20 $u$L of recombinant DNA for

23

| PHMcc Mutant Oligos | Oligos |
| --- | --- |
| WT | AGCATGGATACTGTCCACCATATGCTGCTGTTTGGATGC |
| H108A | AGCATGGATACTGTCCAC**GCT**ATGCTGCTGTTTGGATGC |
| H107108A | AGCATGGATACTGTC**GCCGCT**ATGCTGCTGTTTGGATGC |
| M109I | AGCATGGATACTGTCCACCAT**ATA**CTGCTGTTTGGATGC |
| The forward primers are shown above with the mutated codons in bold, while the reverse primers are complementary. WT PHMcc sequence is available for comparison. | |

**Table 2.1.** *Oligonucleotides used in the construction of PHM variants*

transfection.

Chinese hamster ovary (CHO) DG44 cells were transfected with the recombinant DNA using Lipofectamine 2000 (Invitrogen). The transfected cells were subsequently selected for *Dhfr* cell lines in $\alpha$- minimum Eagle's medium containing 10% dialyzed fetal bovine serum (Kolhekar, Keutmann, et al. 1997; Oyarce et al. 2001). Only those cells that retained the *Dhfr* gene (co-located with PHM on the plasmid) were capable of growth under these conditions. Monoclonal cell lines were created by serial dilution into 96-well plates and wells that contained single-cell colonies were selected for further analysis (Figure 2.1). These colonies were passed individually into a fresh 96-well plate, grown to confluence, and screened via Western blot for PHMcc expression levels under similar conditions.

*2.1.1.1 Western Blot Analysis.* CHO DG44 cells were incubated in DMEM/F12 containing 0.5% Fetal Clone II (FCII, Fisher) for at least 24 hours before a sample
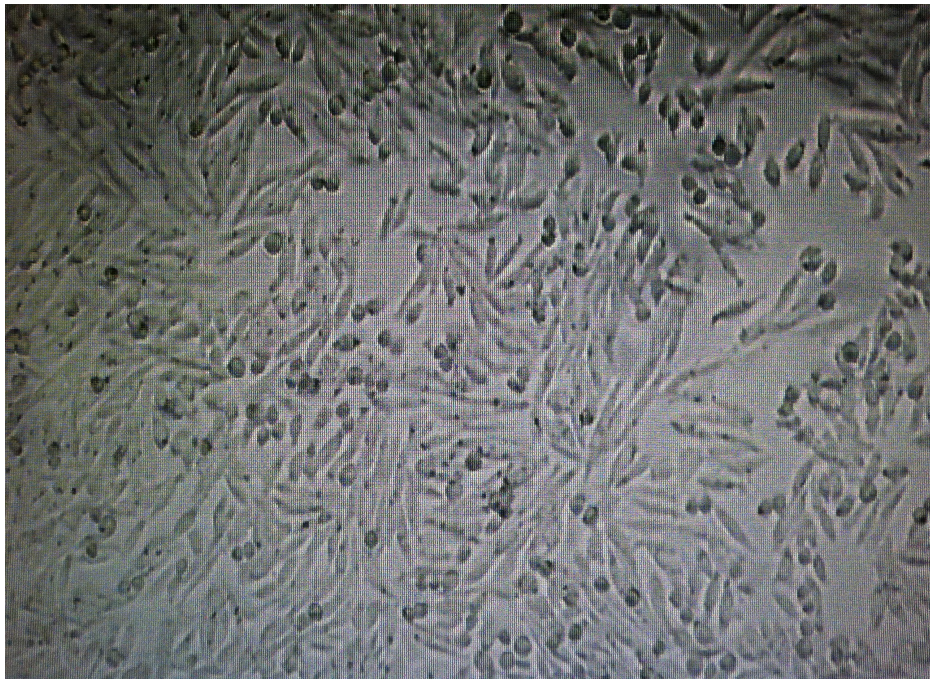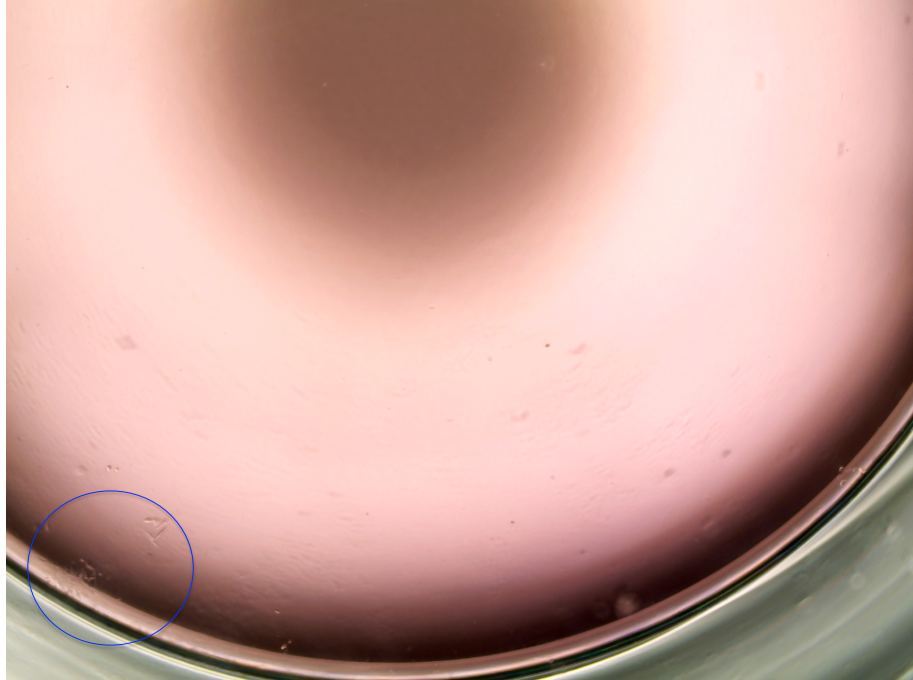
*Figure 2.1.* *CHO monoclonal cell lines. The top image represents a single-cell colony growing in a 96-well plate, circled in blue. The bottom image is a well that has grown confluent with cells.*

was collected. This aliquot was then combined with 5X SDS, and heated for five minutes at 100° C. Each sample was separated using an 8-25% (GE Healthcare) sodium dodecyl sulfate-polyacrylamide gel electrophoresis (SDS- PAGE) and then transferred to an Immobilon P membrane (Millipore) using the Amersham Biosciences PHAST system. PHM proteins were visualized using rabbit antibody 246 [rPAM(116- 13l)] (Husten and Eipper 1991) diluted 1:1500, and secondary antibody-anti-rabbit IgG (Sigma) diluted 1:1000, followed by an AP Conjugate Substrate Kit (Bio-Rad Laboratories). The monoclonal cell line producing the thickest and darkest enzyme band from the Western blot results were selected for growth in a Hollow Fiber Bioreactor, 5 MWCO (Fibercell Systems, Inc). Figure 2.2 shows an example of 5 monoclonal cell lines from PHM M109I, in which we selected clone in lane 4 to be expressed in the Hollow Fiber Bioreactor system.

   *2.1.1.2 Growing PHMcc.* PHMcc H108A, H107108A and M109I variants were constructed in house and all grown as described previously (Eipper et al. 1995; Jaron and Blackburn 1999; Evans, Blackburn, and Klinman 2006; Bauman, Ralle, and Blackburn 2007; Bauman et al. 2011; Kline, Mayfield, and Blackburn 2013; Chauhan et al. 2014). Briefly, stably transfected (CHO) DG44 cell lines were thawed from freezer stock into a T75 flask with 20 mL of DMEM/F12 medium containing 10% FCII serum (Fisher). At 80 percent confluence, the cells were equally separated and passed into five NUNC triple flasks (500 cm$^2$ area per flask), which were also each grown to confluence. Cells were trypsinized and resuspended in 50 mL medium with 10% FCII serum prior to inoculation into the extra-capillary space (ECS) of a Hollow Fiber Bioreactor (Fibercell Systems 4300-C2008, MWCO 5 kD, 3000 cm$^2$
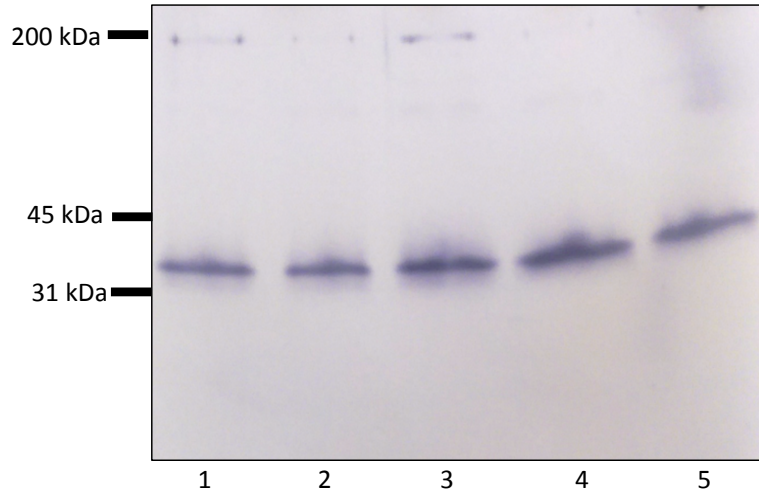
***Figure 2.2.*** *Western blot of PHM M109I monoclonal cell lines*

surface area) pre-cultured with 2 L of 50 mM PBS pH 7.35 followed by 2 L of

DMEM/F12 10% FCII serum (Figure 2.3) (Jaron and Blackburn 1999; Bauman et al.

2011; Kline, Mayfield, and Blackburn 2013; Bauman, Ralle, and Blackburn 2007).

The cell suspension was gently flushed through the ECS, back and forth between the

side port syringes to insure an even distribution of cells. Individual bioreactors

containing each of the variants were fed with DMEM/F12/10% FCII serum for a

week prior to changing the media and collecting the spent media every other day.

After a month the serum level was reduced to 0.5% FCII serum (Bauman, Ralle, and

Blackburn 2007). At this point, the bioreactors were fed with 0.5% serum-

containing medium every other day, and spent medium (20 mL) from the ECS was

collected and frozen at -20°C for later purification.

    *2.1.1.3 Purifying PHMcc Protein.* About a month worth of bioreactor harvest

(approximately 300 mL) for each variant was purified at a time, as previously

described (Bauman, Ralle, and Blackburn 2007). Ammonium sulfate was added to
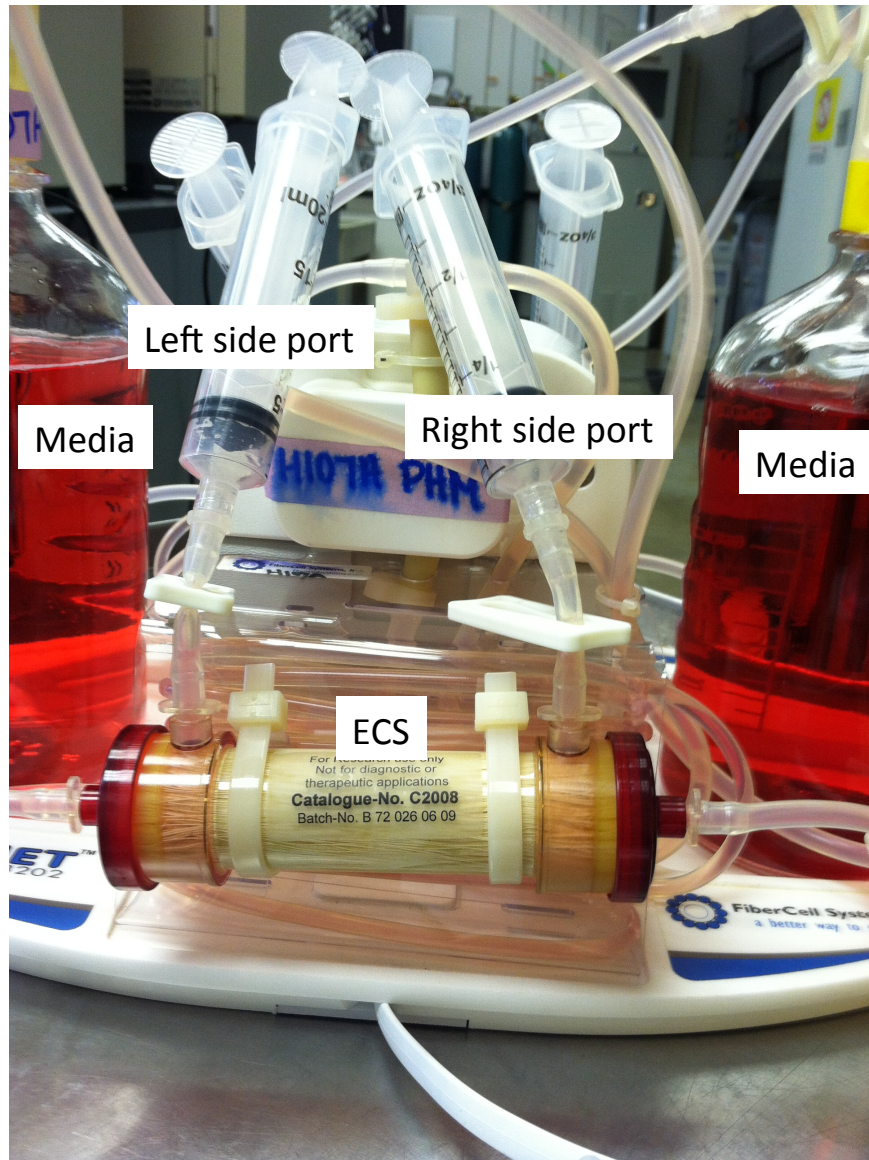
***Figure 2.3.*** *Image of the FiberCell Systems Inc hollow fiber bioreactor. Two hollow fiber cartridges can be maintained per bioreactor unit, using 1 L of media per cartridge every other day. The CHO cells were inoculated into the extra-capillary space (ECS) using the right and left side ports. In order to feed the cells, 20 mL of fresh media was added to the ECS from one end of the side port while spent media was collected from the other end, and stored for later use.*

the spent media in the 4°C fridge and left to stir for 45 minutes in order to precipitate out the PHM protein. The precipitate was pelleted using centrifugation and resuspended gently with no more than 25 mL of 50 mM potassium phosphate buffer (pH 7.5), containing 0.01% Triton X-100. The sample was centrifuged, and filtered through a 0.45 um sterilefilter before being applied to a 26/60 Hiload Superdex 75 prep grade gel filtration column (Pharmacia) at a flow rate of 3.7 mL/min. In order to have good resolution, only 12 mL of sample was injected at once, with no more than two injections a day (Figure 2.4). The main protein fractions were pooled, concentrated, and dialyzed against a buffer containing 20mM Tris-acetate buffer, pH 8.2-8.4 overnight in a 4°C fridge.

The sample was then applied to an anion exchange column on the Biocad 700E Work Station for Perfusion Chromatography (Applied Biosystems) for further purification. The anion exchange column was loaded with no more than 7 mL of protein at 2 mL/min after first being primed, calibrated, and equilibrated. The protein peak was monitored using a UV/vis dual wavelength detector set to 214 and 280 nm. PHM protein was eluted using a salt (NaCl) gradient, with the purest fractions collected between 144 and 180 mM salt. The fractions found to be greater than 95% pure using SDS-PAGE analysis were pooled, concentrated, and dialyzed against 20mM sodium phosphate buffer, pH 8.0 overnight in a 4°C fridge prior to reconstitution with cupric sulfate.

## 2.1.2   CLONING, EXPRESSION, AND PURIFICATION OF ATP7A HM LOOP WT AND VARIANTS WITH AND WITHOUT SELENIUM LABELING
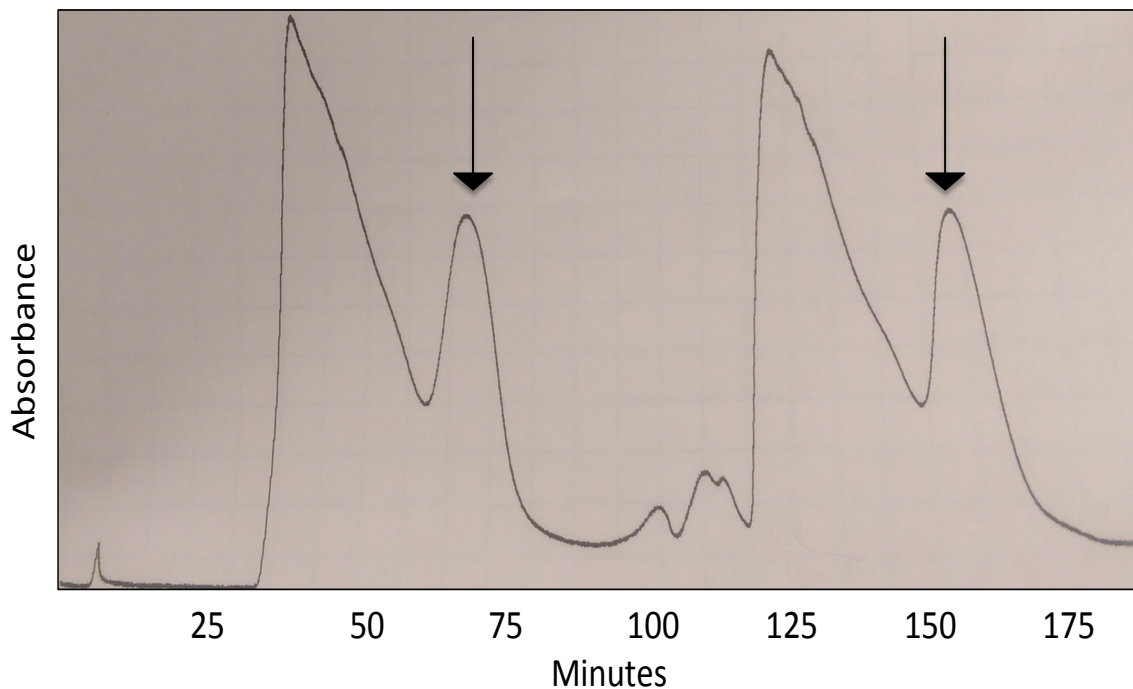
**Figure 2.4.** *Gel filtration chromatograph of PHM WT. PHM can be seen eluting approximately 60 minutes after being loaded onto the column (black arrow), which can be followed by a second injection.*

The HM Loop of ATP7A was constructed as a chimeric protein by replacing the copper-binding $^{45}CXXXC^{49}$ motif of BSco with lumenal loop Histidine-Methionine (HM) rich peptide ($^{674}$MDHHFATLHHNQNMSKEEMINLHSSM$^{699}$) from Menke's protein (ATP7A), as previously reported (Figure 2.5) (Barry et al. 2011; Otoikhian et al. 2012). The HM loop was further constructed by polymerase chain reaction (PCR) amplification to include His$_6$ and a Tev cleavage site at the N-terminus (for ease of purification with the nickel-NTA affinity column) in the petDuet vector using SacI/KpnI restriction enzymes. Sequence analysis was performed and the construct was re-named HM Loop WT. Plasmids were
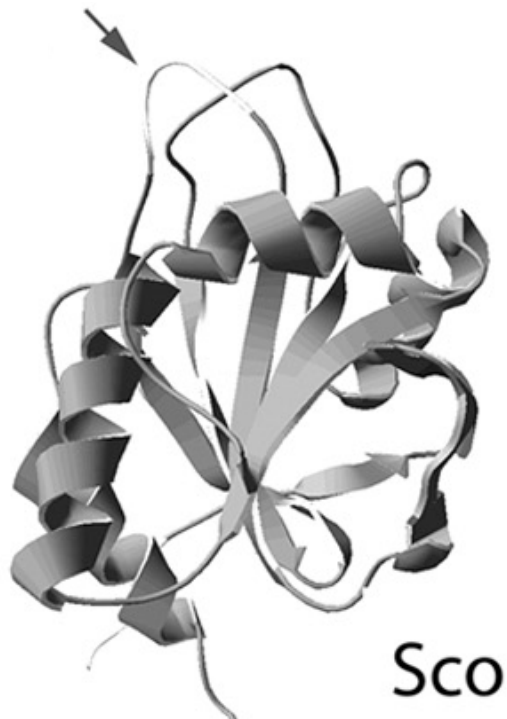
ScoHM

MGQQIKDPLNYEVEPFTFQNQDGKNVSLESLKGEVWLADFIFTN**MDHHFATLHHNQNMSKEEMINLHSSM**PPITAA
ITDLQKKLKAENIDVRIISFSVDPENDKPKQLKKFAANYPLSFDNWDFLTGYSQSEIEEFALKSFKAIVKKPEGEDQVIAQS
SFYLVGPDGKVLKDYNGVENTPYDDIISDVKSASTLK

*Figure 2.5. Structure of B. subtilis Sco (dark gray) with the CETIC sequence replaced with the HM Loop shown in light gray and with an arrow. The sequence of the scaffold construct used in this study is shown below, with the inserted HM Loop sequence in green (Barry et al. 2011).*

transformed into *Escherichia coli* strain BL21 DE3 for normal methionine expression and selected constructs were additionally transformed into *Escherichia coli* strain B834 DE3, a methionine auxotrophic used for selenium labeling experiments.

Double and triple methionine variants were constructed in order to identify the copper bound ligand. Methionine residues were mutated to isoleucine and

| Nomenclature | Amino Acid Sequence |
|---|---|
| HM Loop WT | **M** D H H F A T L H H N Q N **M** S K E E **M** I N L H S S **M** |
| M1 | **M** D H H F A T L H H N Q N **I** S K E E **I** I N L H S S **I** |
| M2 | **I** D H H F A T L H H N Q N **M** S K E E **I** I N L H S S **I** |
| M3 | **I** D H H F A T L H H N Q N **I** S K E E **M** I N L H S S **I** |
| M4 | **I** D H H F A T L H H N Q N **I** S K E E **I** I N L H S S **M** |
| M1,2I | **I** D H H F A T L H H N Q N **I** S K E E **M** I N L H S S **M** |
| M1,3I | **I** D H H F A T L H H N Q N **M** S K E E **I** I N L H S S **M** |
| M1,4I | **I** D H H F A T L H H N Q N **M** S K E E **M** I N L H S S **I** |
| M2,3I | **M** D H H F A T L H H N Q N **I** S K E E **I** I N L H S S **M** |
| M2,4I | **M** D H H F A T L H H N Q N **I** S K E E **M** I N L H S S **I** |
| M3,4I | **M** D H H F A T L H H N Q N **M** S K E E **I** I N L H S S **I** |

***Table 2.2.*** *Nomenclature and Amino Acid Sequence for HM Loop Variants. M1, M2, M3 and M4 denotes the methionine that is retained in the HM Loop sequence (bold), while the other three methionine residues are mutated to isoleucine (in red).*

individually constructed in the petDuet vector via SOEing. Sense and antisense oligonucleotide primers encoding about 15 bases downstream and upstream of the mutations were used for site-directed mutagenesis and paired with primers upstream and downstream of two restriction enzyme sites, SacI & KpnI. The mutant clones were checked by DNA sequencing and appropriately named (Table 2.2). All plasmids were transformed into *Escherichia coli* strain BL21 DE3 for expression.

    *2.1.2.1 Expression of HM Loop WT and Met Variants.* Expression of His$_6$ HM

Loop WT, double, and triple Met mutants were carried out using protocols described previously (Chacon and Blackburn 2012; Barry et al. 2011; Otoikhian et al. 2012). Briefly, ten mL of culture medium (LB and 10X ampicillin, LBamp) was inoculated early morning from a freshly streaked plate of BL21 DE3 cells and used to inoculate a 1 L LBamp flask mid afternoon. The culture was induced by addition of 0.5 mM isopropyl-β-D-thiogalacto-pyranoside (IPTG) and incubated overnight at 17 °C once the culture reached an $OD_{600}$ of 0.6-0.9 with shaking. Cells were harvested by pelleting via centrifugation in a Sorvall GS-3 rotor at 5000g for 30 min and frozen at −80 °C (as needed).

   *2.1.2.2 Expression of Selenium Labeled HM Loop.* Expression was carried out using protocols described previously (Chacon and Blackburn 2012). Ten mL of LBamp was inoculated from a freshly streaked plate of B834 DE3 cells and incubated at 37 °C for three hours. One hundred microliters of this culture was added to a 10 mL flask of minimal culture medium which included L-methionine for overnight incubation at 37 ° C with shaking. A 1 L flask of minimal medium that contained seleno-methionine (SeM) in place of methionine was inoculated with the 10 mL minimal culture until an $OD_{600}$ of 0.6-0.9 was reached. The 1 L culture was then induced by addition of IPTG and incubated overnight at 17 °C. Cells were harvested as previously stated.

*2.1.2.3 Purification of HM Loop and Variants.* Purification was carried out using protocols described previously (Chacon and Blackburn 2012; Barry et al. 2011; Otoikhian et al. 2012). Briefly, apoproteins were purified from the soluble lysate by resuspending the pelleted cells in 50 mM Tris buffer, 400 mM NaCl at pH 8.0

containing EDTA-free protease inhibitor (Roche). Cells were lysed in a French Press

at 1000 psi and centrifuged at 8500g for 30 min. The supernatant was passed

through a 0.45 μm syringe filter and purified by chromatography on a nickel-NTA

affinity column The $His_6$ tag was then cleaved by overnight incubation with

recombinant tobacco etch virus (r-TEV) protease followed by dialysis against

imidazole-free buffer, and a second metal affinity chromatography step removed the

cleaved $His_6$ tag. Eluted protein fractions were assayed for purity by SDS- PAGE

analysis using gradient 8–25% (GE Healthcare) and stained with Coomassie brilliant

blue R-250, which showed a single band at about 23 kDa. Figure 2.6 is the SDS-PAGE

that shows one lane over from the ladder the soluble portion (which is overloaded);

the second lane contains the filtrate, and the third and fourth lanes are two separate

fractions of the purified His-tagged protein. Following purification, the protein was

dialyzed in 20 mM phosphate buffer, pH 8.0 and stored at −80 °C.

## 2.2    PHYSICAL METHODS

### 2.2.1  COPPER RECONSTITUTION OF PHM AND VARIANTS

Purified enzyme was dialyzed against 20 mM sodium phosphate buffer, pH

8.0 and then reconstituted with cupric sulfate by slow addition of 2.5 molar

equivalents Cu (II) per protein and allowed to stir for one hour. Two cycles of

dialysis were included to remove unbound cupric ions. After finding copper-to-

protein ratios close to 1 for PHM H107108A, (Chauhan et al. 2014) the single-site

mutants were thereafter reconstituted with 1.3 equiv of cupric sulfate, dialyzed
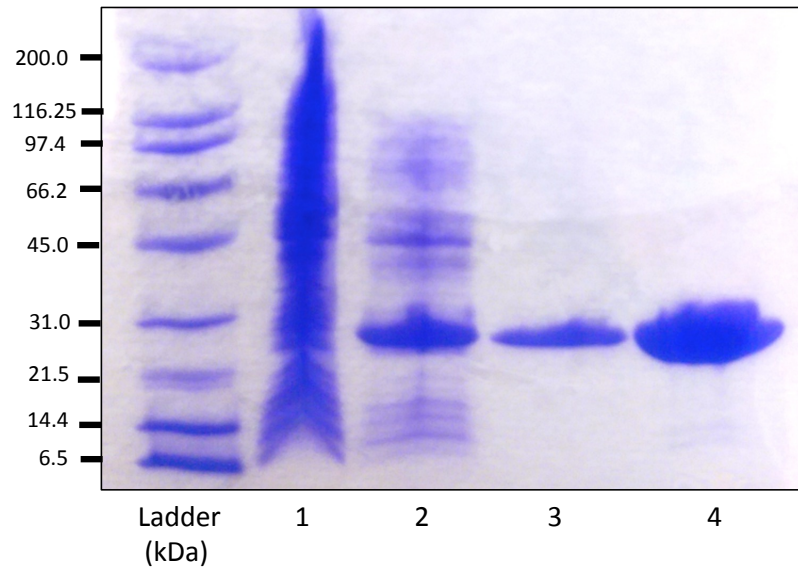
***Figure 2.6****. SDS-PAGE of HM Loop WT. One lane over from the ladder contains the soluble protein portion expressed from bacterial cells (which is overloaded); the second lane contains the filtrate; the third and fourth lanes are two separate fractions of the purified His-tagged protein.*

overnight against 20 mM sodium phosphate buffer, concentrated using ultrafiltration, and passed through a desalting spin column to remove any remaining unbound cupric ions. Protein concentrations were determined using $OD_{280}(1\%) = 0.980$ on a Cary 50 spectrophotometer(Bauman et al. 2011). Copper concentrations were determined using a Perkin-Elmer Optima 2000 DV inductively coupled plasma optical emission spectrometer (ICP-OES) with copper-to-protein ratios reported in Table 2.3. Reduced protein samples were prepared under anaerobic conditions to which 5-fold equivalent ascorbate had been added and used immediately in anaerobic experiments, or flash-frozen in liquid nitrogen for use in XAS experiments.

| Protein | Cu:Protein |
| --- | --- |
| PHM WT | 2.02 ± 0.15 |
| H172A (Jaron and Blackburn 1999) | 1.40 ± 0.30 |
| M314H (Bauman et al. 2011) | 1.60 ± 0.28 |
| M109I | 2.08 ± 0.14 |
| H107A | 2.01 ± 0.01 |
| H108A | 2.04 ± 0.23 |
| H107108A (Chauhan et al. 2014) | 1.09 ± 0.15 |
| H242A (Jaron et al. 2002) | 1.11 ± 0.03 |
| M314I (Jaron and Blackburn 1999) | 1.20 ± 0.38 |

**Table 2.3.** *Copper reconstitution values for PHM WT and variants.*

## 2.2.2 COPPER RECONSTITUTION OF HM LOOP AND VARIANTS

Purified protein was reconstituted with cupric sulfate by slow addition of 1.2 mol equivalent Cu (II) per protein followed by exhaustive dialysis to remove unbound cupric ions. Protein concentrations were determined using the bicinchoninic acid (BCA) assay while copper concentrations were analyzed using ICP-OES. (Otoikhian et al. 2012; Chacon and Blackburn 2012) The copper to protein ratios were found to be about 1:1. Reduced samples were prepared using Tetrakis(acetonitrile)copper (I) hexafluorophosphate (referred to as Cu (I)-ACN), only to determine later that reduction of the Cu (II) samples with 5 fold equivalent ascorbate had the same end result.

The Cu (I)-ACN samples were prepared in a Coy anaerobic chamber by first stirring the protein samples over an ice pack. The Cu (I)-ACN compound was meticulously weighed out and dissolved in pure acetonitrile (ACN) such that the ACN concentration was limited to 10% of the total protein solution by volume, additionally comprising a metal to protein ratio of no more than 1.5:1. The mixture was allowed to stir and incubate one hour before three spin columns were applied to remove excess metal. The desalting columns were equilibrated with 20 mM phosphate buffer containing 10%, 5%, and 0% ACN. The metal-to-protein concentrations were then verified by ICP-OES and the BCA assay before being flash-frozen in liquid nitrogen for use in XAS experiments.

### 2.2.3   COMBINATION BUFFER

The following mixed buffer systems were made by mixing equal volumes of either 50 mM or 100 mM *N*-cyclohexyl-2-aminoethanesulfonic acid (CHES), 4-(2-hydroxyethyl)-1-piperazineethanesulfonic acid (HEPES), 2-(*N*-morpholino)ethanesulfonic acid (MES), and formic acid, and then adjusting the pH (3-10) using sodium hydroxide (Bauman et al. 2011).

### 2.2.4   SPECIFIC ACTIVITY MEASUREMENTS OF PHM

Enzymatic activity was measured by monitoring oxygen consumption in a Rank Brother's oxygen electrode at 37° C, as previously reported (Bauman, Jaron, et al. 2006). Each reaction was performed in a water-jacketed vessel in 2 mL total volume containing 100 mM MES pH 5.5, 200 µL of a 6 mg/mL catalase solution

37

(47,000 units per mg), 100 $\mu$L of 100 $\mu$M Cu (II) solution, 10 $\mu$L of 2 M stock ascorbate, and 80 $\mu$M dansyl-YVG substrate.  In some cases, various concentrations of imidazole up to 10 mM were added in an attempt to rescue activity. The reaction was allowed to equilibrate for approximately 1 minute, the reaction vessel was capped, and a baseline was measured for 50 seconds prior to initiation of the reaction.  The reaction was initiated by addition of 10 to 20 $\mu$L of enzyme (concentrations varied depending on the activity of the particular variant) through the cap using a Hamilton syringe. The oxygen consumption was monitored and analyzed as previously reported (Bauman et al. 2011; Bauman, Jaron, et al. 2006). Steady state kinetic measurements were performed as above, varying concentrations of dansyl-YVG between 2.5 and 400 $\mu$M. Kinetic constants were determined by fitting raw data to the Michaelis-Menten equation using nonlinear regression.  Similar assay conditions were used for the measurement of pH-activity profiles in the pH range 3 – 9, except that a mixed buffer system was employed containing equal volumes of 100 mM each of MES, HEPES, CHES, and formic acid adjusted to the desired pH with sodium hydroxide.

### 2.2.5  HPLC

Reverse-phase high-pressure liquid chromatography (HPLC) is a technique used to separate, identify, and quantify complex samples using a hydrophobic stationary phase (Berg, Tymoczko, and Stryer 2002). HPLC is like an enhanced version of column chromatography, where the fine material in the column interacts with the components in the samples differently, thus allowing greater resolving

power. Applied pressure is additionally required for the appropriate flow rate, resulting in high resolution and rapid separation of the complex mixture.

HPLC was performed with a Varian Pro Star solvent delivery module equipped with a Varian Pro Star model 410 autosampler (250 uL syringe, 100 uL sample loop) on a 250 mm × 4.6 mm Varian Microsorb-MV 100-5 C18 column as reported in Bauman *et al.*, 2011. A Waters 474 scanning fluorescence detector was used to measure the dansyl fluorescence $\lambda_{ex}$ at 365 nm, and $\lambda_{em}$ at 558 nm and therefore the concentration of peptide substrate, dansyl-YVG (American Peptide Co.) and hydroxylated product (produced by the PHM-catalyzed reaction). Product was separated from substrate via an isocratic method using 25% Solvent B in A where Solvent A was 0.1% trifluoroacetic acid in water, and solvent B was 0.1% trifluoroacetic acid in acetonitrile. HPLC was used in conjunction with the $O_2$-electrode and found that oxygen consumption was coupled to product formation for PHM WT and variants.

Reactions were performed in a water-jacketed glass reaction vessel, under similar reaction conditions as for the specific activity measurements mentioned above (substrate and enzyme concentrations were adjusted for each experiment). The reaction was allowed to equilibrate for 1 minute prior to initializing the reaction with enzyme. After 150-200 seconds of reaction time, an aliquot of 200 $\mu$L from the reaction vessel was quickly removed and quenched with 20 $\mu$L of 20% TFA with the oxygen concentration additionally noted. In the case of M109I, an aliquot of 200 $\mu$L from the reaction vessel was removed and added to 200 $\mu$L of 20% TCA in order to quench the reaction. Substrate and product were separated via HPLC, and
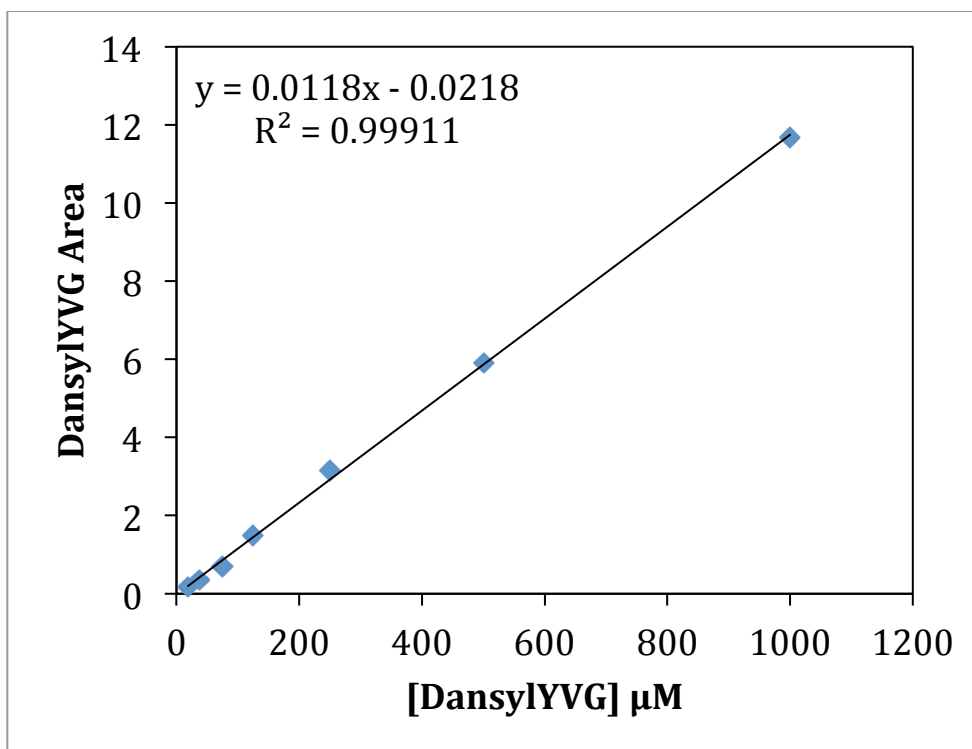
*Figure 2.7.* *Calibration curve for peptide substrate DansylYVG*

concentrations of peptide substrate remaining were determined by reference to a

standard curve (Figure 2.7) (Bauman et al. 2011; Bauman, Jaron, et al. 2006).

Micromoles of oxygen consumed were determined by subtracting the $O_2$

concentrations at the time of sampling from the value immediately before reaction

initiation.

### 2.2.6 XAS

X-ray absorption spectroscopy (XAS) is a powerful tool used to study the

molecular and electronic structure of metalloproteins in solution, making use of the

energetic photons. X-ray diffractions provide three-dimensional (3D) atomic

structures from crystalline samples, in contrast to XAS, which offers structural

| Energies (KeV) | | |
| --- | --- | --- |
| | K | $L_{III}$ |
| S | 2.5 | |
| Mn | 6.5 | 0.6 |
| Fe | 7.1 | 0.7 |
| Ni | 8.3 | 0.8 |
| Cu | 9.0 | 0.9 |
| Se | 12.6 | 1.4 |
| Mo | 20.0 | 2.5 |
| Ag | 25.5 | 3.3 |
| Tb | 52.0 | 7.5 |
| W | 69.5 | 10.2 |
| Hg | 83.1 | 12.3 |

**Table 2.4.** *Ionization Energies (Que 2000).*

information on amorphous samples. The X-rays used are generated as synchrotron radiation, which provide a high intensity X-ray source in the range of 200- 30,000 eV and can be tuned with a crystalline monochromator in order for a specific metal to absorb (Que 2000). An X-ray absorption spectrum is a measurement of the energy-dependent absorption coefficient required to remove an electron from the 1s (K-edge), 2s or 2p (L-edge) shells, leaving a core hole. Absorption does not occur until the X-rays have reached an energy capable of ionizing the core electron of a specific atom, with examples of selected elements and their ionization energies reported in Table 2.4.
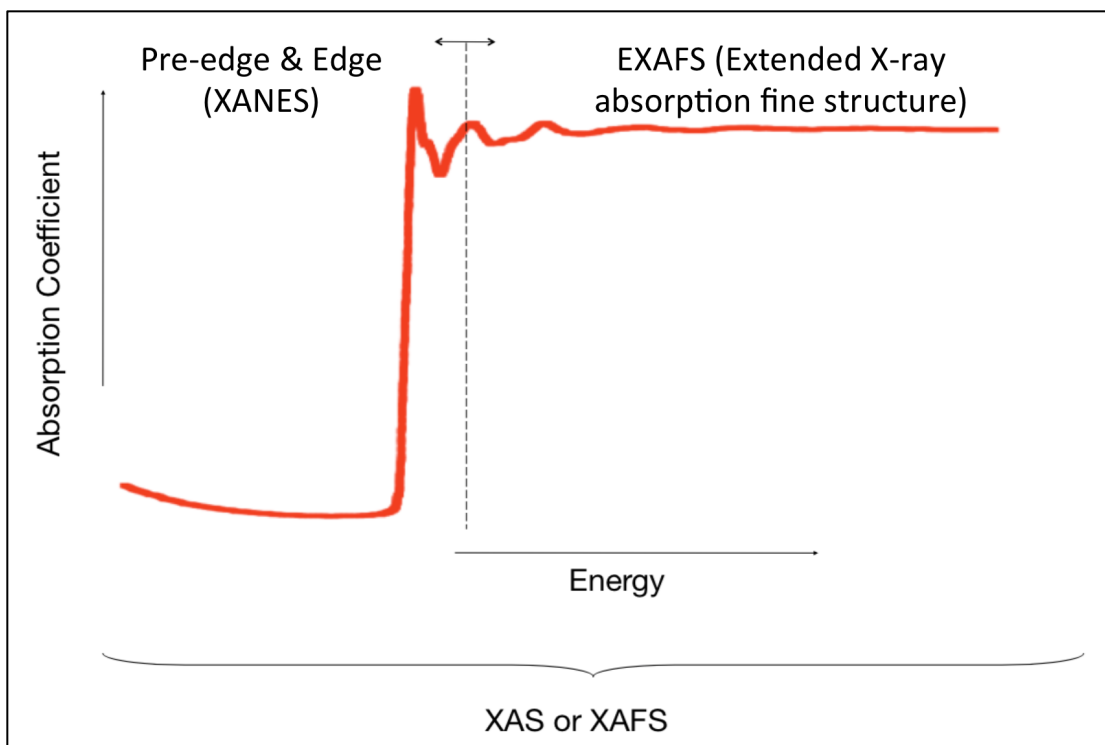
*Figure 2.8* X-ray absorption spectrum plotted as absorption coefficient photon energy. Spectrum showing the pre-edge, edge, and extended X-ray absorption fine structure (EXAFS) regions (Que 2000).

The X-ray energy region allows investigation of K edges ranging from approximately P to Sn, while $L_{III}$ edges extend from Y to Lr.(Que 2000) The exact ionization energy required by the absorbing atom can be affected by the valence or oxidation state. For example, a Cu (II) oxidation state is more difficult to ionize compared to Cu (I), and thus shifts the K edge to a slightly higher energy. Once the atom of interest absorbs the appropriate X-ray energy, a core electron is ejected and electrons from higher orbitals fill the core hole, which emits fluorescent X-ray photons. $K_{\alpha}$ emission refers to an electron from the L shell filling the core hole of the

K shell, whereas K$_\beta$ emission is an electron from the M shell filling the K shell. A typical XAS spectrum is formed when an electron is excited at a particular photon energy, causing an abrupt rise in absorption coefficient shown in Figure 2.8. The spectrum can be thought of as two different energy regions giving rise to the Edge and EXAFS regions. The spectral features in the edge region are sensitive to the electronic and geometric information occasionally referred to as X-ray absorption near-edge structure (XANES) or as NEXAFS (near-edge X-ray absorption fine structure). Detailed analysis of the edge region can provide information about oxidation state, covalency, molecular symmetry of the site, and coordination number. On the other hand, qualitative analysis of the edge region can also help determine the molecular geometry around the absorbing atom often providing distinct differences between tetrahedral 4- coordinate and square planar 4-coordinate complexes (Que 2000). The quasiperiodic modulations occurring approximately 50 eV above the absorption edge are known as the EXAFS (extended X-ray absorption fine structure) region and can provide detailed structural information around the absorbing atom.

The core electron ejected from the absorbing atom (a) will interact with neighboring atoms as a photoelectron, providing the information content for the EXAFS technique (Que 2000). The ejected photoelectron can be considered a de Broglie wave that backscatters when interacting with neighboring, or scattering atom (s). The backscattering amplitude can interfere with the forward wave of the photoelectron to produce a maximum due to constructive interference, or a minimum due to destructive interference. Therefore the oscillatory variation only

appears when scattering atoms surround the absorbing atom, with the type and distance of the scattering atoms affect the wave's frequency, phase shift, and amplitude. These details provide molecular information regarding how many, of what type of ligands, are at what distance from the absorbing metal of interest. Frequency provides information about the distance between the absorbing and scattering atoms, while the phase shift helps define the type of scattering atoms (for a given sample), and amplitude provides a measurement for the number of atoms. As a result EXAFS can provide local information about the atomic neighborhood with details about distances, coordination numbers, types of ligands, and clusters extracted from the EXAFS equation 2.1 given below (Que 2000).

$$\chi(k) = \sum_s \frac{N_s \, [f_s \, (\pi, k)]}{kR_{as}^2} \exp\left(-2\sigma_{as}^2 \, k^2\right) \sin[2kR_{as} + \alpha_{as}(k)] \qquad \text{(Equation 2.1)}$$

The equation is comprised of terms representing amplitudes, frequencies, and phase shifts from the shells of the absorbing (a) and scattering (s) atoms described above. The summation of waves is proportional to the number of scattering atoms ($N_s$) and their backscattering amplitudes $[f_s \, (\pi, k)]$, with long-distance shells causing much weaker EXAFS compared to nearby atoms ($R_{as}^{-2}$). The Debye-Waller factor is described by $\sigma_{as}^2$ and can be thought of as a stretching vibration (or disorder) between the a-s bond, which can be static or dynamic. These variations have characteristic temperature dependencies and can dampen the EXAFS signals.(Que 2000) The sine function describes the frequency ($2R_{as}$) and phase shift ($\alpha_{as}(k)$),

which is proportional to the a-s distance and nature of both atoms, respectively. EXAFS can therefore calculate distances up to $\pm$ 0.02 Å, coordination numbers with $\pm$ 20-25% accuracy, and the scattering atom Z $\pm$ 1 (Z=6-17) and Z $\pm$ 3 (Z= 20-35).

*2.2.6.1 XAS Samples.* XAS is particularly useful comparing various conditions such as pH, substrate addition, redox state, and mutations in order to elucidate differences at the metal active site that are crucial for enzymatic activity. Oxidized protein samples were prepared in a single step by 5-fold dilution of approximately 2 mM protein in 20 mM phosphate pH 8.0 (and 4 mM in Cu (II) for 2:1 protein samples) with the appropriate mixed buffer containing 20% ethylene glycol (Bauman et al. 2011). Reduced protein samples were prepared under anaerobic conditions by 5-fold dilution of a 2 mM sample of the oxidized enzyme into the appropriate buffer containing 5 mM ascorbate and 20% ethylene glycol. (pH-adjusted anaerobic buffers contained equal volumes of 50 mM MES, HEPES, CHES, and formic acid adjusted with sodium hydroxide).  Samples were transferred to an XAS cuvette via a syringe  and flash frozen in liquid nitrogen. Final copper concentrations ranged from 300 to 1200 $\mu$M, being careful not to exceed 3mM in selenium concentrations for the SeM labeled HM Loop samples.

*2.2.6.2 Collection of XAS Data.*  Copper K-edge (8.9 keV) EXAFS and edge data were collected at the Stanford Synchrotron Radiation Lightsource (SSRL) operating at 3 GeV with currents near 500 mA maintained by continuous top-off. Samples were measured at Cu (8.9 keV) or Se (12.6 keV) on beamline 9-3 and 7-3 using a Si 220 monochromator with crystal orientation $\varphi$ = 90° and a Rh-coated mirror located upstream of the monochromator set to 13 keV (Cu) or 15 keV (Se) cutoff to
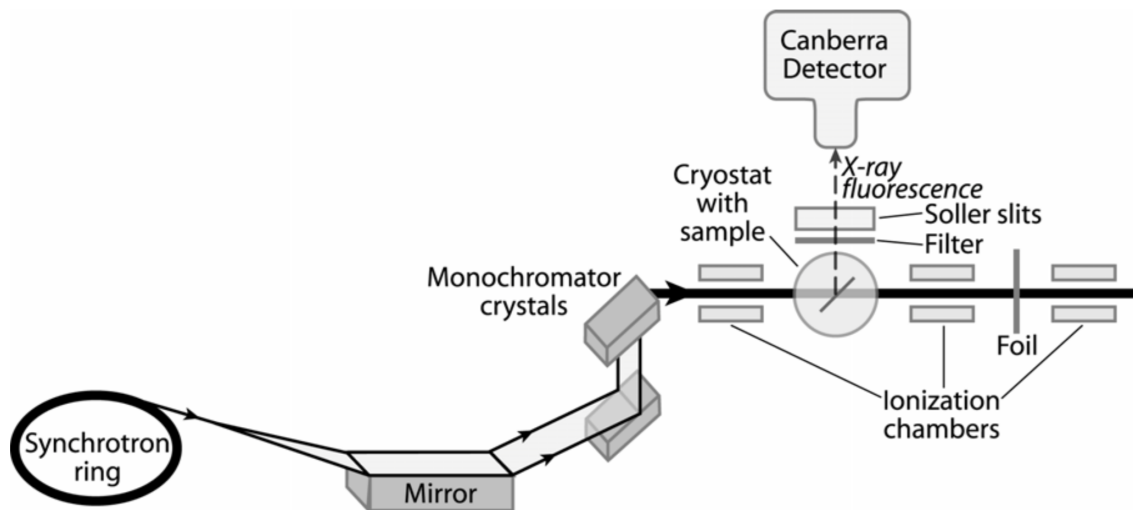
**Figure 2.9.** *Schematic view of the experimental set-up for X-ray absorption spectroscopy (Que 2000).*

reject harmonics (Figure 2.9). Samples were measured as frozen aqueous glasses in ~20% ethylene glycol at temperatures between 7 and 15 K, and the XAS was detected as Kα fluorescence using either a 100 element (beamline 9-3) or 30 element (beamline 7-3) Canberra Ge array detector. A Z-1 metal oxide filter (Ni for Cu, and As for Se) and Soller slit assembly were placed in front of the detector to attenuate the elastic scatter peak. Four to eight scans of protein samples and a buffer blank (20 mM sodium phosphate pH 8.0) were measured at each absorption edge. Energy calibration was achieved by placing a Cu or Se metal foil between the second and third ionization chamber.

*2.2.6.3 Analysis of XAS Data.* Data reduction and background subtractions were performed using the program modules of EXAFSPAK.31 (Gurman, Binsted, and

Ross 1984, 1986; George 1995; George and Pickering 2000). Briefly, the collected protein data were averaged and subtracted from the raw data to produce a flat pre-edge and eliminate residual Ni (or As in the case of Se EXAFS) $K_\beta$ fluorescence of the metal oxide filter. (Data from each detector channel were inspected for dropouts and glitches before being included into the final average). The modulations above the edge are isolated by spline subtraction and are normalized to obtain what we define as EXAFS. The energy (E) is then converted to $k$ space using the threshold energy ($E_0$), which is equivalent to the ionization potential. It is common practice to work with $k^3$ weighted $\chi$(k) data in order to emphasize the oscillations at high $k$-values. And lastly, a Fourier transformation of a sum of sine waves generates peaks in the appropriate distance space for each neighboring atom. A Fourier Transform (FT) is thus a useful way to plot the EXAFS data, providing a way to easily observe the neighboring atoms at different distances from the metal of interest.

Spectral simulations were carried out using the program EXCURVE 9.2 as previously described (Bauman, Jaron, et al. 2006; Bauman et al. 2011; Gurman, Binsted, and Ross 1984, 1986; George 1995; Binsted and Hasnain 1996). The neighboring atoms around the metal of interest are then simulated from the EXAFS data with an initial set of parameters that is then refined by least squares minimization. Refinement of structural parameters include distances (R), coordination numbers (N), Debye–Waller factors ($2\sigma^2$) and simulations using a mixed-shell model consisting of imidazole from histidine residues and sulfur/selenium from methionine coordination. The goodness of fit (or F- value) is calculated using the sum of the squares for the differences between experiment and

theory as described by equation 2.2 below (Que 2000).

$$F^2 = \frac{1}{N} \sum_{i=1}^{N} k^6 \, (Data - Model)^2 \qquad \text{(Equation 2.2)}$$

## 2.2.7  FTIR SPECTROSCOPY

Absorption of electromagnetic radiation in the infrared region of the

spectrum changes the vibrational energy of molecules (Que 2000). The absorption

of energy can only occur if there is a net change in the molecules' dipole moment.

Energy changes fall between 250-4000 $cm^{-1}$ (40- 2.5 um) and are caused by

molecular vibrations in which the chemical bonds can bend and stretch. For

example, the symmetrical stretch of $CO_2$ is inactive in IR if there is no change in the

dipole moment of the molecule (Que 2000). Hydrogen, nitrogen, and chlorine are

linear molecules that cannot produce an IR signal either, whereas carbon monoxide

and iodine chloride can absorb IR radiation (Que 2000). Free CO has a stretching

frequency of 2143 $cm^{-1}$ and shifts to lower frequency when bound to most metal

compounds. Briefly, molecular orbital theory explains that a synergic process occurs

whereby the σ- bond causes electron donation from CO to the metal's empty orbital

while additionally providing π- back-donation from the dπ-electrons of the metal to

the antibonding orbitals of CO as shown in Figure 2.10 (Nakamoto 1986). Ultimately

the electrons flow from the metal to the CO, which weakens the C—O bond and

shifts the v(CO) to lower frequencies.

An IR spectrum is more like a "molecular fingerprint" since the spectrum is
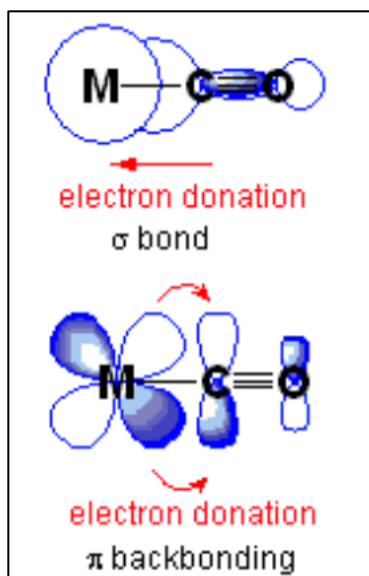
***Figure 2.10.*** *The σ- and π- bonding in metal carbonyls (Nakamoto 1986).*

often much more complex with no two compounds having the same exact IR

frequency. The complexities of the IR spectra give chemist information about the

molecule since the energy values of specific molecular vibrations occur in

characteristic regions of the spectra and are also dependent on the type of bonded

atoms. However, the relative intensities of IR signals are not quantitatively related

to the number of bonds (Que 2000).

The basic components of IR spectrometers include a source of

electromagnetic energy, a sample chamber, detector, and computer much like the

set-up for a UV/vis experiment. A typical way to report the IR data is to refer to the

stretching frequency of a particular diatomic molecule in terms of wavenumbers

with units of $cm^{-1}$. Wavenumbers are directly proportional to frequency (v) with the

electromagnetic radiation equal to the speed of light (c) over lambda (Que 2000).

Wavenumbers are also proportional to energy with some IR spectra plotting the

horizontal axis in units of micrometers (um). One cm is equal to $10^4$ um with the relationship between wavenumber and lambda given below (equation 2.3) (Que 2000).

$$v = 10^4 / lambda \qquad \text{(Equation 2.3)}$$

*2.2.71 CO Binding.* Purified PHM WT and variants were concentrated to approximately 2 mM (4 mM in copper) in 20 mM phosphate pH 8.0, and pH adjusted with four volumes of 50 mM mixed buffer MES/HEPES/CHES/Formate at either pH 3.5 or 7.5 in a septum-sealed conical vial. Samples were purged with CO before the addition of a 5-fold excess (5 mM) of anaerobic buffered ascorbate, and then incubated under an atmosphere of pure CO for 10 – 15 minutes. Protein solutions were loaded into the IR cell at a final concentration of 500 $\mu$M (1 mM in copper). After the protein data were collected, the cell was flushed with buffer and re-measured to collect a baseline. FTIR data were recorded on a Bruker Tensor 27 FTIR spectrometer at room temperature with a sample chamber that was continuously purged with $CO_2$-free dry air. Samples were equilibrated inside the instrument sample chamber for 15 minutes to allow purging of water vapor and $CO_2$ prior to data collection. One thousand scans were collected from 2250-1900 cm$^{-1}$ at a nominal resolution of 2 cm$^{-1}$ for each sample and buffer spectrum. Baseline subtraction and spectral analysis were performed using the GRAMS AI Spectroscopy Software (Thermo).

# CHAPTER 3

# SUBSTRATE-INDUCED CARBON MONOXIDE REACTIVITY SUGGESTS MULTIPLE ENZYME CONFORMATIONS AT THE CATALYTIC M-CENTER OF PHM

## 3.1 INTRODUCTION

Peptidylglycine hydroxylating monooxygenase (PHM) catalyzes Cα hydroxylation of glycine extended pro-peptides, the first step in the biosynthesis of their C-terminally amidated bioactive forms (Eipper et al. 1993). PHM contains two nonequivalent, mononuclear Cu sites, termed CuM and CuH that are separated by 11 Å of solvent. CuM is coordinated by His242, His244 and Met314, while CuH is bound to His107, His108, and His172. The catalytic reaction requires both copper ions to cycle between Cu (II) and Cu (I) oxidation states, but mechanistic aspects such as substrate triggering of oxygen activation, and/or the nature of the catalytic intermediates are not understood. Previous research has led to the consensus that the role of CuM involves catalysis, reacting with oxygen and hydroxylating the nearby substrate, while CuH is responsible for electron transport.

      The unusual nature of the ligand coordination chemistry at each of the

mononuclear copper centers has been of interest for many years. Cu (I) is the redox active metal, and due to its diamagnetism, is difficult to detect spectroscopically. The added fact that there are two copper centers, with similar ligand sets but distinct chemistry, makes unraveling their specific enzymatic roles challenging. The copper ligand distances and angles differ only slightly under various conditions, with a planar T-shaped CuH-site and a tetrahedral CuM-site (Prigge et al. 2004). The crystal structures of PHM WT depict various small molecules like CO, azide, peroxide and nitrite binding to the CuM center in an "end-on, bent" ligand formation (Figure 3.1 PDB ID 1MLJ), while PHM CuH does not appear reactive towards small molecules (Chufa´n et al. 2010; Rudzka et al. 2013). Spectroscopic and kinetic evidence suggests that both the coordination and dynamics of the two copper centers are essential for oxygen activation and reduction, but the way in which substrate influences this chemistry remains elusive.

Detailed kinetic and thermodynamic studies of PHM have revealed an equilibrium ordered mechanism in which substrate binds prior to oxygen (McIntyre et al. 2010; Francisco et al. 1998; Francisco et al. 2002a; Evans, Ahn, and Klinman 2003). The first step in the catalytic cycle involves reduction of both copper centers, followed by substrate binding. Oxygen is then capable of reacting to form an oxygen intermediate species believed to be a cupric superoxo (Abad, Rommel, and Kaestner 2014; Chen and Solomon 2004b; Evans, Ahn, and Klinman 2003; Prigge et al. 2004) responsible for C-H atom abstraction and thus hydroxylation of substrate. McIntyre *et al.*, 2010 further demonstrated that the catalytic mechanism of PHM relies on two types of motions, which are termed the pre-organizational state and the
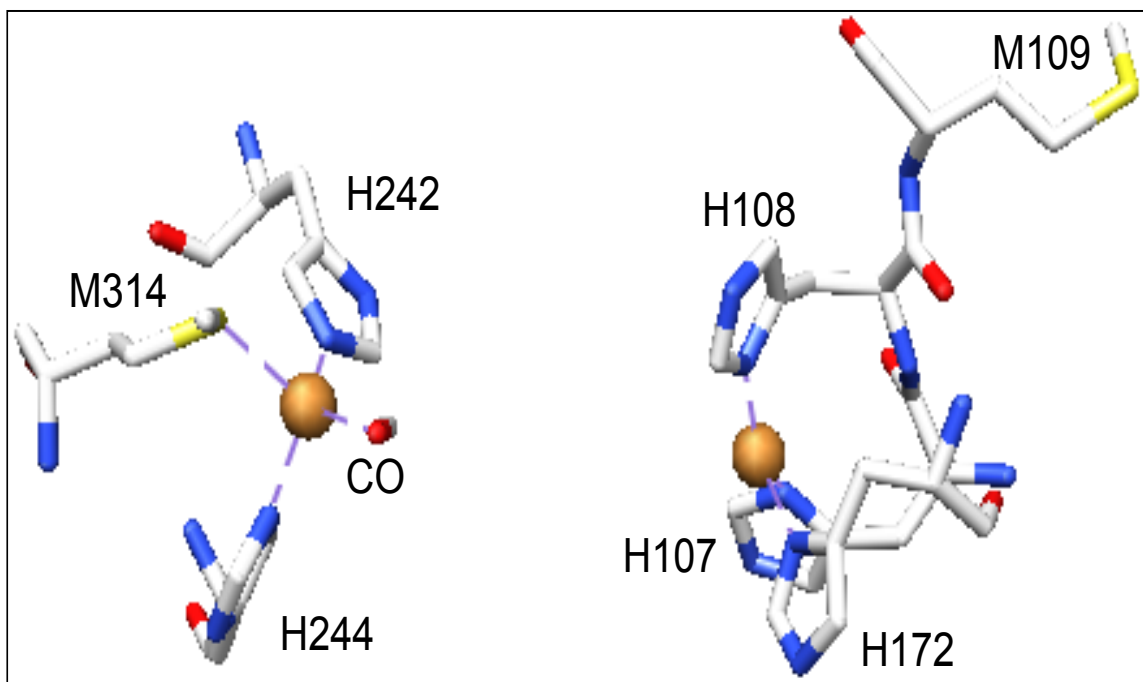
**Figure 3.1.** *Crystal structure of CuM and CuH sites of reduced WT PHM-CO complex at 2.15 Å (PDB ID code 3MLJ) (Chufa´n et al. 2010).*

reorganizational state. The pre-organizational state refers to the motions of enzyme and substrate required to attain an E-S complex while the reorganizational state refers to the gating motions or vibrations within the protein required for optimizing reactivity.

Klinman and co-workers found that the kinetic complexity controlling the C-H activation in enzymes, like PHM are linked to dynamic motions. For example, Soybean lipoxygenase (SLO) has a deeply buried active site where the hydrogen atom transfer is controlled by ligand reorganization (Francisco et al. 2002a). However, PHM was found to be more flexible and dependent on gating motions compared with SLO, even though PHM's active site is exposed to solvent. In addition,

PHM substrates that contain benzoyl groups have greater conformational sampling compared to N-decanoylglycine which have 25-fold higher $V_{max}/K_m$ and 13- fold lower $K_m$. Therefore control of catalytic activity in PHM appears to be more dependent on global as opposed to local conformational dynamics (Bauman, Jaron, et al. 2006; Bauman et al. 2011; Kline, Mayfield, and Blackburn 2013).

Despite the clear kinetic evidence for substrate triggering of the catalytic chemistry, structurally-based techniques like X-ray absorption spectroscopy (XAS) and X-ray crystallography have failed to detect any variation in metrical parameters at the metal centers in the presence of substrate. The one approach that *has* indicated substrate perturbation is CO binding. Previous Fourier Transform Infrared (FTIR) spectroscopy, in the absence of substrate, detected a PHM-CO complex at a single CO stretching frequency of 2092 cm$^{-1}$ (Boswell et al. 1996; Jaron and Blackburn 1999; Jaron et al. 2002; Kline, Mayfield, and Blackburn 2013; Chauhan et al. 2014). Results from the homologous dopamine β- monooxygenase (DβM) established that this CO band is bound at the CuM, coordinated by two histidines and one methionine. DβM shares mechanistic, sequence, and structural homology to PHM and has a very similar CO stretching frequency at 2089 cm$^{-1}$ (Kunishita et al. 2012; Pettingill, Strange, and Blackburn 1990). Half apo derivatives of both PHM and DβM were capable of maintaining CO reactivity and were observed via XAS to coordinate a sulfur ligand, providing further evidence for the assignment of a CuM-site carbonyl (Reedy and Blackburn 1994; Jaron and Blackburn 2001). Additionally, PHM CuM site mutants H242A and M314I did not react with CO in the

presence or absence of peptide substrate (Jaron and Blackburn 1999; Jaron et al. 2002; Chauhan et al. 2014).

In PHM WT, the presence of substrate induces a second CO band at 2063 cm$^{-1}$ (Jaron and Blackburn 1999; Jaron et al. 2002). The frequency of this second carbonyl species is identical to the CO stretching frequency found for molluscan hemocyanin and was therefore assigned to a CO complex at the CuH-site (Jaron and Blackburn 1999; Jaron et al. 2002; Fager and Alben 1972). Hemocyanin is an oxygen-binding dicopper protein with each copper coordinated by three histidine residues and can have CO stretching frequencies ranging from 2043 cm$^{-1}$ to 2063 cm$^{-1}$ depending on species (Alben and Fager 1972; Fager and Alben 1972; Deen and Hoving 1979). These data demonstrate that slight changes in the local molecular environments rather than a change in ligand sets can affect the CO stretching frequency.

In this study we further explored the CO reactivity of PHM and its variants as a surrogate for oxygen binding and reactivity. We have determined that upon carbonylation (i) a major CO band at 2092 cm$^{-1}$ and a second minor CO band at 2063 cm$^{-1}$ is observed in the absence of peptide substrate Ac-YVG; (ii) the presence of peptide substrate amplifies the minor CO band and partially inter-converts with the CO band at 2092 cm$^{-1}$; (iii) the substrate induced CO band is associated with a second conformer at CuM; and (iv) the CuH-site mutants eliminate the substrate induced CO band together with catalytic activity. These data provide evidence for at least two conformers at CuM, one of which is induced in the presence of peptide substrate, with the implication that this represents the conformation that allows

binding and activation of $O_2$.

## 3.2 RESULTS

### 3.2.1 FTIR SPECTROSCOPY OF CO BINDING TO PHM WT

Carbon monoxide is used to model the oxygen binding sites of copper proteins due to its electronic similarities with $O_2$. Previous X-ray crystallography data has shown that CO interacts with the CuM, but not the CuH center (Figure 3.1). In a previous study of PHM WT and the variant H172A, CO stretching frequencies were measured in the presence and absence of peptide substrate Ac-YVG (reported in Table 3.2) (Jaron and Blackburn 1999; Jaron and Blackburn 2001; Jaron et al. 2002). When CO reacted with the fully reduced di- Cu (I) form of the enzyme a band at 2092 $cm^{-1}$ was observed and assigned to a carbon monoxide adduct bound at the M-center. However, in the presence of substrate a second band of similar intensity was observed at 2063 $cm^{-1}$ which was assigned to a CO adduct at the H-center on the basis of the similarity of the $\nu(C\equiv O)$ to that of Cu (I) carbonyls with three histidine ligands (Jaron and Blackburn 1999).

With the availability of a number of additional variant forms, we have reinvestigated the CO binding chemistry in order to obtain a better picture of how the CO reactivity is influenced by binding of substrate. The new FTIR data on PHM WT demonstrate that in addition to the 2092 $cm^{-1}$ reported previously, a weak CO band is observed at 2063 $cm^{-1}$ even in the absence of substrate Ac-YVG (Figure 3.2a). This evidence suggests an alternative explanation, that two populations of
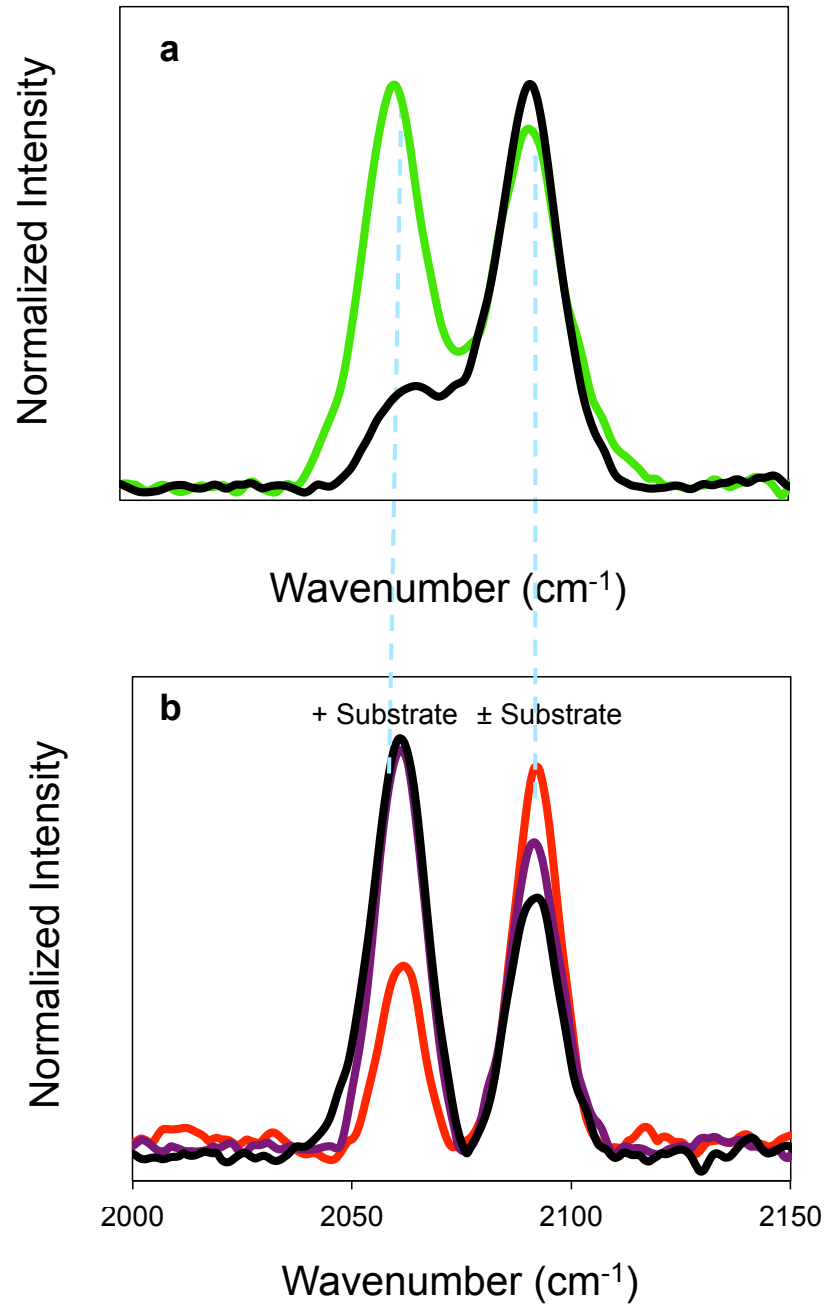
***Figure 3.2.*** *Infrared Spectra of CO complexes formed with reduced PHM WT. (a) CO complexes of reduced PHM WT in the presence (green) and absence (black) of peptide substrate. (b) PHM WT-CO complexed with increasing ratios of peptide substrate Ac-YVG; 0.5 equivalents in red; 2 equiv in purple; 4 equiv in black. The IR data was normalized to the protein concentration.*

CO-bound species at CuM exist in equilibrium, one which is favored upon substrate binding. In order to further probe the CO assignments, we titrated PHM WT with Ac-YVG, and carefully normalized the CO intensities to the protein concentration (Figure 3.2b). Increasing equivalents of peptide substrate Ac-YVG (0.5, 2, and 4) added to PHM WT increased the peak intensity observed at 2063 cm$^{-1}$, with a maximum intensity reached after 2 equivalents. Careful quantitation indicates that the CO band at 2092 cm$^{-1}$ decreases as the intensity at 2063 cm$^{-1}$ increases, although not at a 1 to 1 ratio.

Figure 3.3 shows CO band intensities plotted as a function of added substrate for both bands. The top spectra in Figure 3.3, compares the intensity of 2092 cm$^{-1}$ to that of the 2063 cm$^{-1}$ peak as black and red bars respectively, while the intensity of each peak is plotted in an additive fashion in the bottom figure. The sum of both peaks demonstrates a remarkably constant total intensity (Figure 3.3c). This data shows that although a portion of the 2092 cm$^{-1}$ CO band is converted into the 2063 cm$^{-1}$ band, both species still remain at equilibrium. This behavior is more consistent with two conformations of the M-site CO complex interconverting in response to substrate binding.

## 3.2.2 FTIR SPECTROSCOPY OF CO BINDING TO M314H

To distinguish between assignment of the 2063 cm$^{-1}$ band as an H-site or M-site carbonyl, previous attempts were made using mutants M314I and H242A, neither of which could be found to absorb IR in the appropriate region. We therefore turned to the M314H mutant where the S(Met) donor is replaced with a N(His)
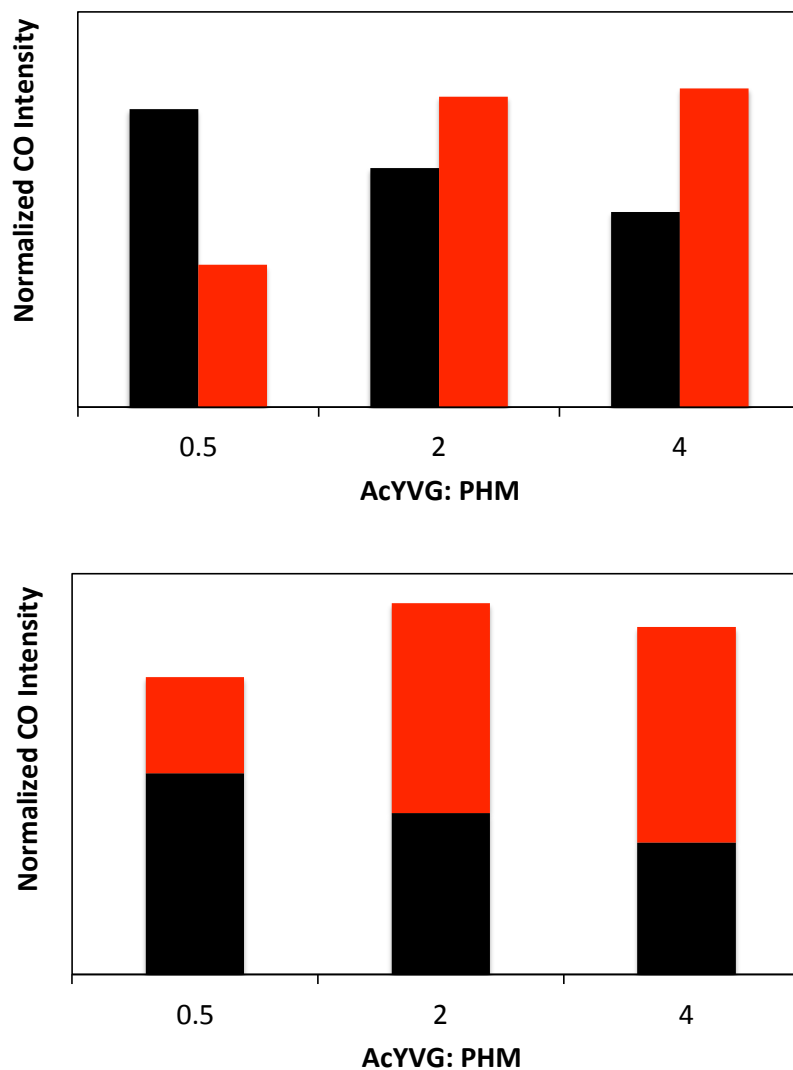
*Figure 3.3.* *Bar graph comparing the CO intensities of PHM WT with increasing amounts of peptide substrate Ac-YVG at 2092 cm$^{-1}$ and 2063 cm$^{-1}$. with 0.5 equivalents in red, 2 equiv in purple, and 4 equiv in black. The bar graphs represent the IR data plotted by normalizing the CO peak intensities to protein concentration. The top figure compares the CO intensities at 2092 cm$^{-1}$ (black) and 2063 cm$^{-1}$ (red) of reduced PHM WT as increasing amounts of substrate are added. The total peak intensity for both 2092 cm$^{-1}$ (black) and 2063 cm$^{-1}$ (red) was plotted as the sum of the two peaks in the bottom figure.*

donor. The increased sigma donor capacity of the histidine ligand is expected to decrease the stretching frequency of a CO ligand bound at the M-center by increasing the back-bonding interaction, but to leave an H-site CO complex unchanged (Lee et al. 2009). Previous EXAFS results reported between 2.5-3 N(His) bound to M314H in the oxidized protein at neutral pH, and in the reduced form approximately 2.5 N(His) were fit to the data (Bauman et al. 2011).

FTIR results for PHM WT and variant M314H in the presence and absence of peptide substrate Ac-YVG are shown in Figure 3.4. As predicted, in the absence of substrate, PHM M314H produced a carbonyl species that down-shifted approximately 20 cm$^{-1}$ relative to that of WT with a $\nu$(CO) at 2075 cm$^{-1}$ (Figure 3.4b, Table 3.2). In the presence of peptide substrate Ac-YVG, a second peak appeared at 2052 cm$^{-1}$. This peak also shifted from the original 2063 cm$^{-1}$ observed in the presence of Ac-YVG. The strong dependence of frequency on CuM-site ligands unambiguously assigns the substrate-induced CO band as a CuM- carbonyl in a different conformation than the 2092 cm$^{-1}$ band.

### 3.2.3 FTIR SPECTROSCOPY OF CO BINDING TO CUH-SITE MUTANTS WITH AND WITHOUT SUBSTRATE

Kline *et al.*, 2013 showed that histidine mutants at the CuH center decrease the catalytic activity by > 95% and yet still maintain coupling of oxygen and product (Kline, Mayfield, and Blackburn 2013). This profound effect indicates that the CuH scaffold is required for full activity, and raises the possibility that H-site ligation and conformation might be important for substrate activation of CO/$O_2$. Therefore we
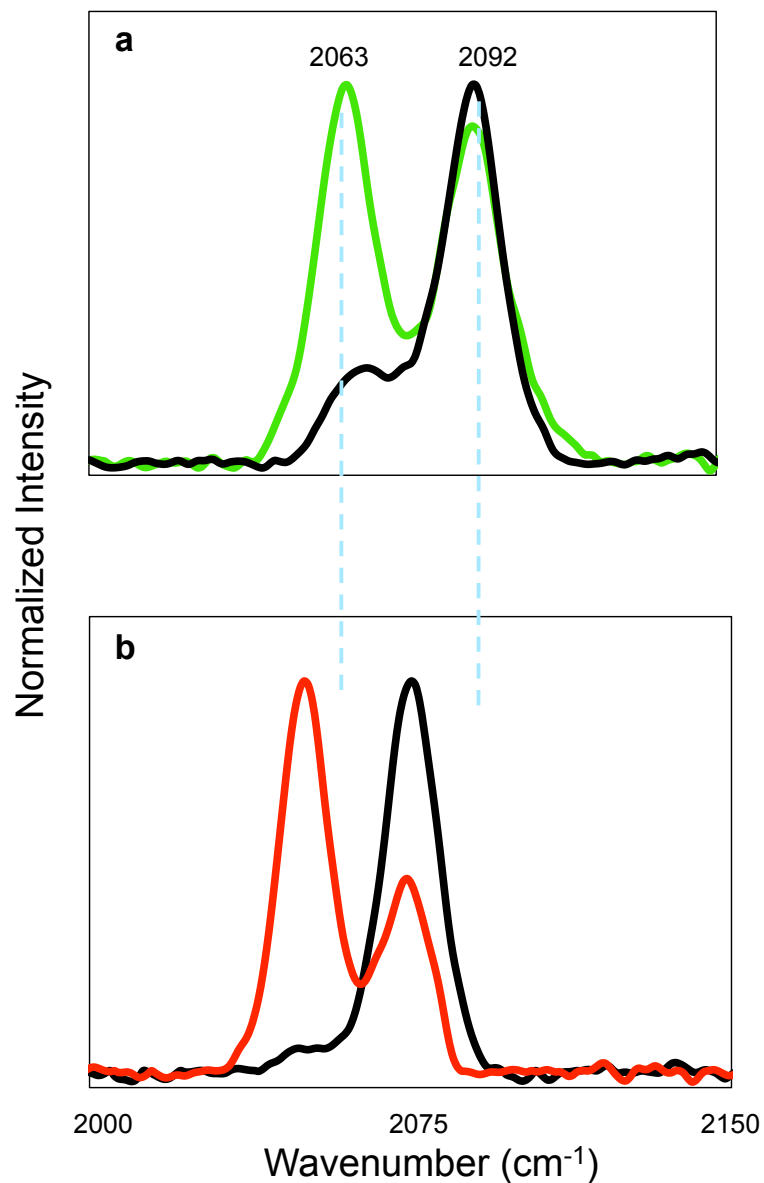
*Figure 3.4.* IR spectra comparing the CO complexes formed for PHM WT and variant M314H in the presence and absence of peptide substrate Ac-YVG. (a) WT PHM-CO complexed with substrate (green) and without substrate (black). (b) PHM M314H-CO complexed with substrate (red) and without substrate (black). Spectra are normalized to the intensity of the CO band at 2092 cm$^{-1}$ and 2075 cm$^{-1}$ for WT and M314H respectively in the absence of substrate. In the presence of substrate, WT was normalized to 2063 cm$^{-1}$ and M314H normalized to 2052 cm$^{-1}$.

also investigated the FTIR spectra of the variants H107A, H108A, H172A, H107108A, and M109I in the presence and absence of peptide substrate Ac-YVG to document the effects on CO stretching frequency.

FTIR shows that CO binds to the mutants with a similar frequency observed for PHM WT at ~2092 cm$^{-1}$ (Figure 3.5 & Figure 3.6). Each of the CuH-site mutants have copper at both the CuM and CuH center except for the double mutant H107108A in which the H-site is empty (Jaron et al. 2002; Kline, Mayfield, and Blackburn 2013; Chauhan et al. 2014) and cannot reproduce WT-CO chemistry in the presence of substrate. In the absence of peptide substrate, single mutants H107A and H108A do not perturb the $\nu$(CO) at 2092 cm$^{-1}$, while double mutant H107108A decreases the CO stretching frequency by 3 cm$^{-1}$ (Figure 3.5a-c, with reported values listed in Table 3.2 as $\nu$(CO) 1). Interestingly upon peptide substrate addition, these three mutants completely eliminate the second carbonyl species, and in some cases actually cause a downward shift in the original $\nu$(CO) of 2092 cm$^{-1}$ (Figures 3.5a-c, again listed as $\nu$(CO) 1 in Table 3.2). In the presence of substrate, PHM mutant H107A exhibited an identical IR spectra of that without substrate, whereas H108A and H107108A decreased the original $\nu$(CO) by 5 cm$^{-1}$ and 9 cm$^{-1}$, respectively. The substrate activated CO band could not be rescued in H107A or H108A using imidazole as an exogenous ligand (data not shown). A weak shoulder is observed in H107108A upon peptide substrate addition.

The only CuH-site mutant to resemble PHM WT CO chemistry was variant H172A (Figure 3.6) (Kline, Mayfield, and Blackburn 2013). In our previous study H172A reacted with carbon monoxide in the presence and absence of peptide
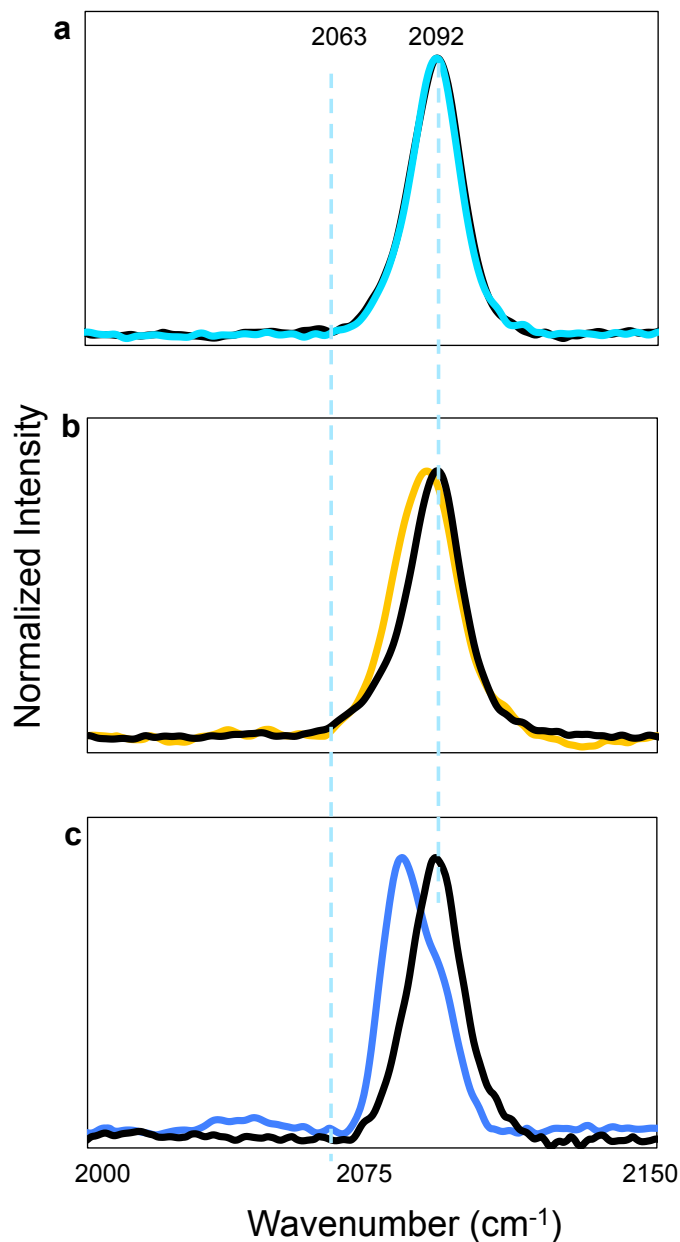
***Figure 3.5.*** *FTIR spectra of the CO complexes of PHM CuH site histidine variants, H107A, H108A, and H107108A in the presence and absence of substrate Ac-YVG. (a) H107A with substrate (teal) and without substrate (black); (b) H108A with substrate (yellow) and without substrate (black); (c) H107108A with substrate (blue) and without substrate (black). Spectra are normalized to the intensity of the only CO band observed, ~ 2092 cm$^{-1}$.*
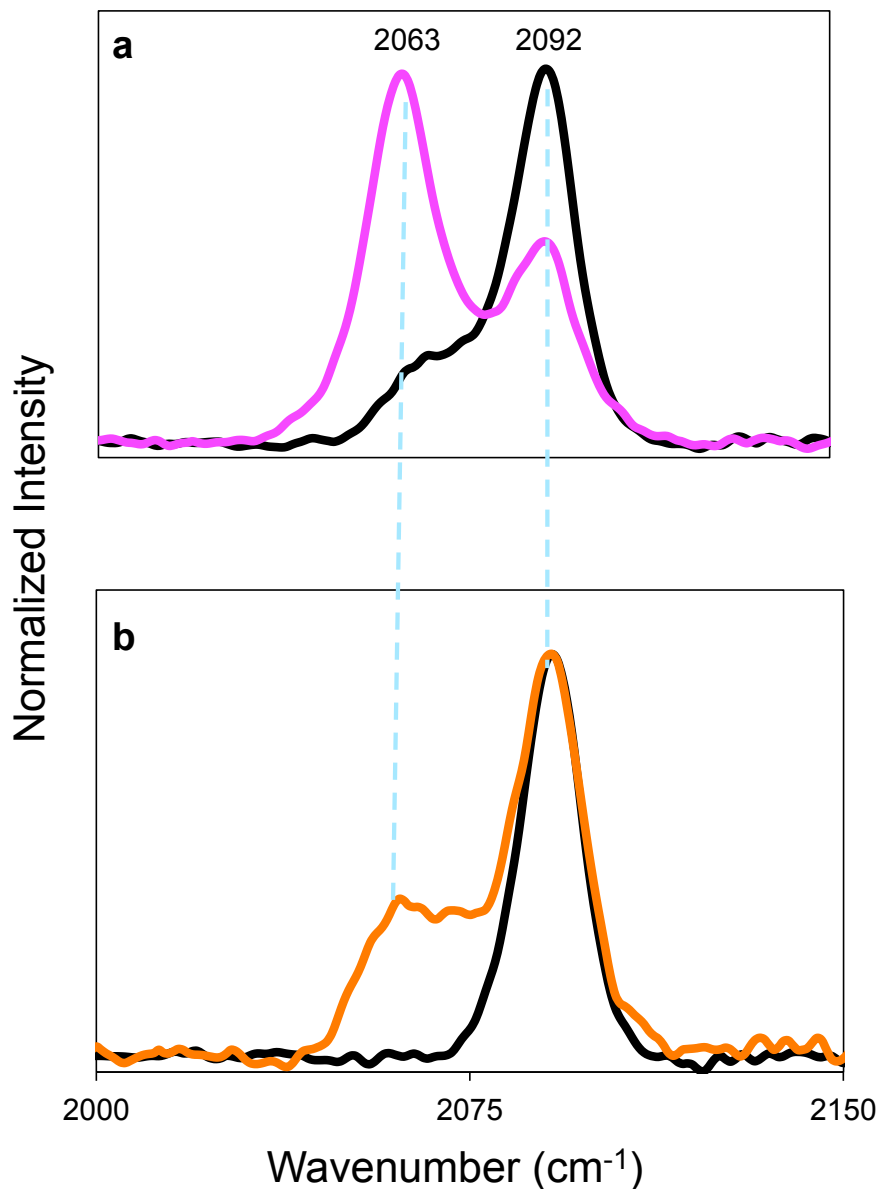
*Figure 3.6.* IR spectra of the CO complexes of PHM CuH site histidine variants M109I and H172A in the presence and absence of substrate Ac-YVG. (a) M109I with substrate (magenta) and without substrate (black); (b) H172A with substrate (orange) and without substrate (black). In the absence of peptide substrate, spectra are normalized to the intensity of the CO band at 2092 cm$^{-1}$ for both M109I and H172A. In the presence of substrate, M109I was normalized to 2063 cm$^{-1}$ while H172A was normalized to 2092 cm$^{-1}$.

substrate to produce both CO bands at the appropriate frequencies. However, more recent IR data have demonstrated variable behavior observing a less intense CO band at 2063 cm$^{-1}$ in the presence of peptide substrate, if at all.

Next, we wanted to know if non-coordinating residues at the copper active sites would affect the CO stretching frequency, and if so, to what extent? PHM M109I was used because we previously reported that it does not coordinate CuH at neutral pHs (Kline, Mayfield, and Blackburn 2013; Bauman et al. 2011). PHM M109I reacted with CO to produce a stretching frequency at 2092 cm$^{-1}$, and in the presence of peptide substrate a second CO band appeared at 2063 cm$^{-1}$ (Figure 3.6a and Table 3.2). However, unlike WT, M109I perturbs the equilibrium of the two peaks, causing more of the 2092 cm$^{-1}$ CO band to interconvert to 2063 cm$^{-1}$ in the presence of peptide substrate.

The overall total intensities of the CO peaks in the presence and absence of peptide substrate remained relatively constant for PHM WT and its variants (Figure 3.7). Carbonylation of reduced PHM WT in the absence of peptide substrate produced an intense CO band at 2092 cm$^{-1}$, with a minor peak intensity found at 2063 cm$^{-1}$ (Figure 3.7, labeled ν(CO) 1 and 2 respectively). The addition of substrate causes the ν(CO) at 2063 cm$^{-1}$ to become more apparent while 2092 cm$^{-1}$ decreases slightly. The sum of these two peak intensities is similar to the sum of the two CO peak intensities in the experiments excluding substrate. The total CO intensity of the H-site mutants where the substrate-induced band is not observed is also similar to the sum of the two bands in WT/M314H/M109I and to each other. If the band intensities reflect the sum of all M-site CO species, this suggests that the H-site
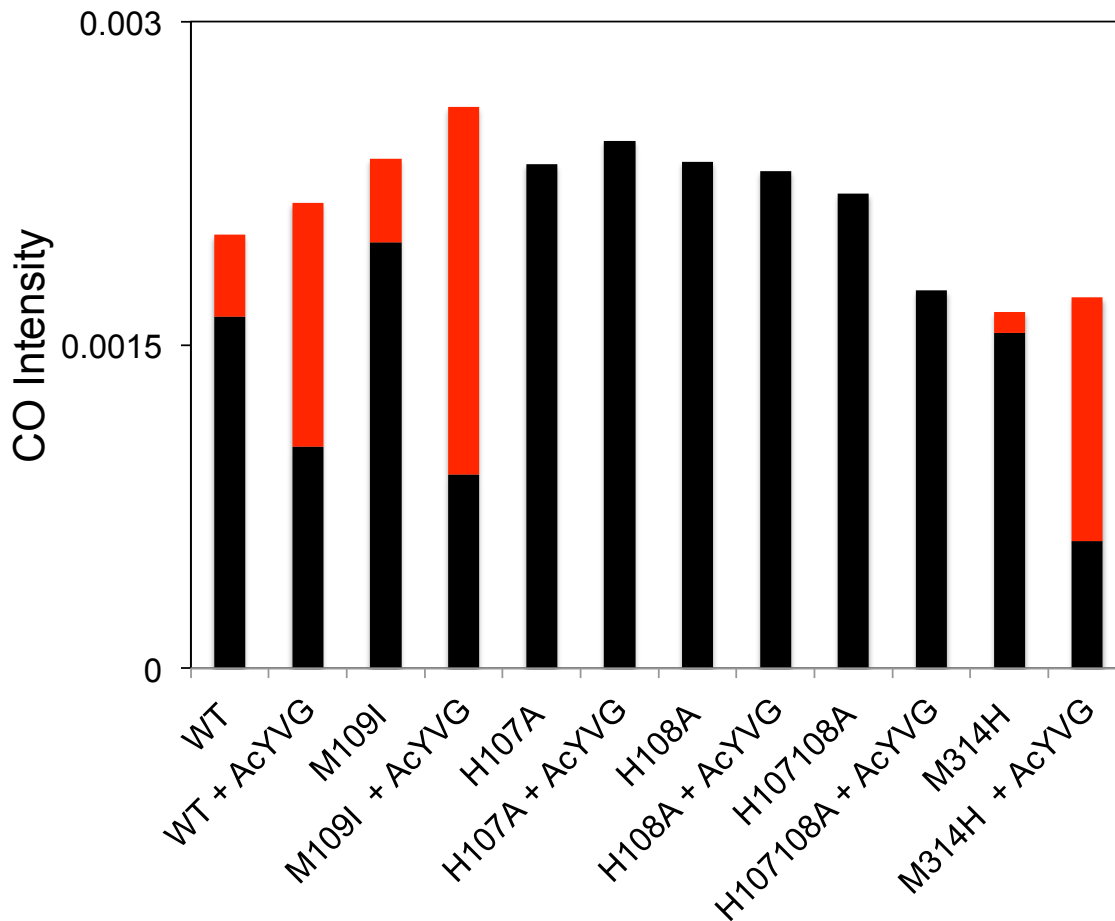
***Figure 3.7.*** *Stacked bar graph comparing the total raw CO intensities of PHM WT and variants in the absence and presence of peptide substrate Ac-YVG. The main CO intensity observed in the absence of substrate at ~ 2092 cm$^{-1}$ is denoted major $v(CO)$ and is black while the second minor $v(CO)$ is red.*

variants generate a single conformation at M, all of which reacts with CO to form the carbonyl.

**3.3 DISCUSSION**

X-ray crystallography structures are available for PHM WT in the oxidized and reduced,(Prigge et al. 1997) oxidized plus substrate,(Prigge et al. 1999) an inhibitor-bound pre-catalytic oxygen complex, (Prigge et al. 2004) and in the presence of small molecules (Chufa´n et al. 2010). However, no structure of a reduced, substrate-bound form is available. XAS studies have been reported for the reduced and reduced plus substrate but do not indicate any observable changes in structure when substrate binds to the reduced form (Blackburn et al. 2000). Despite the lack of spectroscopic evidence upon substrate addition in PHM, kinetic data have established that substrate binding precedes oxygen binding and activation (McIntyre et al. 2010). Strict coupling of oxygen consumption and product formation also suggests that oxygen is activated and ready to commit to catalysis only after substrate binds (Bauman et al. 2011; Kline, Mayfield, and Blackburn 2013). FTIR spectroscopy has been the only technique to detect a change upon substrate addition and thus has been utilized here as a probe of substrate-induced structural and electronic perturbations at the catalytic M-center.

PHM WT was found previously to exhibit a major CO band at 2092 cm^{-1} unambiguously assigned to the CuM center, (Pettingill, Strange, and Blackburn 1990; Blackburn et al. 1990; Boswell et al. 1996; Jaron and Blackburn 1999; Jaron and Blackburn 2001; Jaron et al. 2002; Kline, Mayfield, and Blackburn 2013) and upon substrate addition a second band appeared at 2063 cm^{-1} (Jaron and Blackburn 1999; Jaron et al. 2002). The present study highlights the fact that a minor CO band at 2063 cm^{-1} is apparent *prior* to substrate addition suggesting that it may relate to a catalytically competent state.  The new data indicate that this state is favored when

substrate binds, and may thus represent a spectroscopic marker for substrate triggering of reactivity. The results from PHM variant M314H absolutely assigns the substrate induced CO band to the CuM center, suggesting a second conformer. The additional histidine ligand causes increased sigma donation, which allows more back bonding with the metal and decreases the CO stretching frequency. Upon carbonylation of M314H, both CO bands downshift to 2075 cm$^{-1}$ and 2052 cm$^{-1}$ respectively, where the effect of the substrate likewise lowers the CO frequency, albeit by a smaller amount than in the WT protein. The downshift suggests a second conformation at the CuM center, which if applied to O$_2$ would imply an activated state.

The new IR data shows that both IR bands are actually present in the absence of substrate, but the lower frequency band is of much lower intensity. Upon the addition of substrate the two bands partially interconvert, with a maximum intensity reached after 2 equivalents (a relatively constant total CO intensity is maintained throughout the titration experiments). CuH site variants, which exhibit extremely low levels of catalytic activity also eliminate the substrate-induced band, suggesting a correlation between substrate-induced M-site perturbation and activation of oxygen chemistry. These mutants appear to have a single CO band at 2092 cm$^{-1}$ whether or not substrate is present, and the overall peak intensity is similar to the sum of the two peak intensities observed for PHM WT.

These observations on the relative intensities of the CO bands are consistent with M-site reactivity towards CO where all conformations are reactive, where the distribution of CO-bound conformers is proportional to the fractional occupancy,

and where the total intensity of all CO bands is determined by the total M-site
copper occupancy. Furthermore, the elimination of substrate-induced bands in H-
site variants implies that the two copper centers work together to provide a precise
geometric scaffold necessary for M-site $CO/O_2$ activation. These data further
support the argument that the multiple CO stretching frequencies do not represent
CO binding at two independent copper sites, rather that the CO bands are in
equilibrium and partially interconvert with two varying populations at the CuM
center. The X-ray structures corroborate this evidence demonstrating that only the
CuM center is reactive towards small molecules and illustrating that CO binds in an
end-on, bent configuration (Figure 3.1) (Chufa´n et al. 2010).

The factors likely to contribute to this second CO conformational state could
include (i) a second CO ligand coordinated at the M-site; (ii) changes in the M-site
ligand set; (iii) a reorganization of the electronics at the CuM center; or (iv)
alterations in the hydrogen-bonding network which affect the orientation of the CO
ligand. Taking each of these possibilities in turn, a second CO bound to CuM might be
discarded since both CO frequencies would be expected to change when the second
molecule of CO becomes ligated. Changes in the M-center ligand set are also
unlikely.

Karlin and co-workers have reported model complexes built using the HH
and HGH copper-binding motif containing either Cu-Nδ or Cu-Nε imidazole
coordination. These complexes form 3-coordinate carbonyls with frequencies
ranging from 2092 cm$^{-1}$ to 2112 cm$^{-1}$ for the four complexes studied (Table 3.1) (Lee
et al. 2006). In addition, the ε-HGH complex that most resembles the CuM-site

coordination has an IR frequency at 2092 cm$^{-1}$ and is coincidentally reported as the only complex reacting with $O_2$. These model studies might suggest that the PHM 2092 cm$^{-1}$ band could represent a Met-off configuration while the lower frequency band could arise from a Met-on state. This would imply that coordination of the Met ligand generated a significant increase in back bonding from Cu (I) to CO. Two observations argue against this interpretation. First a similar mechanism applied to the M314H variant would predict no downshift in the absence of substrate (His314 in an "off" conformation) but a larger downshift in the presence of substrate due to the expected increase in sigma donor power of N(His) over S(Met) in the "His-on" conformation. Second, previous XAS studies of WT CO complexes in the absence of substrate show clear evidence for Cu-S coordination (Jaron and Blackburn 1999). Therefore it is probable that both conformations contain (His)$_2$S(Met)CO ligand sets.

On the other hand, it is certainly conceivable that substrate binding perturbs the electronic interaction between Cu (I) and one or more ligands in a fashion that is not directly observable by XAS. In particular, changes in orientation of the S orbitals with respect to Cu (I) might influence the overall electronic structure of the carbonyl complex. This is an attractive idea, since the Met ligand is essential to catalysis (Eipper et al. 1995; Bauman et al. 2011; Hess et al. 2008). Recent biomimetic studies have established an important role for thioether coordination in C-H bond activation, but one that is very dependent on the electronic state and architecture of the other ligands in the complex. A variety of different classes of inorganic cupric superoxo species have been characterized as models for the putative superoxo intermediate in PHM and DβM, and included the side on "Kitajima" complex, (Chen

70

et al. 2003; Fujisawa et al. 1994) the end-on "Sundermeir/ Karlin" complex, (Schatz et al. 2004; Lanci et al. 2007; Maiti et al. 2007; Woertink et al. 2010; Peterson et al. 2011; Ginsbach et al. 2013; Peterson et al. 2013) and the end-on "Itoh" (Tano et al. 2013; Kunishita et al. 2012; Kunishita et al. 2009) complex. Unlike the PHM M-center, these are built on 3- or 4-coordinate *N-donor* scaffolds and do not contain thioether coordination.

Attempts to incorporate thioether ligands into the complexes met with mixed success. In one study, a $N_2S$ containing model complex deemed to be a good model for PHM M-center (Cu-S distance of 2.203 Å, close to the 2.24 Å reported for the Cu-S(M314) PHM distance) and reacted with oxygen and hydrogen peroxide.(Lee et al. 2006) Reaction with $O_2$ led to oxidation of the thioether, with no observable Cu (I)-$O_2$ intermediate. Studies on related Cu (II)- (Lee et al. 2007) and Cu (III)-peroxo (Aboelella et al. 2006) species also showed little or no stabilization via thioether coordination. However, Karlin and coworkers have recently reported a new $N_3S$(thioether)-Cu (I) complex which reacts with oxygen to form a superoxo intermediate at -125°C with $\lambda_{max}$=425 nm and $\nu(O-O)$= 1117 cm$^{-1}$, and undergoes further reaction with the Cu (I) precursor to form *trans-$\mu$*-peroxo di-Cu (II) (Kim et al. 2015). Studies on the reactivity of the superoxo species suggest that the thioether moiety in this complex *increases* reactivity towards hydroxylation of C-H bonds through an increase in electrophilic character. The differences in reactivity between these various thioether-containing models indicate the need for careful tuning of Cu-S electronic structure in order to turn on oxygen reactivity.

Electronic tuning of metal-thioether reactivity has also been reported in

radical-SAM containing enzymes, where S-adenosyl methionine is bound to one of the Fe atoms of a 4Fe-4S cluster (Dey et al. 2011). The radical-mediated catalysis is required for important biological processes such as DNA repair, biotin synthesis, and glycl radical formation, among others. XAS data and density functional theory (DFT) calculations revealed that substrate binding alters the degree of metal-to-sulfur back bonding, leading to cleavage of the C-S bond.  This study demonstrates that non-coordinating interactions such as substrate binding in an active site pocket can influence metal-methionine electronic interactions although the positive charge residing on the S-adenosyl-methionine ligand may profoundly influence the metal-sulfur electronic interactions.

Interestingly, the peptide substrate hippuric acid (N-benzoylglycine, $C_6H_5CONHCH_2COOH$) appears to induce a second CO band not at 2063 cm$^{-1}$ (observed for peptide substrate Ac-YVG) but at 2075 cm$^{-1}$ and does not appear to affect the $\nu$(CO) at 2092 cm$^{-1}$ (Table 3.2). The observed differences in CO stretching frequencies could be due to the different modes of substrate binding near the CuM-site that have different effects on the electronics of the CuM center as argued above. A change in the orientation of bound CO could also induce a second stretching frequency especially if the CO enters into hydrogen bonding interactions either with the substrate or with ordered solvent. The crystal structure of PHM-CO measured in the absence of substrate shows CO bound in a bent, end-on configuration at the CuM center (Figure 3.1),(Chufa´n et al. 2010) in marked contrast to the expected linear binding mode.  Inspection of the structure reveals that the O of the CO moiety interacts with the amide of Gly308, on the opposite side from where substrate

would bind.  Thus, reorientation of the CO towards the substrate when the latter is bound could result in disruption of the interaction with the glycine main chain amide, and the formation of a new interaction leading to an altered stretching frequency.

Multiple CO absorption bands arising from different populations of active site conformers was also inferred from flash photolysis studies of CO binding to cytochrome c oxidase $a_3$.(Fager and Alben 1972; Deen and Hoving 1979) Cytochrome c oxidase is the terminal respiratory enzyme in the mitochondrial electron transfer chain responsible for reduction of molecular oxygen to water. In strongly visible light, CO is dissociated from the heme$_{a3}$ pocket and rebinds to the $Cu_B$ with a major CO stretching frequency at 2062 cm$^{-1}$ and a minor $\nu$(CO) at 2043 cm$^{-1}$. The 20 cm$^{-1}$ wavenumber difference was attributed to having highly ordered versus a more flexible Cu-CO complex. The behavior of the CcO system emphasizes the fact that changes in CO frequency due to conformational complexity can exist without any change in ligand set around the coordinating metal ion.

The multiple absorption bands observed via IR may also reflect dynamics important in controlling PHM catalysis. The PHM catalytic reaction is known to proceed via a H-tunneling mechanism in which the enzyme must reach a critical configuration for H-atom transfer from substrate to the developing oxygen intermediate (Francisco et al. 2002b; Klinman 2006a, 2015; McIntyre et al. 2010). The enzyme is able to sample many dynamical states via specific vibrational modes along the reaction coordinate which couple the local motions of the metal-oxygen activated intermediates with critical substrate modes such as the pro-S C-H bond,

until the optimal configuration for H-atom abstraction is achieved. It is likely from the effects of H-site mutations on M-site CO chemistry that dynamics at the H-center is also important for M-site preorganization. For example the conformational flexibility of the CuH center has previously been demonstrated via its ability to engage in a pH-dependent conformational switch (Evans, Blackburn, and Klinman 2006; Osborne et al. 2013) where a histidine ligand protonation induces coordination of Met109 to the CuH center. It is clear that cross talk between the two copper centers represents an important element of the catalytic process.

In summary, we believe that the multiple CO stretching frequencies observed in this study represent two conformations at CuM in which the minor CO stretching frequency depends on the mode of substrate binding and may thus report on a substrate-induced catalytically active configuration. Upon substrate addition, the minor ($\nu$)CO band is amplified while the other decreases, but not at a 1:1 ratio, indicating an equilibrium which is shifted in the presence of substrate. The multiple CO stretching frequencies observed for PHM WT and variants exhibit a fairly constant intensity in the presence and absence of peptide substrate. We propose that substrate-induced electronic structural changes at CuM activate the oxygen complex towards catalysis. These changes may also involve or be induced by changes in the hydrogen bonding network or solvent structure. Finally, the CuH-site coordination scaffold is essential not only for the electron transfer, but also for specifically tuning the CuM-site reactivity.

| Protein name | $\nu$(CO) 1 | $\nu$(CO) 2 |
|---|---|---|
| Hemocyanin (Kline, Mayfield, and Blackburn 2013) | | |
| -molluscan | 2063 | |
| -limulus | 2053 | |
| -arthopodal | 2043 | |
| cytochrome c oxidase | | |
| -a$_3$ (Fager and Alben 1972; Deen and Hoving 1979) | 2062 | 2043 |
| -bo$_3$ (Alben et al. 1981) | 2065 | |
| D$\beta$M | 2089 | |
| D$\beta$M + Tyramine | 2086 | |
| PAM | 2093 | |
| Model Complexes (Puustinen et al. 1997) | | |
| ($\delta$-HGH)$_2^{2+}$ | 2103 | |
| ($\varepsilon$-HGH)$^+$ | 2092 | |
| ($\delta$-HH)$^+$ | 2110 | |
| ($\varepsilon$-HH)$_2^{2+}$ | 2112 | |

***Table 3.1.*** *Infrared Frequencies for Copper Carbonyl Proteins and Model Complexes*

| PHM variant | ν(CO) 1 | minor ν(CO) 2 | Cu:Protein |
|---|---|---|---|
| PHM WT | 2092 | | 2.02 ± 0.15 |
| PHM WT + Ac-YVG | 2092 | 2063 | |
| PHM WT + Hippuric Acid (Park et al. 2014) | 2093 | 2075 | |
| H172A (Jaron and Blackburn 1999) | 2092 | | 1.4 ± 0.3 |
| H172A + Ac-YVG | 2092 | 2065 | |
| M314H | 2075 | | 1.6 ± 0.28 |
| M314H + Ac-YVG | 2075 | 2052 | |
| M109I | 2092 | | 2.08 ± 0.14 |
| M109I + Ac-YVG | 2092 | 2063 | |
| H107A | 2092 | | 2.01 ± 0.01 |
| H107A + Ac-YVG | 2092 | | |
| H108A | 2093 | | 2.04 ± 0.23 |
| H108A + Ac-YVG | 2087 | | |
| H107108A (Chauhan et al. 2014) | 2090 | | 1.09 ± 0.15 |
| H107108A + Ac-YVG | 2083 | | |
| H242A (Jaron et al. 2002) | no peak | | 1.11 ± 0.03 |
| M314I (Jaron and Blackburn 1999) | no peak | | 1.2 ± 0.38 |

**Table 3.2.** *Infrared Frequencies and Stoichiometry for Carbonyl Complexes of PHM WT and Variants.*

# CHAPTER 4

# THE HHM MOTIF AT THE CUH-SITE OF PHM IS A PH-

# DEPENDENT CONFORMATIONAL SWITCH

## 4.1    INTRODUCTION

Mononuclear copper monooxygenases represent a small but important group of

metalloenzymes involved in neurotransmitter and peptide hormone biosynthesis.

They include the enzymes dopamine β-monooxygenase (DβM) (Klinman 2006a) and

tyramine β- monooxygenase (TβM) (Hess, Klinman, and Blackburn 2010) involved

in catecholamine biosynthesis, and peptidylglycine hydroxylating monooxygenase

(PHM) which catalyzes the amidation of neuropeptides hormones, the first step of

which is the conversion of a glycine-extended pro-peptide to its α-hydroxyglycine

intermediate (Prigge et al. 2000). The active sites of these enzymes appear to be

homologous as determined by a combination of crystallographic, (Prigge et al. 1997;

Prigge et al. 1999; Siebert et al. 2005; Chufaʹn et al. 2010; Rudzka et al. 2013)

spectroscopic, Chen kinetic (Evans, Ahn, and Klinman 2003; Evans, Blackburn, and

Klinman 2006; Klinman 2006a; Hess, Klinman, and Blackburn 2010) and

computational studies, (Rudzka et al. 2013; Chen and Solomon 2004a; Chen et al. 2004; Crespo et al. 2006) but PHM remains the only member of the group for which crystal structures are available. The two copper centers termed CuM and CuH are mononuclear, and are separated by 11 Å of solvent-filled channel, in contrast to the better characterized dinuclear centers in hemocyanins, tyrosinases (Chen and Solomon 2004a, 2004b; Magnus et al. 1994; Gerdemann, Eicken, and Krebs 2002; Matoba et al. 2006a) and oxygen activating models (Lewis and Tolman 2004; Citek et al. 2012) in which the Cu-Cu distance is 3–4 Å. A CuM -superoxo intermediate has been suggested on the basis of additional crystallographic (Prigge et al. 2004) and biochemical data (Evans, Ahn, and Klinman 2003; Bauman, Yukl, et al. 2006) while in silico studies have validated Cu (II)-$O_2{}^{\bullet-}$ as a probable reactive oxygen species. It has been further suggested that the large spatial separation of the Cu centers in PHM prevents immediate formation of the peroxide, and thus allows the potent electrophilic reactivity of the mononuclear Cu (II)-superoxo species to be fully expressed in the form of H-atom abstraction from the substrate (Evans, Ahn, and Klinman 2003; Chen and Solomon 2004b) to form a mononuclear hydroperoxo species at CuM and a substrate radical.

The M-site is considered to be the catalytic locus and is coordinated by H242, H244 and solvent ligands in the oxidized form with a weak EXAFS-undetectable interaction with the thioether of M314; on reduction the solvent ligands dissociate and the thioether S from M314 binds to the Cu (I) (Boswell et al. 1996; Chen et al. 2004; Blackburn et al. 2000). A structure of reduced PHM co-crystalized with a slow substrate has allowed the visualization of a "pre-catalytic complex" involving a

dioxygen molecule bound at CuM, the bond length of which is consistent with a Cu

(II)- superoxo species. The O-O bond is oriented away from the C–H bond of the

substrate which binds nearby, but a facile rotation about the Cu-O bond could bring

the distal O and the substrate C–H bond into alignment (Prigge et al. 2004). The

M314 ligand plays a critical role in optimizing the M-site for catalysis since mutation

to His, Cys or Asp results in ~95% loss in activity (Hess, Klinman, and Blackburn

2010; Bauman et al. 2011). Whereas the M-site is the catalytic center, the H-site is

believed to be an electron transfer center responsible for supplying the second

electron necessary to complete the monooxygenation reaction. In the resting

oxidized protein CuH is unremarkable with a [(His)$_3$(OH$_2$)] ligand set, but reduction

again induces loss of solvent, and generates a Cu (I) site with Cu-N(His) distances

more typical of a 2-coordinate system (1.88 Å) (Blackburn et al. 2000; Jaron et al.

2002; Himes et al. 2007). The similarity of the EXAFS of the reduced protein in the

WT and H172A derivatives suggests that of the three copper-coordinating His

residues (107,108, and 172), H172 is only weakly bound in the reduced protein.

Nevertheless, mutation to alanine has a dramatic effect on catalysis with the $k_{cat}$

decreasing by three orders of magnitude (Evans, Blackburn, and Klinman 2006).

Furthermore, crystallographic analysis reveals a structural interaction between the

M and H sites, with the M314I inducing dissociation of the H107 ligand from the H-

center, some 11 Å distant (Siebert et al. 2005). H172 forms a stacking interaction

with the conserved Y79 residue, and it has been suggested from studies on the

related enzyme TβM, (Osborne et al. 2013) that the H172 ligand might form the exit

pathway for the electron as it transfers from H to M using Y79 and oriented water molecules as additional elements of the ET pathway (Cardenas et al. 2011).

WT PHM shows maximum catalytic activity at pH 5.8, and undergoes loss of activity at lower pHs due to a protonation event with a $pK_A$ of 4.6 (Bauman, Jaron, et al. 2006; Bauman et al. 2011). Low pH also causes a unique structural transition in which a new S ligand coordinates to copper with an identical $pK_A$ manifest by a large increase in Cu-S intensity in the XAS. In previous work we tentatively assigned the new Cu-S interaction to binding of M109 to the H-site (part of the HHM conserved motif common to all but one member of the family), induced by protonation of one of the H-site histidine residues (Bauman et al. 2011). These data suggested that the H-site is also conformationally mobile and hint at allosteric gating of ET via long-range structural perturbations. In the present paper we follow up on these findings via studies on the catalytic activity, pH-activity profiles, and spectroscopic properties of a number of H-site variants, including H107A, H108A, H172A and M109I. Our results establish that M109 is indeed the coordinating ligand, and confirm the prediction that this mutant should show no decrease in activity at low pH. The histidine mutants show more complex behavior, but the almost complete lack of activity in all three variants coupled with only minor changes in spectroscopic properties suggests that unique structural elements at H are critical for functionality.

## 4.2 RESULTS

## 4.2.1 STEADY STATE KINETICS

The catalytic activity of all three variants (H107A, H108A, and M109I) was measured under saturating conditions of ascorbate and atmospheric $O_2$ as a function of peptidylglycine substrate (dansyl-YVG), and the data fit by non-linear regression to a standard Michaelis-Menten equation. Kinetic constants are compared with data for the WT enzyme in Table 4.1. The H107A and H108A variants have low activity, which can be seen to be primarily the result of a large decrease in $k_{cat}$. The effect on $K_M$ is different for the two mutants, with H107A binding the peptide substrate more tightly than WT, and H108A binding three times weaker. Given the fact that the substrate binds in the vicinity of the M center, the effects on $K_M$ induced by His to Ala mutation at the H center are intriguing. At the pH optimum for catalysis (5.8), the M109I substitution is not expected to have any effect on H-site copper coordination.

| Variant | $K_M$ ($u$M) | $K_{cat}$ ($s^{-1}$) | Specific acitivity | [dansyl YVG per [$O_2$] | Cu:PHM |
|---------|---------|---------|---------|---------|---------|
| WT | 8.2 | 13.8 | 25.7 | 0.90 ± 0.08 | 2.02 ± 0.15 |
| M109I | 11.8 | 4.6 | 13.7 | 1.01 ± 0.19 | 2.08 ± 0.14 |
| H107A | 3.3 | 0.08 | 0.25 | 0.97 ± 0.05 | 2.01 ± 0.01 |
| H108A | 19.4 | 0.11 | 0.38 | 0.97 ± 0.13 | 2.04 ± 0.23 |

[a]Estimated errors in kinetic constants are ±4%. Values for oxygen coupling in the WT protein is from Evans *et al.*, 2006.

**Table 4.1.** *Kinetic Parameters, Oxygen Coupling Ratios, and Copper Binding Stoichiometry of PHM H-Site Variants Compared with the Wild-Type Enzyme[a].*

However, we consistently observed the somewhat puzzling result of a significant decrease in specific activity, with the major effect on $k_{cat}$. Addition of imidazole to the His to Ala mutants up to a concentration of 10 mM was unable to rescue catalytic activity.

### 4.2.2 COPPER BINDING

One possibility for the dramatic decrease in catalytic rate of the H107A and H108A variants would be a loss of copper due to the loss of a critical histidine residue. Measurement of copper binding stoichiometry showed that this was not the origin of the loss of activity, since both His to Ala mutants bound Cu (II) at a ratio of close to 2:1 (Table 4.1). This result is comparable to that for the H172A mutant which bound Cu (II) with a ratio between 1 and 2 (Jaron et al. 2002; Evans, Blackburn, and Klinman 2006). The data suggests that loss of either H107 or H108 can be compensated by coordination of a solvent to complete the expected 4-coordinate geometry for a cupric ion. Nevertheless, the higher binding ratios for the H107A and H108A mutants relative to H172A may indicate that H172 is more important for stabilizing the H-site structure. The contiguous positioning of H107 and H108 on the same β-strand constrains these ligands to coordinate via their Nδ donor atoms, which may introduce strain into the 4-coordinate $(His)_3(OH_2)$ ligand set in the WT. Therefore, replacement of either H107 or H108 with a solvent ligand may result in a lower energy structure than a similar substitution at H172. The non-coordinating M109I variant reconstitutes with 2 Cu (II) per protein as predicted for the presence of all three coordinating His residues.

### 4.2.3 CHARACTERIZATION OF THE CU (II) CENTERS BY XAS

To gain further insight into the effects of the substitutions, we carried out XAS studies on the oxidized forms using X-ray absorption spectroscopy (XAS) to explore the copper coordination. Figure 4.1 (top) shows a co-plot of the EXAFS of the WT and variants H107A, H108A and M109I at pH 5.5. The spectra overlay exactly, with differences less than the level of noise in the data. Simulations of the spectra (Table 4.2) confirm the result obtained by inspection of the four datasets, namely that they give rise to almost identical parameters, and correspond to the average coordination of 4 N/O ligands per Cu (II) center, reported previously for DβM, (Blackburn et al. 1991) PHM (Blackburn et al. 2000) and TβM (Hess, Klinman, and Blackburn 2010). This is not unexpected since distinguishing features arising from the substitution of one histidine in five (averaged over both copper centers) would only be observable in the shape and/or intensity of the outer-shell features at R = 2.8–4.3 Å, which are the signatures of imidazole coordination. Figure 4.1 (bottom panel) shows a comparison of the Fourier transforms of the WT protein with the three variants, from which it is evident that the intensities of the shell around 3 Å do appear to correlate with the loss of imidazole intensity in the H107A and H108A mutants. However, the trend is much less obvious in the 4 Å shell, where multiple scattering contributions dominate, (Strange et al. 1987) and small differences in imidazole orientation can result in greater intensity shifts than coordination numbers themselves. The EXAFS data therefore suggest that the H-site His residue in H107A and H108A is replaced by coordinated solvent and does not
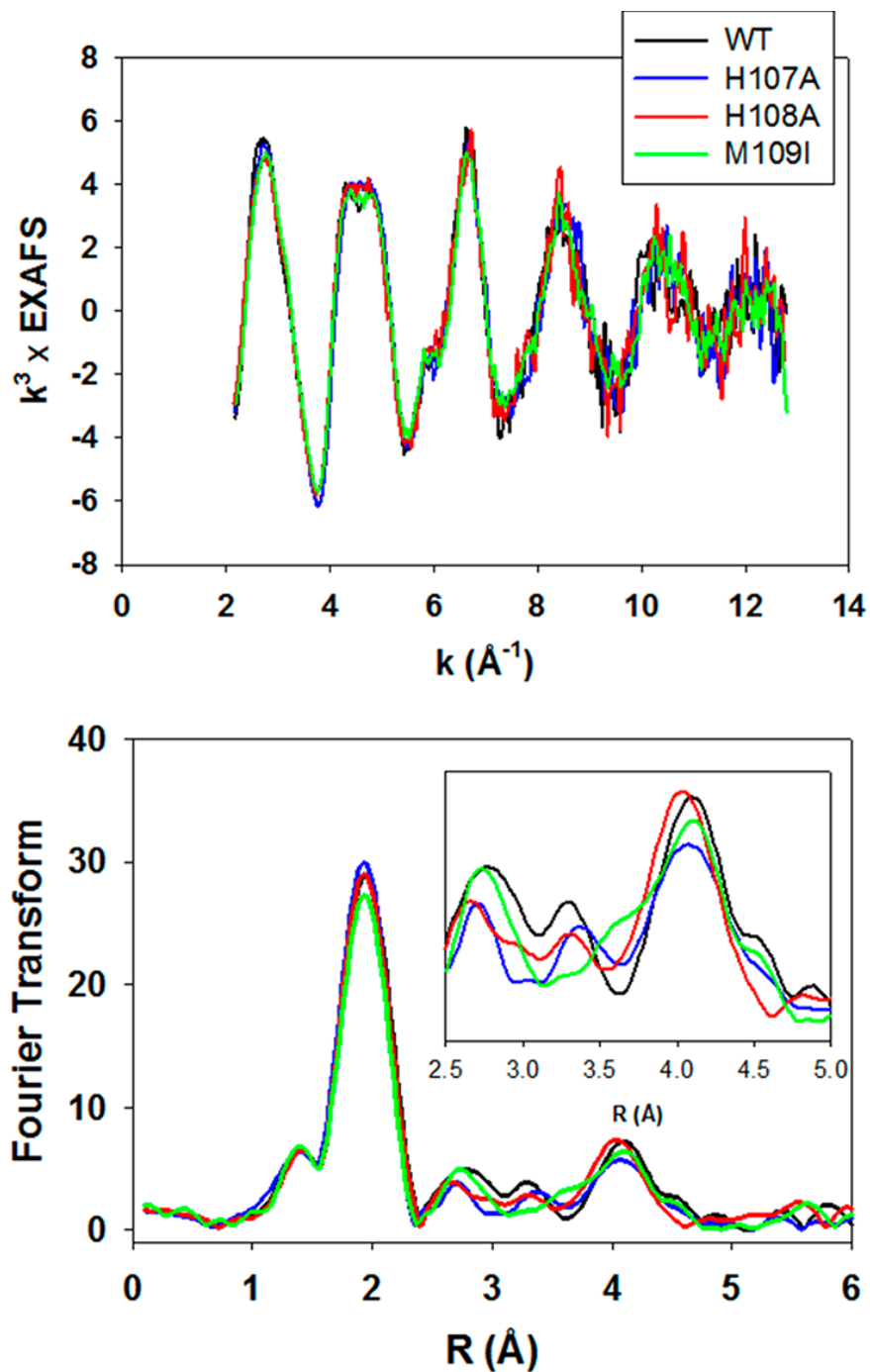
**Figure 4.1.** *Top, overlay of the experimental EXAFS of oxidized PHM variants. Black trace, WT; blue trace, H107A; red trace H108A; green trace M109I. Bottom, overlay of experimental Fourier transforms color-coded as for the EXAFS above. The inset shows an expanded view of the imidazole outer-shell region of the transform.*

perturb the coordination geometry of the site in an observable fashion. The EPR

parameters for the His to Ala variants confirm these conclusions and are

remarkably similar to WT, ruling out large changes in coordination geometry as

the result of histidine removal at the H-center (Kline, Mayfield, and Blackburn

2013).

## 4.2.4 XAS STUDIES ON THE REDUCED PROTEINS

Copper coordination in the reduced proteins was probed by XAS. Figure 4.2

(top panel) compares the Fourier transforms for WT, H107A, and H108A at pH 7.5.

(EXAFS and Fourier transforms for reduced forms of PHM H-site variants are

individually shown in Figure 4.3 at pH 7.5, and pH 3.5 data is shown in Figure 4.4).

The data show more complex behavior than predicted solely on the basis of

histidine shell occupancy with both intensities and peak positions changing, albeit

with shell occupancy decreasing by less than the predicted 20 percent. These data

can be simulated (Table 4.2) with the expected histidine coordination numbers, and

Cu-N bond lengths ranging between 1.95 Å for the WT and 1.88 Å for the H108A

variant, and are broadly consistent with the trend towards a 2- coordinate site at

CuH. A similar trend was observed previously in a study of the H172A variant (Jaron

et al. 2002) (included in Table 4.2 for comparison) where the average Cu-N(His)

bond length also decreased towards the value (1.87 – 1.89 Å) expected for a 2-

coordinate bis-imidazole Cu (I) complex (Himes et al. 2007). However, in contrast to

H172A, the absorption edges of the H107A and H108A (Figure 4.5) do not show the

expected increase in intensity of the 8983 eV edge feature associated with a linear
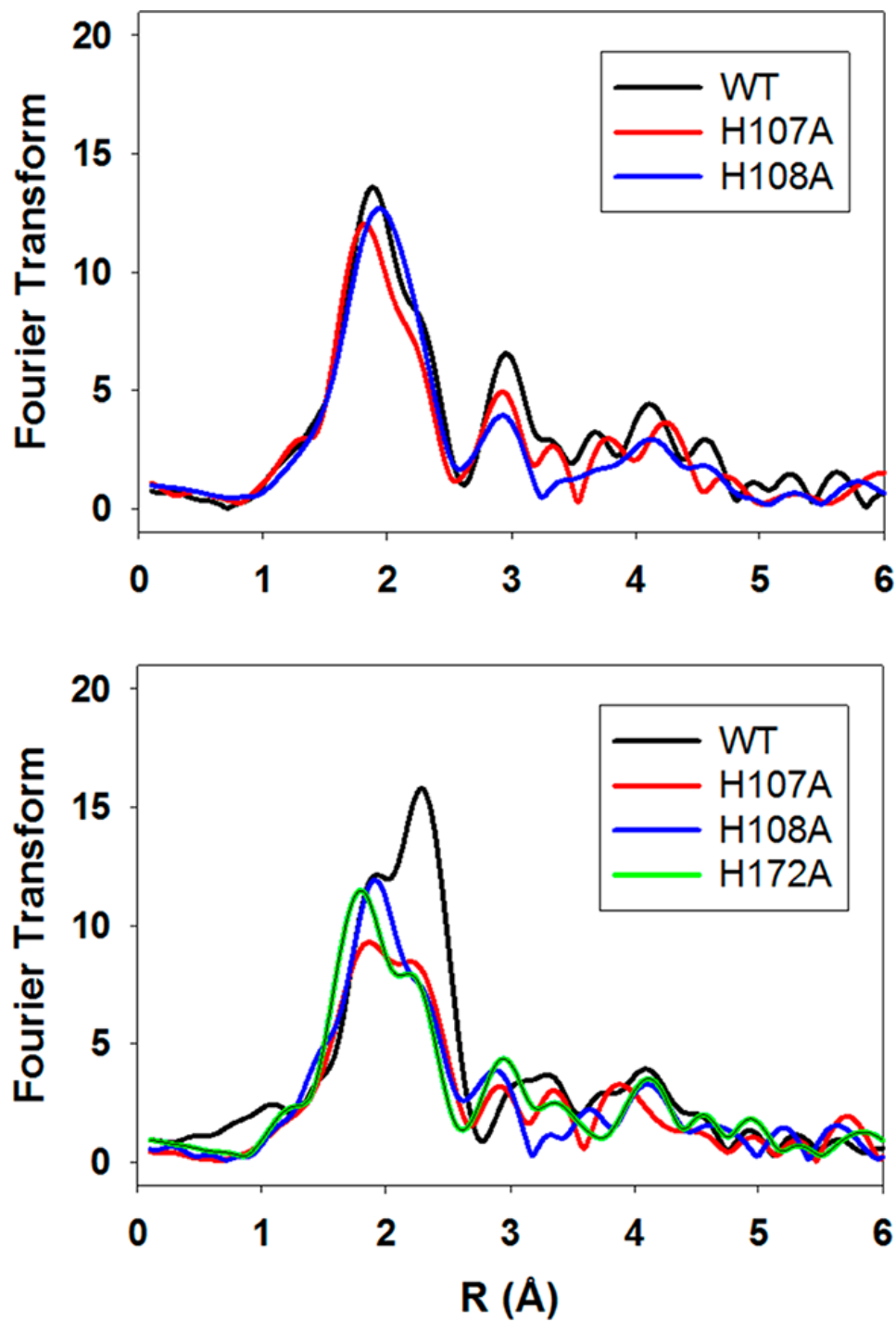
***Figure 4.2.*** *Comparison of the Fourier transforms of ascorbate-reduced PHM H-site variants. Top panel pH 7.5; bottom panel pH 3.5. Spectra are color coded as follows: black, WT; red, H107A; blue H108A; green H172A.*
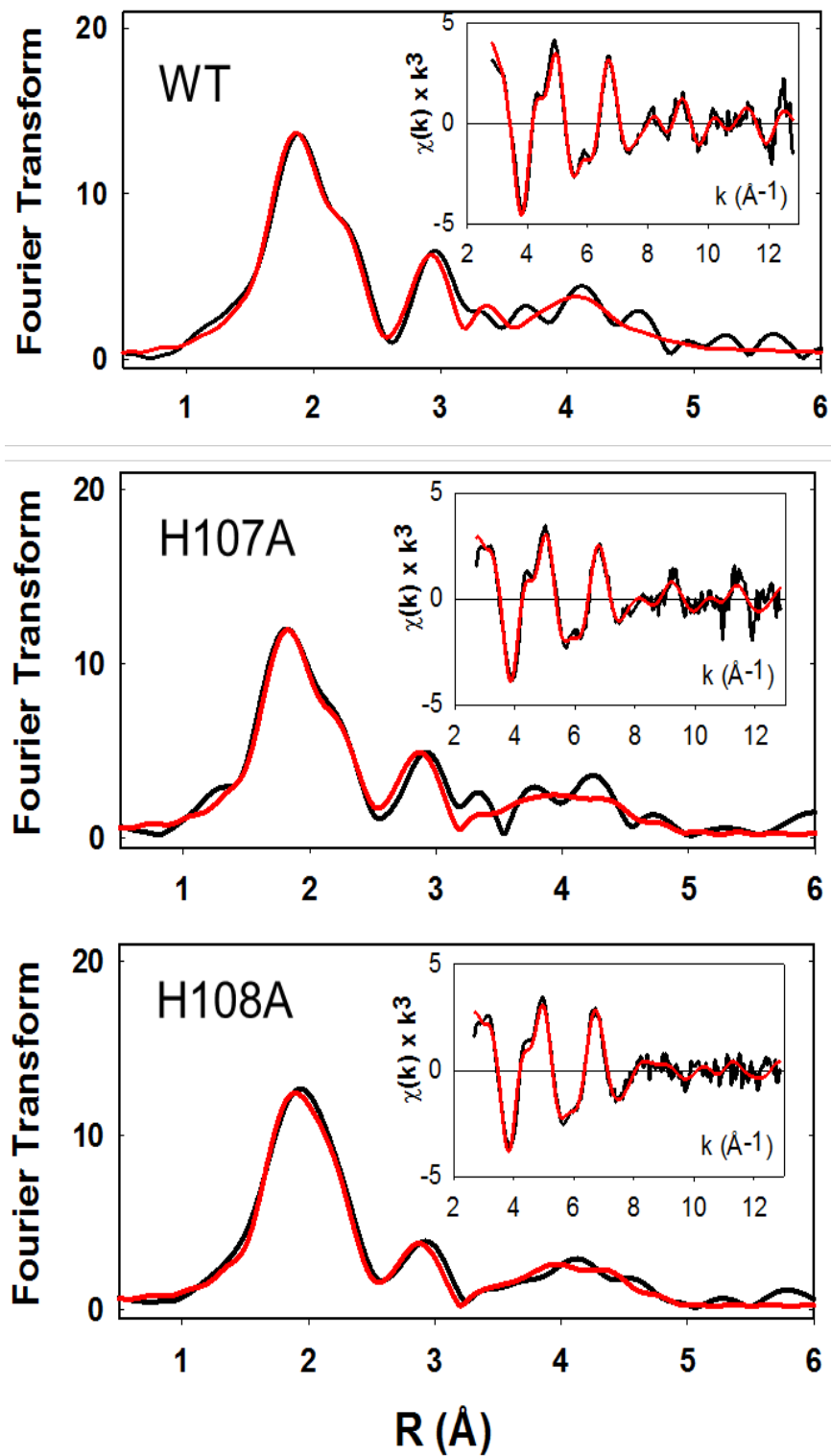
**Figure 4.3.** *Experimental (black) and simulated (red) EXAFS and Fourier transforms for reduced forms of PHM H-site variants at pH 7.5.*
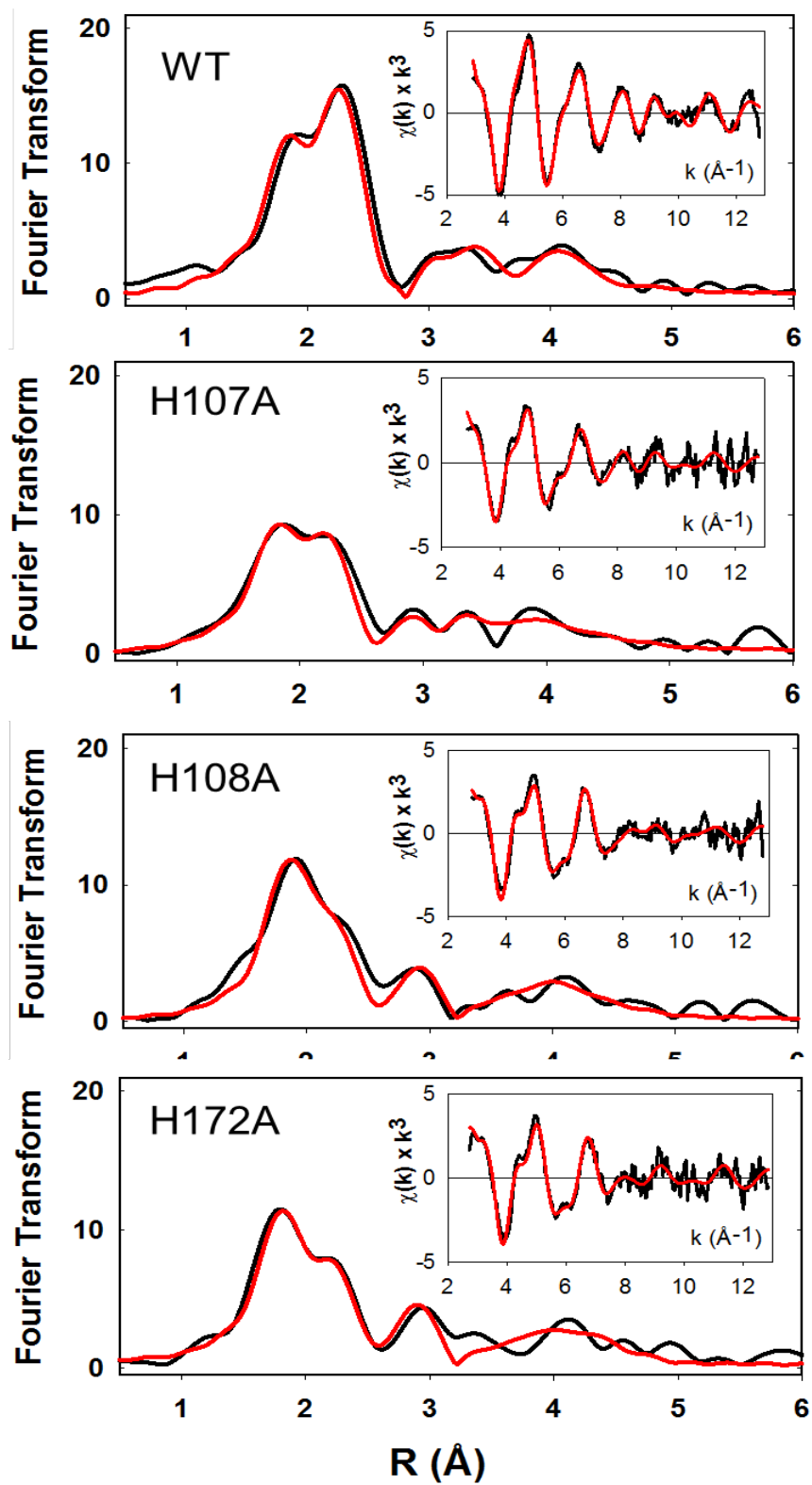
*Figure 4.4. Experimental (black) and simulated (red) EXAFS and Fourier transforms for reduced forms of PHM H-site variants at pH 3.5.*
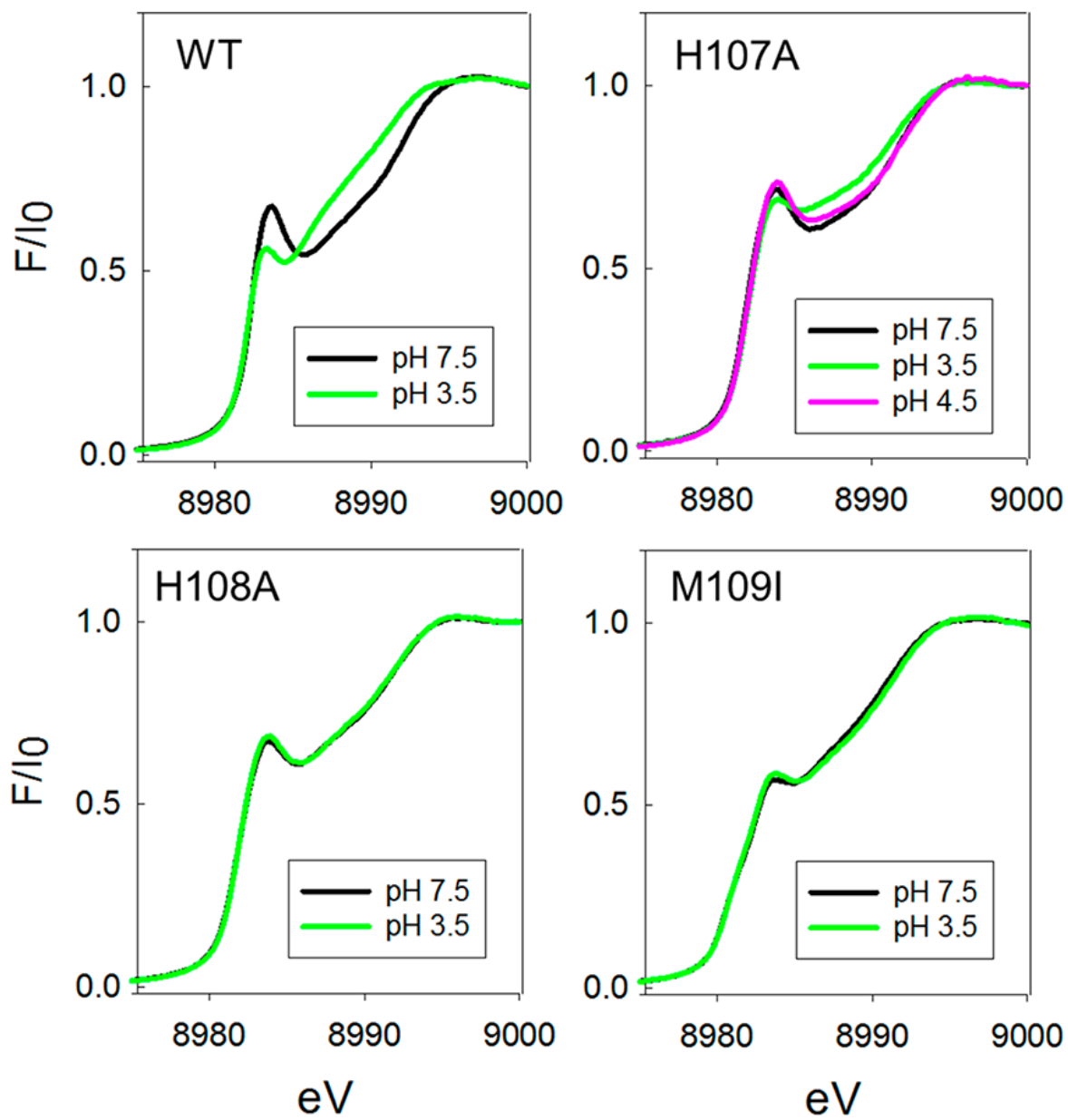
***Figure 4.5.*** *Comparison of absorption edges of ascorbate-reduced PHM WT and Cu H-site variants at neutral and low pH.*

2-coordinate Cu (I) complex (Himes et al. 2007; Himes et al. 2008; Pickering et al. 1993; Sanyal et al. 1991) suggesting that the 2-coordinate H-centers in H107A and H108A are significantly distorted from linearity. The data all show the presence of 0.5 Cu-S due to M314 coordination at the M-center, but interestingly, the Cu-S distance appears to decrease by ∼0.04 Å in H107A and H108A relative to the WT protein. This may suggest that cross talk may influence H and M individual site structure in subtle ways that are difficult to extract from the average coordination as determined by EXAFS analysis. Notwithstanding these uncertainties, it is clear that all the H-site single His variants adopt a 2-coordinate configuration with varying degrees of distortion from linearity. Fits to the EXAFS and FTs of these variants at pH 7.5 and pH 3.5 are given in Table 4.2.

For the WT protein, M109 does not coordinate at pH 7.5 so that the H-site of M109I is expected to be similar to that of WT at this pH. The EXAFS and FT of M109I at pH 7.5 is shown in the top panel to Figure 4.6, and the spectral parameters extracted from simulations are listed in Table 4.2. These data confirm that M109I can be simulated with all three His ligands coordinated at the H-site (average 2.5 over both copper centers), with a longer Cu- N(His) bond length of 1.95 Å similar to the WT protein. However, the Cu–S bond length has decreased to 2.21, which may signal some perturbation at the M-center, as the result of removal of the methionine side chain. While the decrease in $R_{Cu-S}$ is close to the limit of detection, we note that this intriguing result could be related to the unexpected ca. 40% decrease in catalytic activity also observed for this variant.
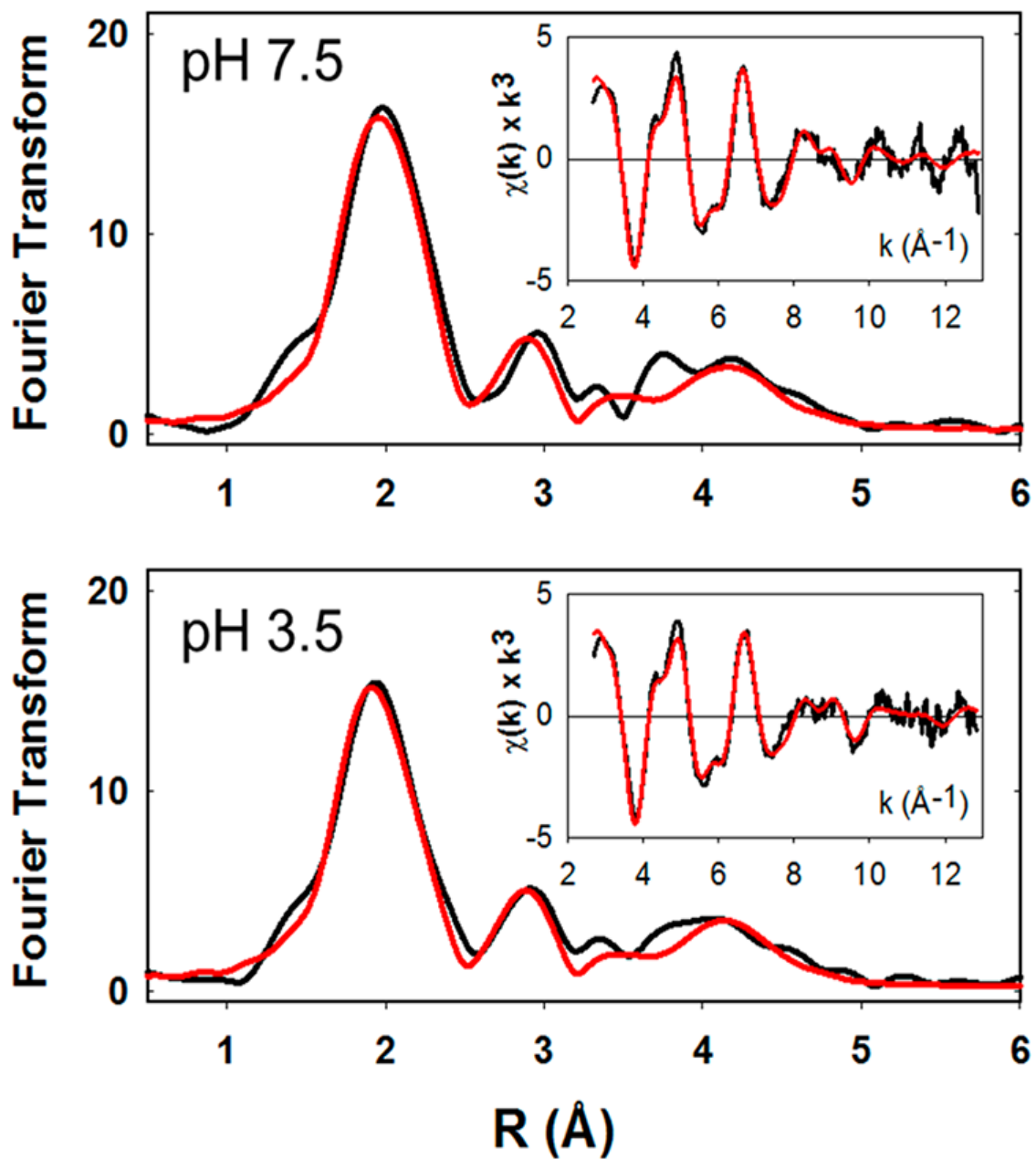
**Figure 4.6.** *pH dependence of the EXAFS and Fourier transforms of the M109I variant. Black traces are experimental data, and red traces are simulated data. The top panel represents data collected at pH 7.5, and the bottom panel is data collected at pH 3.5.*

**4.2.5 PH DEPENDENCE AND THE ROLE OF M109 IN THE LOW PH-TRANSITION**

Our previous studies have suggested that the decrease in activity at low-pH is due to a conformational change induced by a protonation event with $pK_A$ of 4.6–4.7 which results in the coordination of an additional Met ligand at one or other of the two coppers (Bauman et al. 2011). Based on observation of similar behavior in the homologue TβM, and sequence comparisons between PHM, TβM, and DβM we proposed that M109 was the likely origin of the low-pH Met ligand, and that the conformational change was initiated by protonation of one of the His ligands at the H-center. The hypothesis leads to two predictions (i) M109I should show no decrease in catalytic activity at low pH, and (ii) the Met-off to Met-on transition should be absent in M109I. These predictions were tested by measuring the pH dependence of both the catalytic activity and the EXAFS-derived H-site coordination of the M109I variant.

Figure 4.7 compares the pH-activity profile of PHM variants M109I, H107A, H108A, and H172A with that of the WT enzyme. Differences in catalytic rates were factored out by normalizing the rate to unity at the pH optimum of the WT enzyme

so that changes in pH-dependence of the rate profile were directly comparable. In Figure 4.7, the data for WT are represented by the solid black line, which corresponds to the simulation of the WT rate versus pH data published previously (Bauman et al. 2011). The data provides a dramatic confirmation of the prediction, viz that in M109I the rate remains high as the pH decreases below 5.5, and may actually increase in the pH range 5.5– 3.0. In a second set of experiments, we compared the EXAFS of M109I at pH 7.5 and 3.5 as shown in Figure 4.6. The
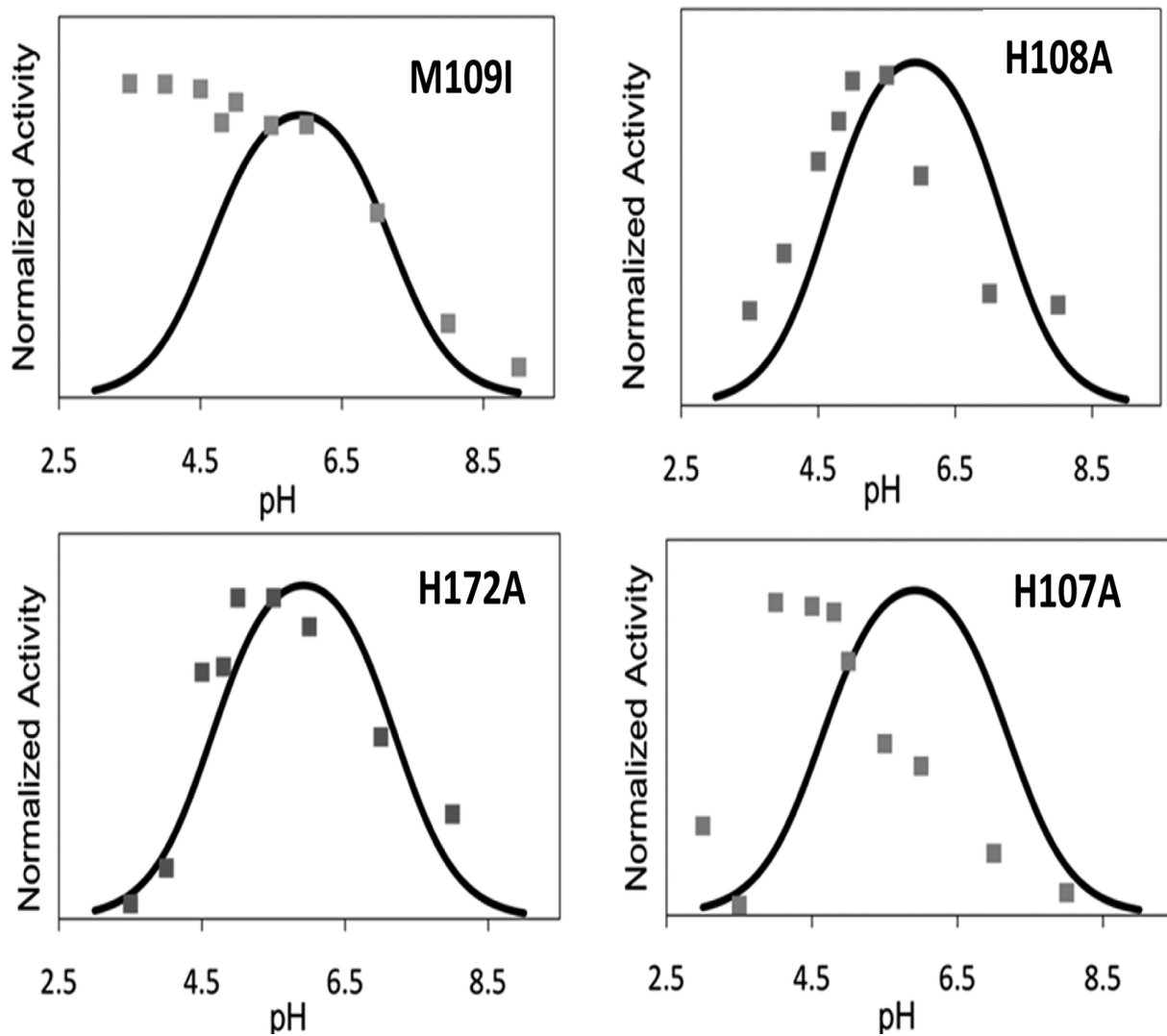
*Figure 4.7.* pH-rate profiles for PHM H-site variants M109I, H108A, H172A, and H107A. Rates were measured using the standard assay conditions at the different pHs as described in the text. To aid in comparison to the WT protein, all rate data have been normalized to unity, despite large differences in activity (as shown in Table 4.1). The solid trace in each panel is the simulated rate profile for the WT enzyme as determined in Bauman et al., 2006.

spectrum at pH 3.5 is identical to that at pH 7.5, and lacks the increased intensity at

2.3 Å due to the additional Cu-S(Met) ligand, which is the hallmark of the low-pH

structural transition (see Figure 4.2 bottom panel and reference) (Bauman et al.

2011). These data confirm our second prediction, namely that the low-pH Cu-S(Met)

interaction is eliminated in the M109I variant. Therefore, we can state with

confidence that M109 coordinates via its thioether S atom in the low-pH form.

An unanswered question is the origin of the group which protonates.

Previously we argued that a p$K_A$ of 4.6 was consistent with protonation of the

coordinated $N_\delta$/$N_\epsilon$ of the imidazole side chain of a histidine ligand. This in turn leads

to the prediction that mutation of the protonatable His residue might also induce

the conformational change, and result in a species which (i) exhibited the met-on

form at all pHs. The EXAFS of H107A and H108A at pH 7.5 (Figure 4.3) do not show

this behavior. Perhaps surprisingly, the mutations also abrogate M109 coordination

at pH 3.5 as show in Figure 4.4 and Table 4.2. Additionally, it might be anticipated

that mutation of the protonatable His residue would also abrogate the decrease in

activity at low pH, producing instead an enzyme form with minimal activity over the

entire pH range. Data on the pH-activity profiles of the H-site His to Ala variants are

shown in Figure 4.7. H172A shows behavior almost identical to WT, while H108A

shows a slight shift in pH optimum to lower pH values. H107A, on the other hand

shows a pH-rate profile, which more closely resembles that of M109I. This would

imply that H107 is the ligand that protonates since its absence abrogates M109

coordination and the associated decrease in catalytic rate, although it is still unclear

why the other His variants do not show M109 Cu-S interaction in their low-pH

EXAFS spectra.

## 4.2.6 CO BINDING TO WT AND M109I AT LOW pH

CO binds to WT enzyme at pH 5.5 and above to generate an M-site carbonyl complex which has been characterized by FTIR (Pettingill, Strange, and Blackburn 1990; Jaron and Blackburn 1999) and crystallography (Chufaʹn et al. 2010). The C≡O stretching frequency is 2092 cm$^{-1}$ which is consistent with a binding site comprised of 2 His, one S(Met) and CO (Pettingill, Strange, and Blackburn 1990; Boswell et al. 1996; Jaron and Blackburn 1999). To gain further insight into the coordination changes at low-pH, we used FTIR to compare the CO-binding chemistry of the WT and the H-site variants at pH 7.5 and pH 3.5. These data are shown in Figure 4.8. As expected, the 2092 cm$^{-1}$ band associated with the M-site carbonyl at both pHs. However, a new band is observed at 2110 cm$^{-1}$ in the WT protein that is absent in M109I, and we therefore assign this band to an H-site carbonyl coordinated by the thioether of M109, two His residues and the CO. This ligand set is identical to that of the M-site CO complex, yet its ν(CO) is 20 cm$^{-1}$ higher, suggestive of weaker back-bonding into the π$^*$ orbitals on the CO ligand. At present we have no explanation for the differences in frequency, but the low-pH carbonyl and absence of the coordinating sulfur at low pH in M109I adds confidence to the assignment of M109 as the coordinating ligand in the low-pH H-site structure. The IR of the H107A and H108A variants at pH 3.5 also shows some intensity at 2110 cm$^{-1}$, but of much lower intensity than the WT protein. This may suggest that a small population of H107A and H108A molecules exist in the thioether-bound
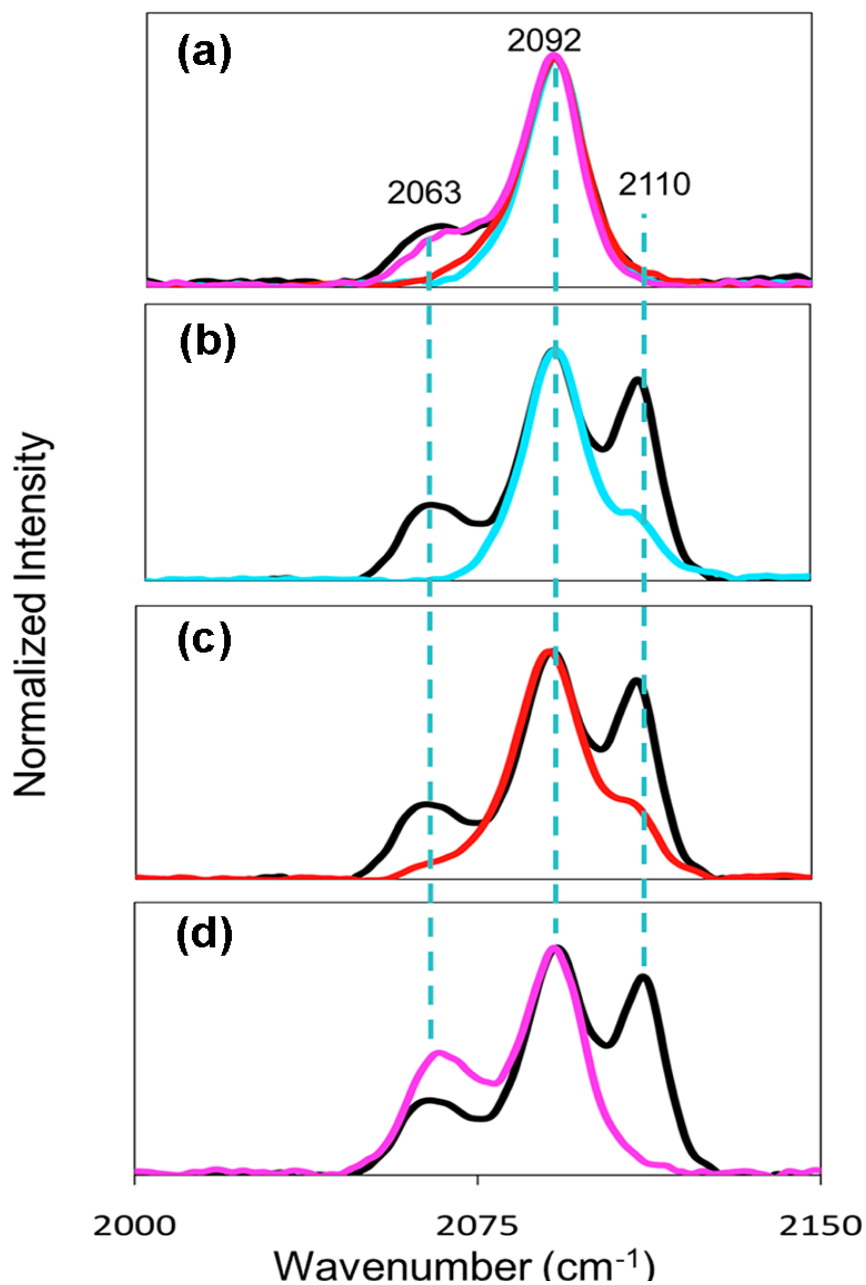
***Figure 4.8.*** *FTIR spectra of the CO complexes of PHM WT and its H- site variants in the CO stretching region. (a) Comparison of IR spectra at pH 7.5 for WT (black), H107A (cyan), H108A (red), and M109I (magenta); (b–d) comparison of IR spectra at pH 3.5 for WT (black) and H107A (cyan) (b); WT (black) and H108A (red) (c); WT (black) and M109I (magenta) (d). Spectra are normalized to the intensity of the WT 2092 cm−1 band.*

conformation, or that CO induces a small shift towards this conformation.

## 4.3 DISCUSSION

Our data establish that mutation of any one of the three His residues at the H-center of PHM reduces activity to detectable yet extremely low levels. Most of the loss is associated with $k_{cat}$, although $K_M$ varies by a factor of 3 with H107A having the highest affinity and H108A the lowest. This loss of activity is not due to inability to bind Cu in either the oxidized or reduced states. Furthermore, the structures as visualized by EPR and EXAFS spectroscopy appear similar in all cases to those observed in the WT fully active enzyme. In the oxidized mutant proteins, solvent appears competent to bind in place of imidazole to generate 4-or 5- coordinate H-site structures, whereas in the reduced proteins any two histidine residues appear competent to bind Cu (I), albeit with some indication from absorption edge intensities of different degrees of distortion from linearity. Since H107 and H108 are contiguous residues on the same β- strand are constrained to bind in a trans - configuration via their Nδ imidazole N atoms and hence are likely most stable in linear 2-coordinate geometry (Himes et al. 2008). This was previously noted in an earlier study of the H172A variant where a significant increase in absorption edge intensity (characteristic of 2-coordinate linear geometry) (Himes et al. 2007; Pickering et al. 1993) was observed. For the H107A and H108A variants the 8983 eV intensity was not significantly increased above that found in the WT protein, suggesting that these variants may be unable to reorient so as to adopt the thermodynamically preferred linear structure. This observation, coupled to the

almost complete loss of activity in single H-site variants, may suggest that the H-site is built on a fairly rigid scaffold where precise orientation of His ligands is an essential element of function.

It is puzzling that solvent readily substitutes for the missing imidazole side chain, yet exogenous ligands do not appear to bind at H. Azide, nitrite and peroxide bind exclusively to the M-center in the oxidized protein while CO binds to M in the reduced form (Chufa´n et al. 2010; Rudzka et al. 2013; Pettingill, Strange, and Blackburn 1990; Boswell et al. 1996; Chen et al. 2004; Jaron and Blackburn 1999). Likewise addition of imidazole to any of the H-site His to Ala mutants fails to rescue activity (Jaron *et* al., 2002 and this work). This may be due to a lack of reactivity (similar to azide), but it may also support the hypothesis advanced above that H-site reactivity is intimately involved with the connectivity of the His ligands to the protein scaffold, which either completes ET circuitry, or organizes other key elements of structure. It is noteworthy that the X-ray crystal structure of the M-site M314I mutant shows a highly perturbed H-site structure with H107 completely dissociated (Siebert et al. 2005). The cross-talk between H and M implied by this structure is also manifest in changes in the $K_M$ for substrate binding of H-site mutants, even though the substrate binds at a site many angstroms distant. Thus subtle changes in H- site structure may propagate through the scaffold to M, where they could inhibit the enzyme from achieving critical conformations necessary for H-tunneling (Klinman 2006b; Francisco et al. 2002a).

The pH dependence of catalytic activity gives further insight into protonation/ deprotonation events that interconvert active and inactive states. In this study, we

have focused on the protonation event that generates an inactive state with a $pK_A$ of

4.6 (Bauman et al. 2011; Bauman, Yukl, et al. 2006). Our earlier work advanced the

hypothesis that pH induced a conformational switch between a catalytically

competent active state of the H-center and an inactive state containing a new Cu-S

ligand. We further speculated that the new S residue was derived from the side

chain of M109 which is part of the H-site conserved HHM motif but points away

from CuH on the opposite side of the β-strand (Figure 4.9). The hypothesis allowed

us to make two predictions (i) that the absence of a thioether at residue 109 would

prevent the M109 S(Met) coordination thereby attenuating the driving force for this

conformational switch, and (ii) that its absence would therefore eliminate the loss of

activity at low pH.

Both of these predictions were borne out by the data. The M109I variant

showed a small increase in activity in the pH range 5.5−3.0 and lacked the high-

intensity Cu−S interaction characteristic of the low-pH state of the WT enzyme. This

allows us to conclude with confidence that in the WT enzyme, the low-activity state

has undergone a conformational switch, which flips the β-sheet, repositioning the

coordinating ligands $pK_A$ that M109 is in a favorable orientation to bind to CuH.

The observed $pK_A$ for the catalytic transition of 4.6 is within the range

expected for protonation of histidine residues coordinated to Cu (I). Well

established cases of this behavior include the reduced forms of cupredoxins (Guss et

al. 1986; Li et al. 2011) and Cu/Zn superoxide dismutases, (Bertini, Luchinat, and

Monnanni 1985; Blackburn et al. 1984; Banci et al. 2002) where protonation is

coupled to addition of an electron so as to keep the overall charge constant. As noted
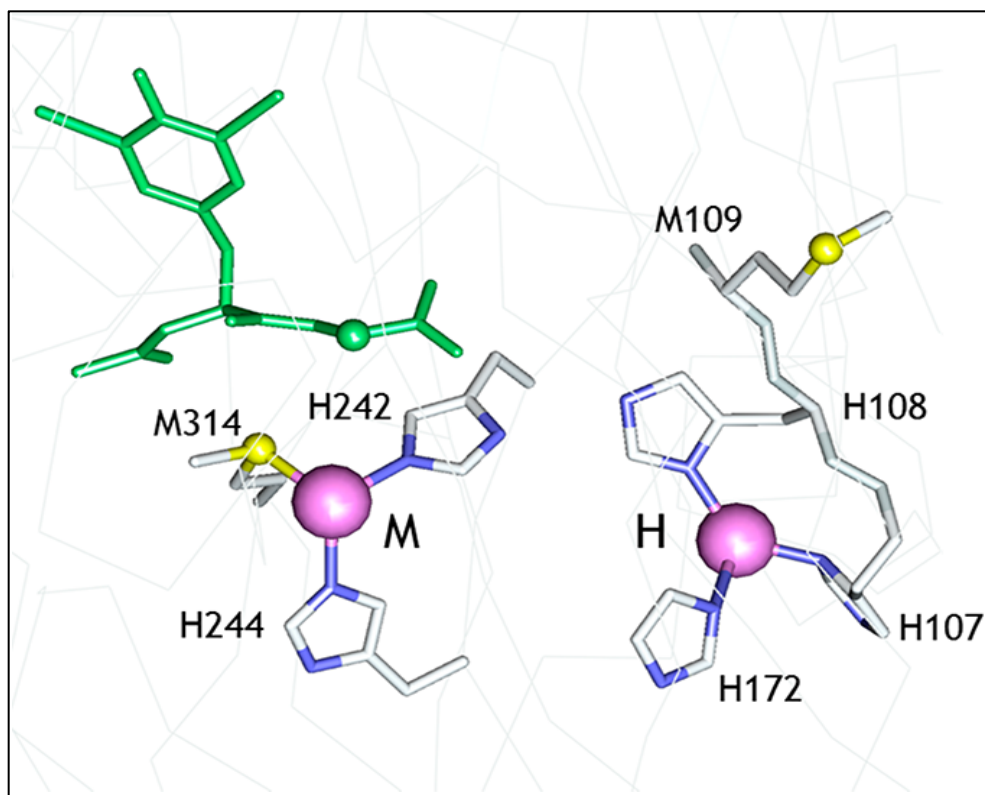
***Figure 4.9.*** *Active site structure of oxidized WT PHM (pdb file 1OPM). The substrate di-iodo-tyrosyl-glycine (I-YG) is shown in green. The H-site shows the relative orientation of the H107H108 M109 motif in the active conformation, with the Met residue pointing away from the copper (Prigge et al. 1999).*

previously, (Bauman et al. 2011) the C- terminal histidine ligand of the cupredoxin site is located in a loop of sequence between the Cys112 and Met121 (azurin numbering), and the $pK_A$ for histidine protonation is sensitive to both the identity and length of the sequence (Li, Banfield, and Dennison 2007)  with values ranging from 2 to 6. For example replacement of the native loop of azurin ($C^{112}$TFPGH$^{117}$SALM, $pK_A$ H$^{117}$ < 2) with shorter loops from amicyanin or

plastocyanin produces chimeras with pK$_A$s for protonation of the corresponding

histidine of 5.5 and 4.3 respectively, while for plastocyanin, the pK$_A$s of the native

protein and the chimera in which the native loop (C$^{84}$SPH$^{87}$QGAGM$^{92}$) is replaced

with the azurin loop-sequence are 4.7 and 4.9. We reasoned that if protonation of an

H-site coordinating histidine was responsible for the conformational switch, then its

mutation to alanine should either eliminate, or at least strongly perturb both the

pH-rate profile, and the structural transition leading to S(Met) binding. The data

show that H172A exhibits WT pH-rate profile, while H108A has a rate profile only

slightly shifted to lower pH. H107A on the other hand has a strongly perturbed rate

profile, which approximates to that of M109I showing an increase in rate between

5.5 and 4, below which the activity crashes to zero. Additionally, close inspection of

the EXAFS data suggests an increase in Cu-S site occupancy for H107A to 0.65 at pH

3.5, while FTIR shows evidence for the S-coordinated H-site carbonyl (2010 cm$^{-1}$).

These observations may suggest an equilibrium between M109-on and -off states in

H107A, and leads us to propose that H107 is the residue which protonates. The

inability of the H107A mutant to induce a complete conformational switch was at

first puzzling, as the prediction was that the absence of the protonating residue

would generate the Met109-on state at all pHs. However, further analysis suggests

that the switch may be driven by the replacement of the coordinating histidine by its

bulky non-coordinating protonated form, and is induced by a combination of

S(M109) coordination and relief of steric crowding. In this model, the hole created

by the Ala substitution would create no steric restrictions, and could therefore be a

stable entity at all pHs. We also note that H107 does not appear to protonate as

readily in the M109I variant, as no decrease in activity is observed with M109I between pH 6 and 3. This observation implies that the $pK_A$ for His protonation is coupled to the ability of the Met ligand to coordinate, without the driving force for S ligation, Cu (I) out-competes the proton for histidine binding.

The M109-on state of the enzyme is catalytically incompetent, and the obvious next question is why? Binding of CO to the low pH inactive (S-bound) form of the WT enzyme induces a new band at 2110 cm$^{-1}$ absent in the M109I variant, which we may logically assign to a 4-coordinate H-site carbonyl with two histidines, one methionine and CO. On the other hand the active state of the H-site does not form a CO complex. These observations give hints to the possible geometrical differences between active and inactive states. Cu (I) carbonyls are generally formed from 3-coordinate precursors to give predominately 4- coordinate tetrahedral complexes (Sanyal et al. 1991; Pasquali and Floriani 1984; Blackburn et al. 1988) and CO reacts poorly if at all with 2-coordinate Cu (I) complexes. A recent study of an H-site PHM model peptide containing the HH motif confirmed this chemistry: the 2-coordinate Cu (I)- $N_\delta$- $N_\delta$ bis-imidazole complex reacted sluggishly with CO to generate a weak 3-coordinate CO complex with a low-intensity $\nu(C\equiv O)$ between 2105 and 2110 cm$^{-1}$. However, in the presence of an additional mole equivalent of imidazole, the 4-coordinate Cu (I)(His)$_3$ CO species was formed stoichiometrically, and exhibited a strong $\nu(C\equiv O)$ at lower frequency (2075 cm$^{-1}$) as expected (Himes et al. 2007). With regards to the low pH WT PHM spectrum, it is possible that the 2110 cm$^{-1}$ is due to a Cu (I)(His)$_2$CO structure, but the strong intensity of the band together with its absence in the M109I variant suggests that the 4-coordinate Cu

(I)(His)$_2$S(Met)CO species is more likely. We believe that the assignment is reasonable since the thioether ligand is a poor donor, and hence may have little impact on the extent of back bonding.

The question remains, if the low activity S-bound H-site readily forms a carbonyl, why not the 3-coordinate high activity site? The answer must lie in the ability of lack thereof of the 3-coordinate precursor to rearrange on CO binding to a tetrahedral coordination. This again suggests that a rigid protein scaffold associated with the H-site active form may be required for electron transfer.

Most cuproproteins including PHM and DβM are packaged into vesicles in the TGN as folded apo-proteins that still require metallation. This function is performed by copper transporting ATPases (Steveson et al. 2003; Petris, Strausak, and Mercer 2000; Setty et al. 2008; Qin et al. 2006) which are members of the P1B family of heavy metal transporters found in all forms of life from bacteria to mammals where they function in copper export across membranes. Mammalian ATP7A resides in the TGN or vesicular membranes and pumps copper from the cytosolic to the lumenal side of the membrane where it is believed to transfer copper directly to PHM without the intermediacy of an intravesicular copper chaperone (El Meskini et al. 2003). ATP7A contains a lumenal loop rich in His and Met residues (MDHHFATL-HHNQNMSKEEMINLHSSM) (Pope et al. 2012; Barry et al. 2011) which has been shown to bind Cu (I) at pH 8.0 with 2-coordinate (His)$_2$ ligation and weak additional interaction with a Met residue (Otoikhian et al. 2012). Based on in vitro data, it was postulated that that this loop binds copper as it exits the membrane channel, and passes it on to cuproproteins such as PHM, which are also associated with the

lumenal membrane (Steveson et al. 2003). As the vesicles mature, their pH drops as the result of $H^+$ import, resulting in an internal pH of ~5.5, close to the pH optimum of the monooxygenases with the consequence that the ATP7A lumenal loop is subject to the same pH constraints as its putative PHM partner. At present, the effect of pH on the Cu (I)-binding properties of the loop has not been investigated but it is intriguing that similar HM signals appear to be present in both systems, suggesting that $HHX_nM$ motifs may have more general utility as Cu-dependent conformational switches that could modulate coordination in response to pH. Further studies are underway to explore this and other aspects of HHM chemistry.

| | $F^a$ | $N_0^b$ | $R(Å)^c$ | $DW(Å^2)$ | $N_0^b$ | $R(Å)^c$ | $DW(Å^2)$ | $N_0^b$ | $R(Å)^c$ | $DW(Å^2)$ | $-E_0$ |
|---|---|---|---|---|---|---|---|---|---|---|---|
| | | | Cu-N(His)[d] | | | Cu-O/N[e] | | | Cu-S | | |
| | | | | Oxidized Proteins pH 7.5 | | | | | | | |
| WT | 0.318 | 2.5 | 1.97 | 0.0123 | 1.5 | 1.97 | 0.0123 | | | | 4.69 |
| H107A | 0.316 | 2.0 | 1.96 | 0.0123 | 2.0 | 1.96 | 0.0123 | | | | 5.21 |
| H108A | 0.447 | 2.0 | 1.97 | 0.0129 | 2.0 | 1.97 | 0.0129 | | | | 4.95 |
| H172A[f] | 0.167 | 2.0 | 1.96 | 0.0120 | 2.0 | 1.96 | 0.0120 | | | | |
| M109I | 0.287 | 2.5 | 1.97 | 0.0137 | 1.5 | 1.97 | 0.0137 | | | | -4.30 |
| | | | | Reduced Proteins pH 7.5 | | | | | | | |
| WT | 0.373 | 2.5 | 1.92 | 0.0175 | | | | 0.5 | 2.24 | 0.0123 | 0.34 |
| H107A | 0.487 | 2.0 | 1.88 | 0.0156 | | | | 0.5 | 2.20 | 0.0123 | -0.57 |
| H108A | 0.360 | 2.0 | 1.91 | 0.0152 | | | | 0.5 | 2.20 | 0.0101 | -0.03 |
| H172A[f] | 0.379 | 2.0 | 1.90 | 0.0130 | | | | 0.5 | 2.23 | 0.0200 | |
| M109I | 0.373 | 2.5 | 1.95 | 0.0150 | | | | 0.5 | 2.21 | 0.0094 | 0.26 |
| | | | | Reduced Proteins pH 3.5 | | | | | | | |
| WT | 0.327 | 2.5 | 1.95 | 0.0182 | | | | 1.0 | 2.26 | 0.0102 | -0.66 |
| H107A | 0.860 | 2.0 | 1.91 | 0.0194 | | | | 0.6 | 2.23 | 0.0120 | -0.26 |
| H108A | 0.629 | 2.0 | 1.91 | 0.0147 | | | | 0.5 | 2.22 | 0.0120 | 0.24 |
| H172A | 0.659 | 2.0 | 1.88 | 0.0165 | | | | 0.6 | 2.22 | 0.0124 | -0.67 |
| M109I | 0.280 | 2.5 | 1.93 | 0.0159 | | | | 0.5 | 2.21 | 0.0139 | -0.15 |

*Table 4.2.*  *Parameters used in the simulation of the EXAFS of the H-site variants of PHM. [a] F is a least-squares fitting parameter defined as $F^2 = (1/N)\sum_{i=1}^{N} k^6(data - model)^2$. [b] Coordination numbers are generally considered accurate to ±25%. [c] In anyone fit, the statistical error in bond lengths is ± 0.005 Å. However, when errors due to imperfect background subtraction, phase shift calculations, and noise in the data are compounded, the actual error is closer to ±0.02 Å. [d] Fits modeled histidine coordination by an imidazole ring, which included single and multiple scattering contributions from the second-shell (C2/C5) and third-shell (C3/N4) atoms, respectively. The Cu– N–Cx angles were as follows: Cu–N–C2, 126°; Cu–N–C3, –126°; Cu–N–N4, 163°; Cu–N–C5, –163°. [e] Distances of the Cu-N(His) and Cu-N/O (non-His) shells were constrained to be equal in fits to the oxidized proteins. [f] Data from reference (Jaron et al. 2002).*

# CHAPTER 5

# PH-REGULATED METAL COORDINATION IN THE HM LOOP OF ATP7A REVEALED VIA XAS

## 5.1 INTRODUCTION

Defects in copper transporting ATPases, ATP7A and ATP7B are responsible for Menke's and Wilson's disease, respectively (Lutsenko, LeShane, and Shinde 2007). Copper transporting ATPases are required to metallate cuproproteins (Steveson et al. 2003) and are co-located with the enzymes in the lumen of vesicles within the trans- Golgi network (TGN) where they are subject to pH gradient environments during maturation (Paroutis, Touret, and Grinstein 2004; Vishwanatha et al. 2014). Transfer of copper between the ATPases and acceptor cuproproteins, such as peptidylglycine monooxygenase (PHM), (De et al. 2007; El Meskini et al. 2003; Steveson et al. 2003) dopamine β-monooxygenase (DβM), (Klinman 2006a) and tyrosinase (TYR) (Setty et al. 2008; Petris, Strausak, and Mercer 2000) is proposed to occur without the intermediacy of a chaperone (Steveson et al. 2003). Significant progress has been made in dissecting the structure and function of the copper ATPases in order to understand the mechanism of copper release and thus transfer.

Recent studies have investigated the role of a lumenal loop connecting

transmembrane (TM) 1 and TM2 of ATP7A in the transfer process (Schushan et al.

2012; Otoikhian et al. 2012; Barry et al. 2011). The His/Met (HM) rich lumenal

segment was previously shown to be important for copper release, where it

was found that  dephosphorylation (a step related to copper release) was retarded

by His and Met mutations (Barry et al. 2011; Otoikhian et al. 2012). A lumenal loop

between TM1 and TM2 is absent in other eukaryotic P1B-type ATPases (ATP7B,

yeast Ccc2), (Lutsenko et al. 2007) and in bacterial transporters such as CopA

(Figure 5.1) (Gourdon et al. 2011), suggesting that these ATPases are not equivalent.

Copper transporting ATPase, ATP7A is a large membrane protein, which is

difficult to express and solubilize. ATP7A contains a number of metal binding sites

in the six subdomains of the N-terminus, and additional binding sites buried in the

8- transmembrane helical region, which makes investigating copper binding to the

HM Loop sequence impossible to study in the full-length protein (Figure 5.1)

(Lutsenko et al. 2007). Therefore in order to examine the copper-binding properties

of the ATP7A lumenal loop the TM1/TM2 loop sequence ($^{674}$MDHHFATLHH-

NQNMSKEEMINLHSSM$^{699}$) was inserted in place of the C$^{45}$ETIC$^{49}$ motif of the *B.

subtilis* Sco protein in which all additional His and Met residues were mutated to Ala

(Barry et al. 2011). The peptide scaffold, now just called HM Loop was also shown

via CD spectroscopy to have a stable secondary structure upon inserting the loop

sequence (Barry et al. 2011).

Previous investigations of the HM loop demonstrated via XAS and EPR that

copper was bound to structurally distinct binding sites dependent upon how much

```
MGLMIYMMVMDHHFATLH-HNQNMSKEEMINLHSSMFLERQ__  human
MGLMIYMMVMDHHFATLH-HNQNMSKEEMINLHSSMFLERQ    orangutan
MGLMIYMMVMDHHFATLH-HSQNMSKEEMINLHSSMFLERQ    macaque
MGLMIYMMVMDHHLATLH-HNQNMSQEEMINSHSSMFLERQ    pig
MGLMIYMMVMDHHLAILH-HNQNMSQEEMINIHSSMFLERQ    dog
MGLMIYMMVMDHHLASLQ-HNQNMSQEEMINIHSSMFLERQ    cattle
MGLMIYMMVMDHHLETLH-HNQNISQEEMIHIHSSMFLERQ    horse
MGGHG----------------------------LKHFI    CopA
```
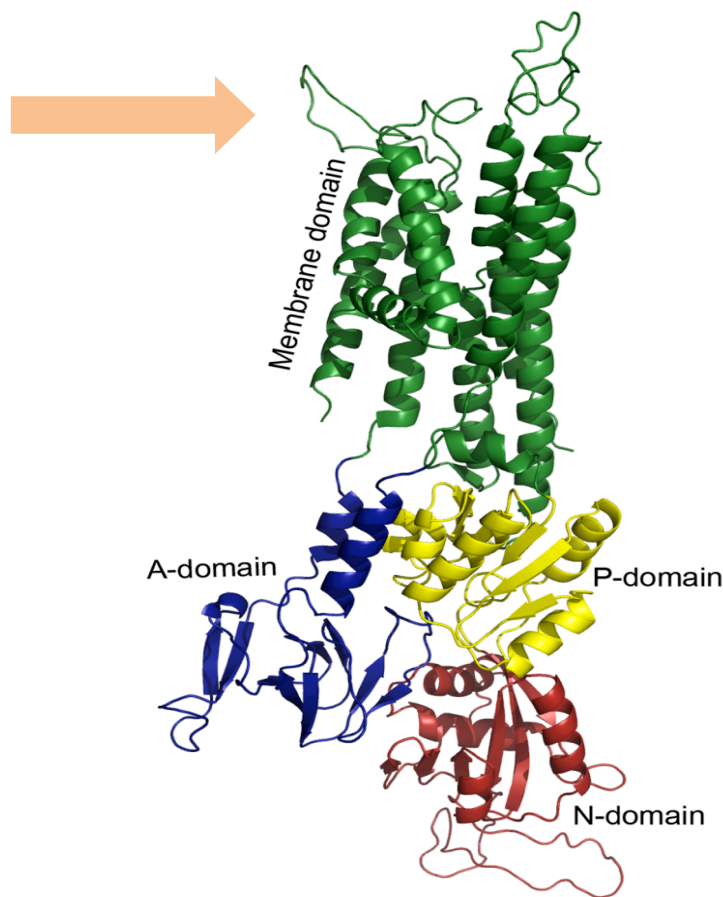


***Figure 5.1.*** *Top, ATP7A lumenal loop sequences (between TM1 and TM2) for mammalian species compared with CopA from Legionella pneunmophilia (Gourdon et al. 2011). The tan bar represents the sequence cloned into the soluble scaffold protein. Bottom, homology model of human ATP7A adapted from reference 34, showing the position of the lumenal loop sequence.*

was loaded, and whether Cu (I) or Cu (II) was bound (Barry et al. 2011; Otoikhian et al. 2012). At low copper to protein ratios, the coordination was dominated by 2 or 3-coordinate mixed His/Met ligands, while higher ratios led to His-only coordination (Otoikhian et al. 2012). In this study we used XAS to further examine the Cu (I) centers of the HM Loop with and without selenium labeling and found 3-coordinate Cu (I) His-Met mixed environments, which werefound to be pH-dependent. At neutral pH's simulations suggested a Met-His$_2$ binding site for Cu (I), while at low pH a structurally distinct Met$_2$-His complex was observed. Triple and double Met mutants were designed in order to assign the Cu (I)-Met binding residue(s), but failed to produce a fully coordinating S(Met) ligand. Overall, our studies show that the Cu (I)-S(Met) coordination observed at either pH is fully dependent on all 4 Met residues in the loop, with the collection of variants identifying Met 3 as an important coordinating ligand. We hypothesize that the conformational mobility of the HM Loop replaces the need for a chaperone and is thus able to regulate the release of copper to target proteins, using factors such as copper loading, redox state, and now pH (shown in this study) to alter coordination.

## 5.2 RESULTS

### 5.2.1 CHARACTERIZATION OF CU (I) BOUND TO HM LOOP AT PH 8 AND PH 3.5 BY XAS

X-ray absorption spectroscopy has previously been exploited to show that a mixture of Cu-N(His) and Cu-S(Met) bind the HM Loop with variable coordination

dependent on factors such as copper loading and redox state. XAS is used in this study to help identify which of the four Met residues in the HM Loop is involved in binding Cu (I), by characterizing the spectra for copper to protein ratios of 1:1 at pH 8.0 and pH 3.5. This pH range represents the range of pH environments that may be encountered within the trans-Golgi secretory pathway. Figure 5.2 compares the EXAFS (insets) and Fourier transforms of Cu (I) 1:1 complexes of WT HM Loop at pH 8.0 (top) and pH 3.5 (bottom) with experimental results in black and simulated fits present in red.

Detailed analysis of the EXAFS data shows a remarkable degree of plasticity in Cu (I) binding. At pH 8.0, the simulations of Cu (I) binding to the S(Met) (unlabeled) in the HM Loop suggest a 3-coordinate structure consistent of a $(His)_2Met$ ligand set. As the pH is lowered to 3.5, the coordination changes to a predominately Cu-S(Met) environment, with the species trading His ligands for Met as the former protonate. The pH 8.0 spectra confirm copper coordination to 1.0 sulfur (Met) at 2.25 Å, and demonstrates the appearance of a second strong sulfur(Met) at low pH (Figure 5.2 and Table 5.1). The first shell peak around 1.9 Å is assigned to Cu-N(His) single scatterer, while peaks at 3 and 4 Å are fingerprints for multiple scattering from the imidazole ligation. The EXAFS data confirmed previous results establishing that Cu (I) to protein ratios of 1:1 bind a mixed His/Met environment, with the spectra depicting a higher degree of sulfur(Met) coordination as the pH decreases.
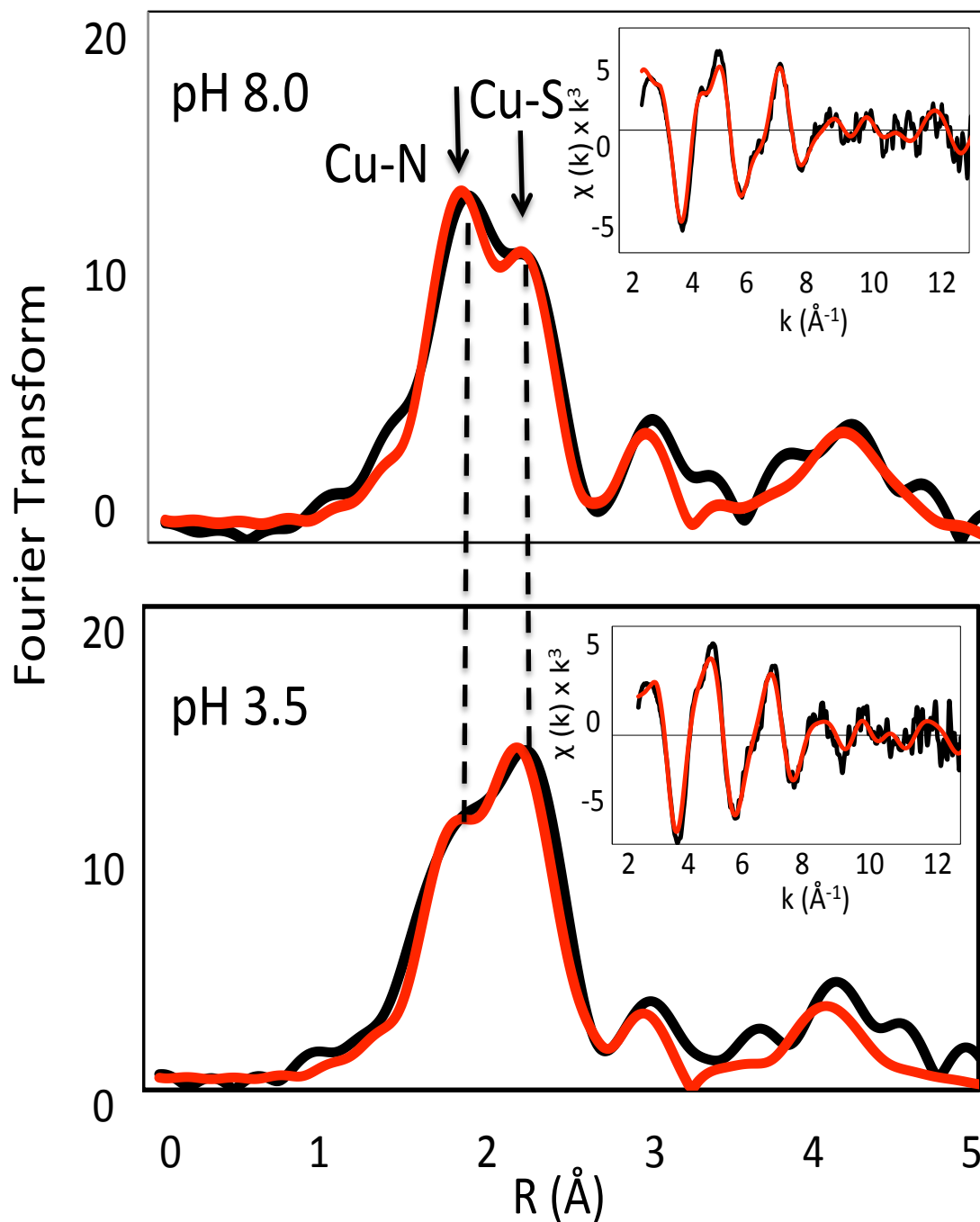
***Figure 5.2****. pH-dependent EXAFS (insets) and Fourier transforms of Cu (I) 1:1 complexes of WT HM Loop. Black traces are experimental data and red traces are simulated data. The top panel represents data collected at pH 8.0 and the bottom panel is data collected at pH 3.5.*

## 5.2.2 CHARACTERIZATION OF CU (I) BOUND TO SELENO-METHIONINE LABELED HM LOOP AT PH 8 AND PH 3.5 BY XAS AT THE CU AND SE K-EDGE

Seleno-methionine (SeM) labeling of the Met residues in the HM Loop allows the pH transition to be studied in more detail, precisely measuring the Cu-Met coordination from the atomic perspective of both Cu and Se. At pH 8.0, conclusions from EXAFS data confirms that copper adopts a 3-coordinate mixed His$_2$Se (Met) coordinated species, while at pH 3.5, the Cu-Se(Met) peak dominates the spectrum, accounting for 2 Se(Met) ligands per Cu (I) (Figure 5.3 and Table 5.1). Therefore, as with the unlabeled construct, the HM Loop toggles between various His and Met ligands, favoring Met as the pH decreases to an extreme of 3.5.

XAS at the Se K-edge provides an additional spectroscopic probe,(Bagai et al. 2008; Chacon and Blackburn 2012) and allows the atomic perspective from both Cu and Se. At pH 8.0, conclusions from EXAFS data validate the conclusions derived from Cu K-edge data. The top panel in Figure 5.4 compares the Se XAS of HM Loop at pH 8.0 (black) and 3.5 (red), where the increase in the Se(Met)-Cu peak at 2.4 Å is observed at low pH, but is not as profound as the FT spectra observed at the Cu K-edge. Corresponding fits are show in the bottom panels of Figure 5.4 (Table 5.1) and suggest that at neutral pH, 0.2 Cu per Se(Met) binds, corresponding to a maximum of 0.8 of the 4 Se(Met) actually bound. At pH 3.5, the Se-Cu ratios increase to 0.5, translating to 2 Se(Met) bound per Cu. Therefore, Cu (I)-Met coordination increases from species containing a sub stoichiometric Se(Met) component at pH 8.0 to one ligated by at least 2 Se(Met) ligands at pH 3.5, fully consistent with the Cu K-edge data. It is likely that each of the binding sites represents a different conformation of
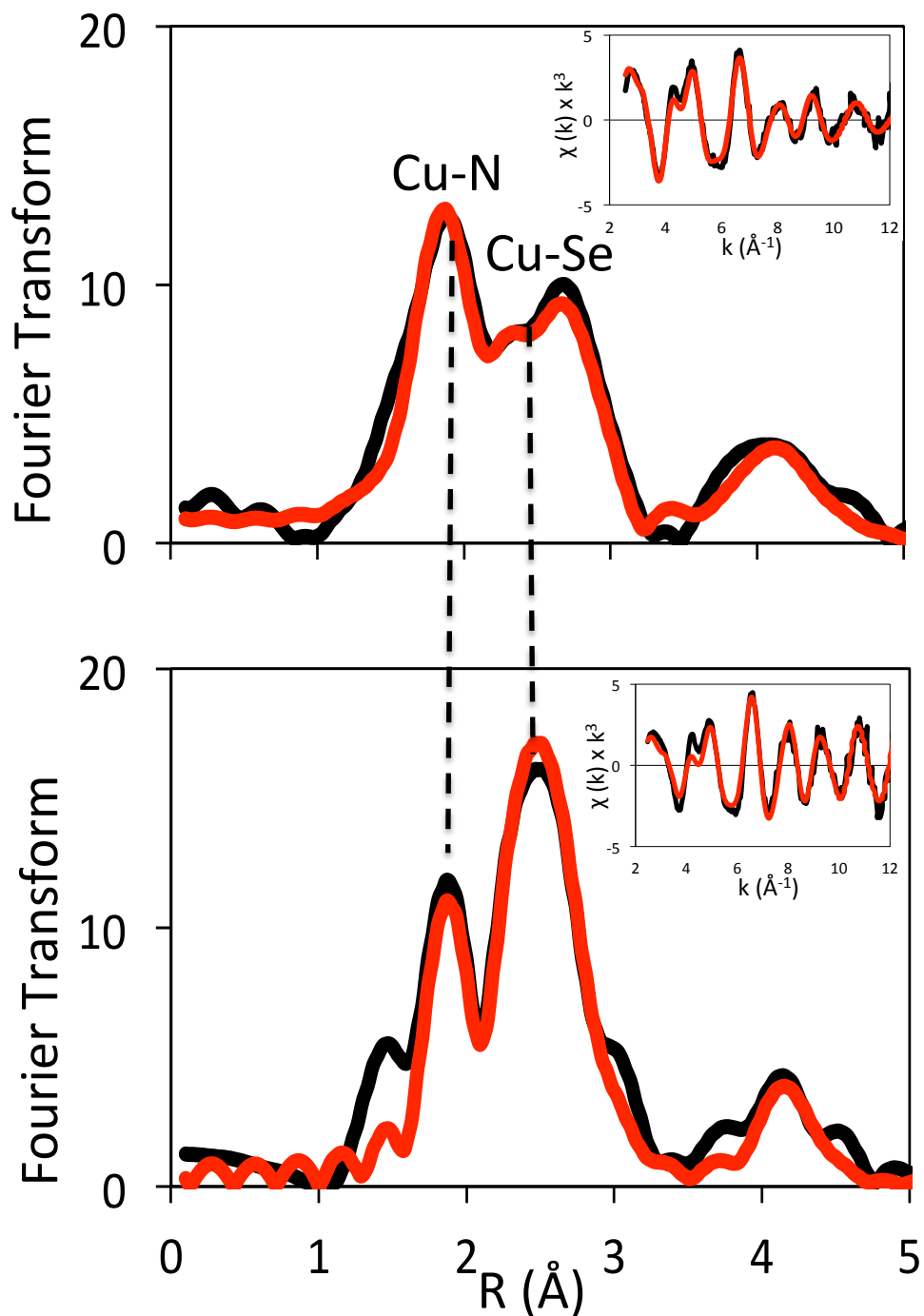
***Figure 5.3.*** *pH-dependent EXAFS (insets) and Fourier transforms of Seleno-Methionine (SeM) labeled HM Loop Cu (I) 1:1, at the Cu K-edge. Black traces are experimental data and red traces are simulated data. The top panel represents data collected at pH 8.0 and the bottom panel is data collected at pH 3.5.*

*Figure 5.4*. *pH-dependent XAS of SeM labeled HM Loop Cu (I) 1:1, at the Se K-edge. Top panel compares the Fourier transforms at pH 8.0 (black) and pH 3.5 (red). Bottom figures are EXAFS (insets) and Fourier transforms at pH 8.0 (bottom left), and pH 3.5 (bottom right) with experimental data in black and simulated data represented as red traces.*

the loop peptide, where one or more coordinated histidines can protonate, inducing coordination of copper to an adjacent Met Ligand. The identity of the coordinating Met ligand is further explored in this study using a series of methionine mutants.

## 5.2.3 CHARACTERIZATION OF CU (I) BOUND TO TRIPLE MET MUTANTS OF HM LOOP AT PH 3.5 BY XAS

Triple met mutants were constructed and analyzed at the Cu edge in order to identify the Met residue that binds copper within the HM Loop. These mutants are denoted M1 through M4 where M1 retains the first methionine in the sequence while the other three methionine residues have been mutated to isoleucine, and so on (Refer to Table 2.2 for details about the nomenclature). M1 and counterpart, SeM1 (SeMet234I), were loaded with Cu (I) and subjected to pH 8.0 and 3.5. Interestingly, no signs of Cu-S(Met) or Cu- Se(Met) were observed at either pH (Figure 5.5 depicts results for SeM1 at pH 3.5 with data not shown for M1). FT and EXAFS data are shown in Figure 5.5 for triple Met mutants M2, M3, and M4 and also showed no signs of Cu-S(Met) at pH 3.5. Simulations of EXAFS data (insets) and the FT yielded typical spectra of 2-coordinate Cu (I)-N(His) complexes with the distances between 1.87 and 1.88 Å (Table 5.2) (Prigge et al. 1997; Blackburn et al. 1991; Blackburn et al. 2000; Himes et al. 2008). A very small component of Cu (I) interacts with 0.1 S(Met) for the M2 and M3 variants. The data provides evidence that constructs containing a single Met experience no pH-dependent switching even in the SeM labeled sample. This implies that one methionine residue is insufficient on its own to bind and may require others, especially since two methionines

115
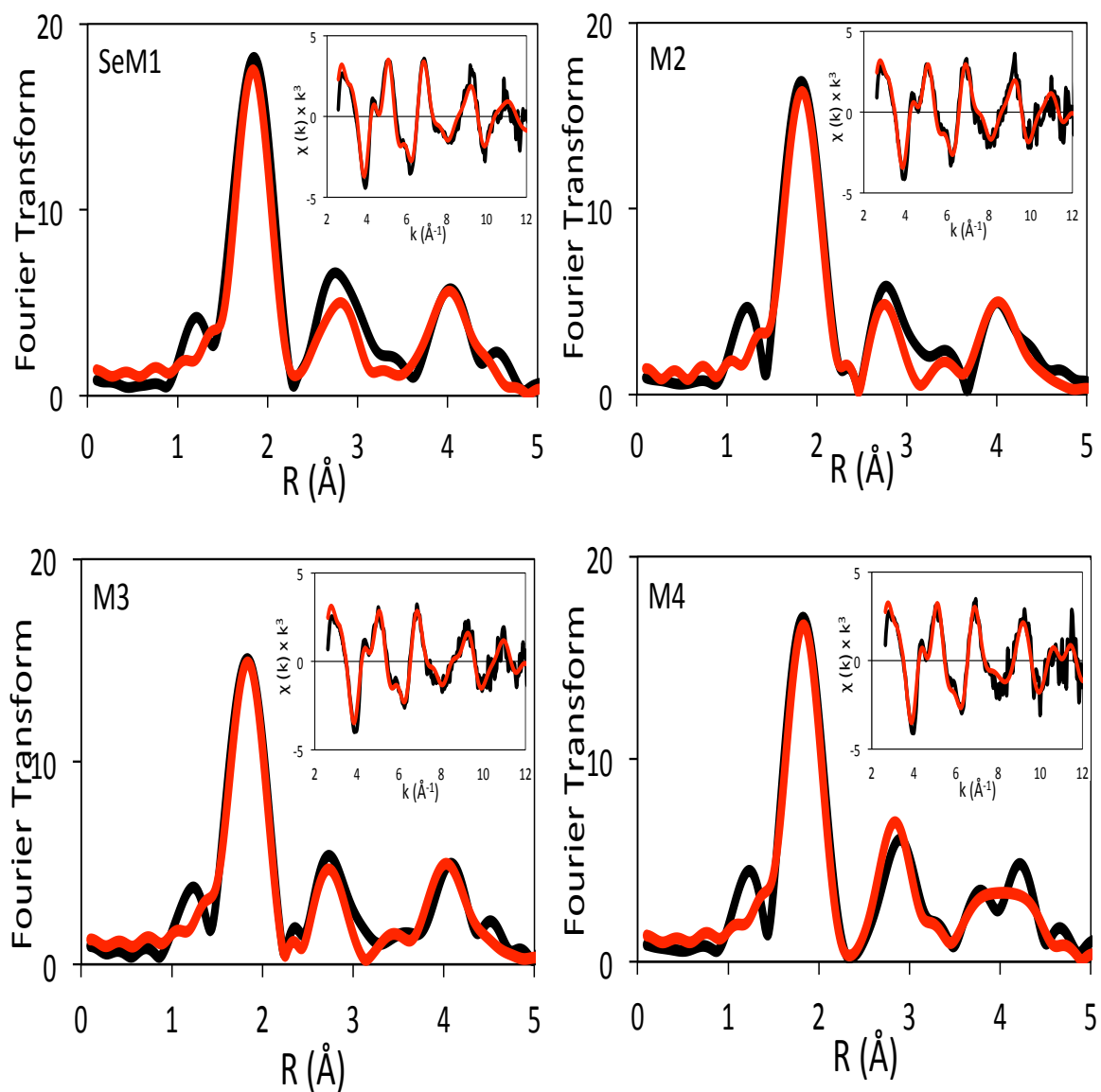
*Figure 5.5.* EXAFS (insets) and Fourier transforms of Cu (I) 1:1 complexes of HM Loop Triple Met Mutants ("SeM1" HM Loop, "M2", "M3", and "M4," see Table 2.2 for nomenclature) at pH 3.5. Black traces are experimental data and red traces are simulated data.

coordinate at low pH.

## 5.2.4 CHARACTERIZATION OF CU (I) BOUND TO DOUBLE MET MUTANTS OF HM LOOP AT PH 8 AND PH 3.5 BY XAS

Double Met mutants of the HM Loop were designed in the hopes of identifying the Met ligand that coordinates copper since previous data suggests a single Met residue alone is not sufficient for coordinating. Figures 5.6 through 5.8 compare the FT and EXAFS (insets) data for double Met mutants of the HM Loop (M1,2I, M1,3I, M1,4I, M2,3I, M2,4I, and M3,4I respectively) at both pH 8.0 and pH 3.5. Once more, the spectra were dominated by His coordination at 1.9 Å with the characteristic fingerprint of multiple scattering (MS) from the imidazole ring at 3 and 4 Å. The difference between the scattering amplitudes at pH 8.0 and pH 3.5 (refer to Figure 5.9 for comparison of the double Met mutants FT spectra) is only semi quantitative, as EXAFS cannot determine shell occupancy better than 25%.(Ralle, Lutsenko, and Blackburn 2003) Additionally, almost all of the double mutant samples can be simulated by 2-N(His) with bond distances at approximately 1.88 Å, reminiscent of 2-coordinate environments (Table 5.3) (Himes et al. 2008; Himes et al. 2007). The EXAFS simulations are confirmed by comparison of the absorption edges where the intensity of the edge feature at 8.9 keV increases in proportion to decreasing coordination number (Pickering et al. 1993). The edge data in Figure 5.10 suggests that most all of the double mutants are 2-coordinate complexes, with the exception of the M1,2I variant.

The M1,2I variant of the HM Loop (which contains both Met 3 and Met 4) most
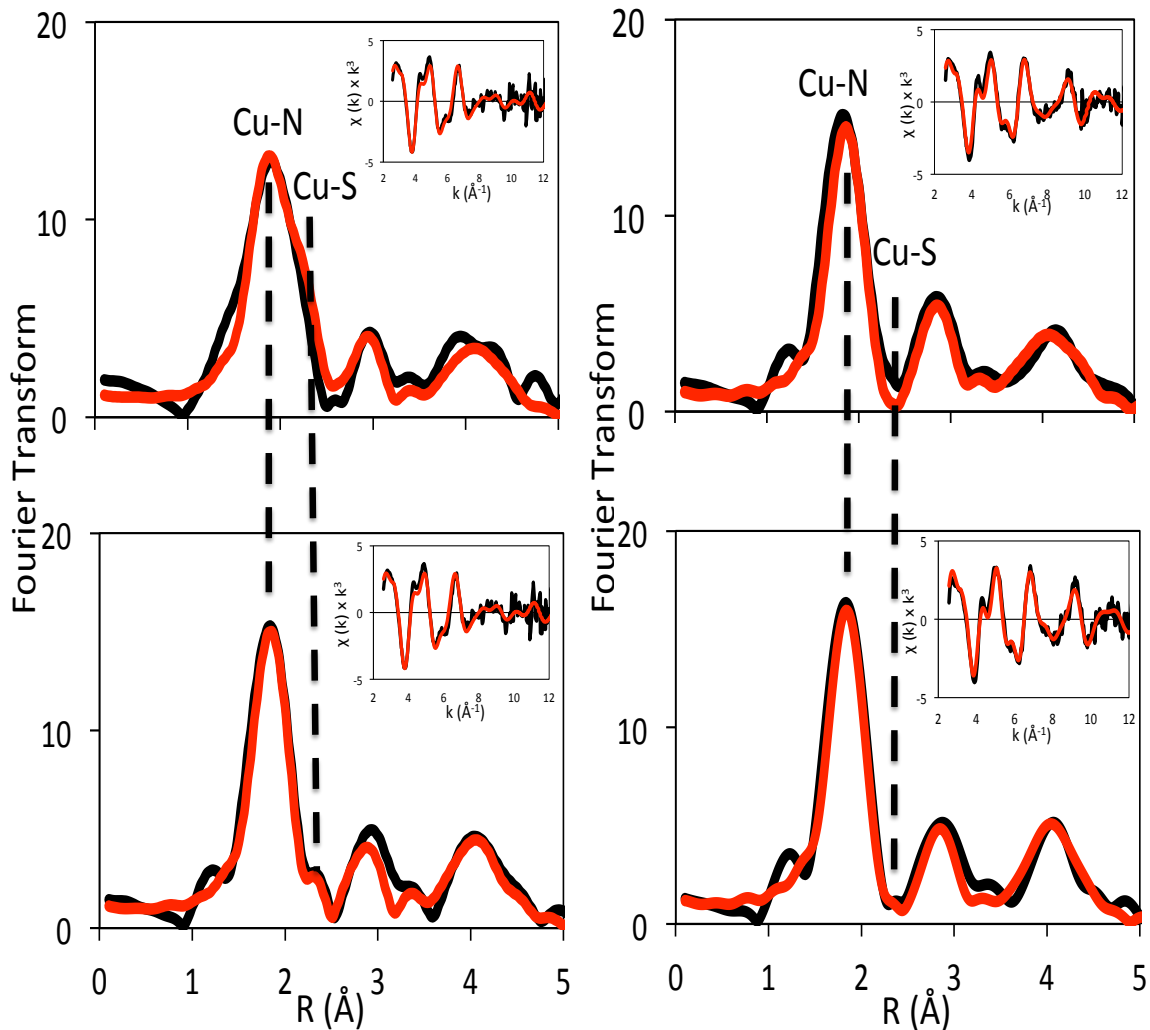
***Figure 5.6.*** *pH-dependent EXAFS (insets) and Fourier transforms of HM Loop variants M1,2I (left) and M1,3I (right), Cu (I) 1:1. Black traces are experimental data and red traces are simulated data. The top panel represents data collected at pH 8.0 and the bottom panel is data collected at pH 3.5.*
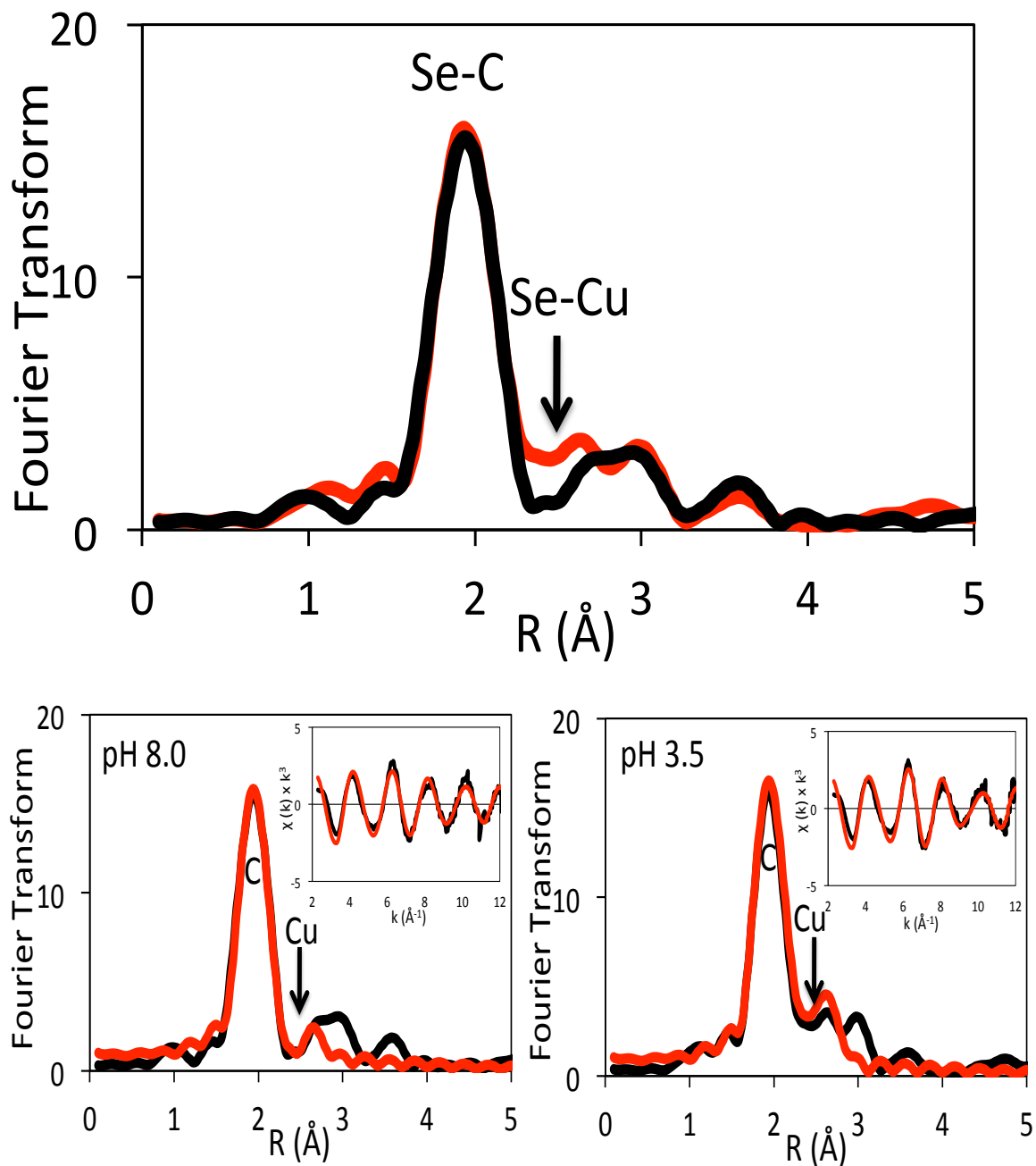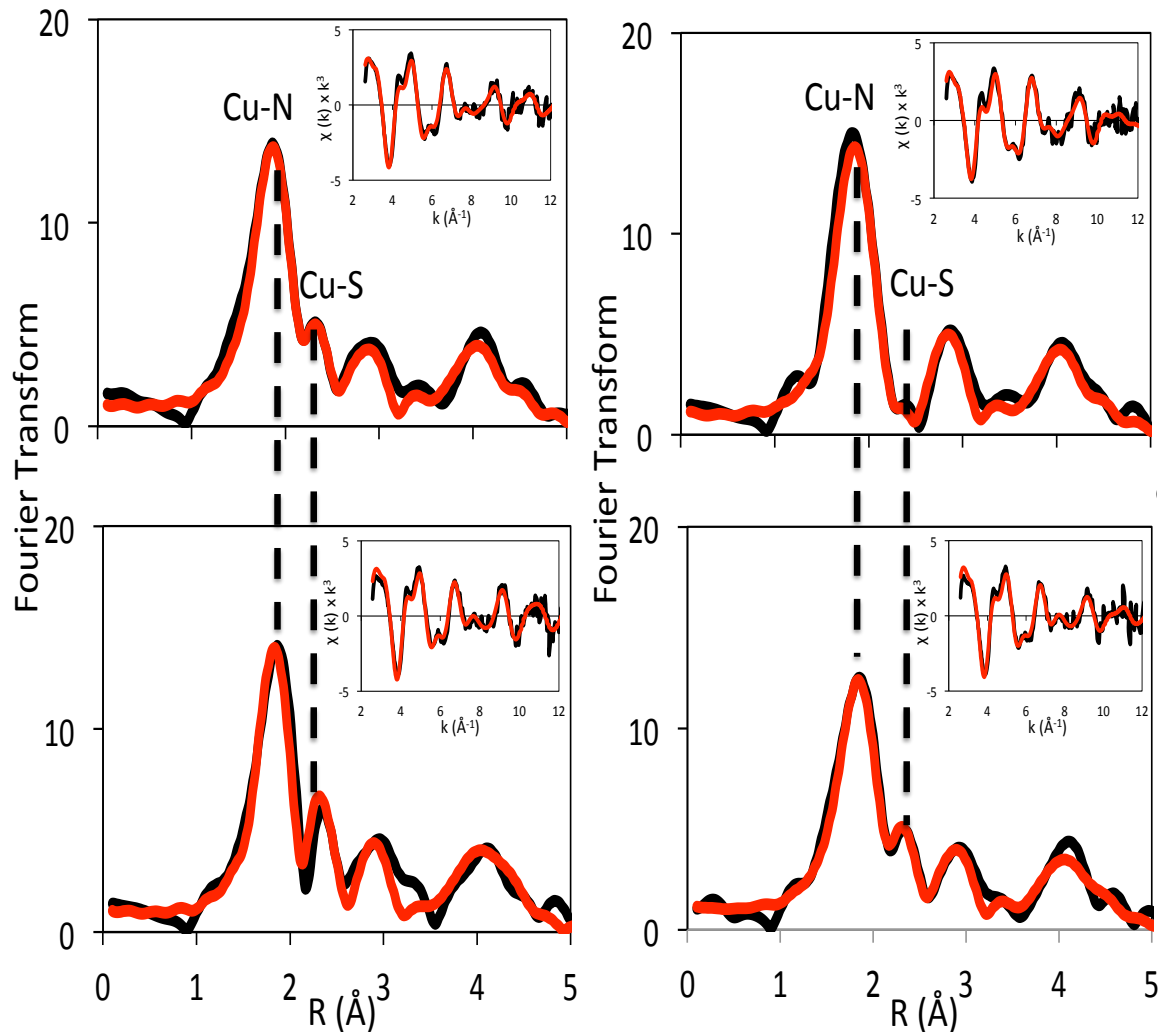
***Figure 5.7.*** *pH-dependent EXAFS (insets) and Fourier transforms of HM Loop variants M1,4I (left) and M2,3I (right), Cu (I) 1:1. Black traces are experimental data and red traces are simulated data. The top panel represents data collected at pH 8.0 and the bottom panel is data collected at pH 3.5.*
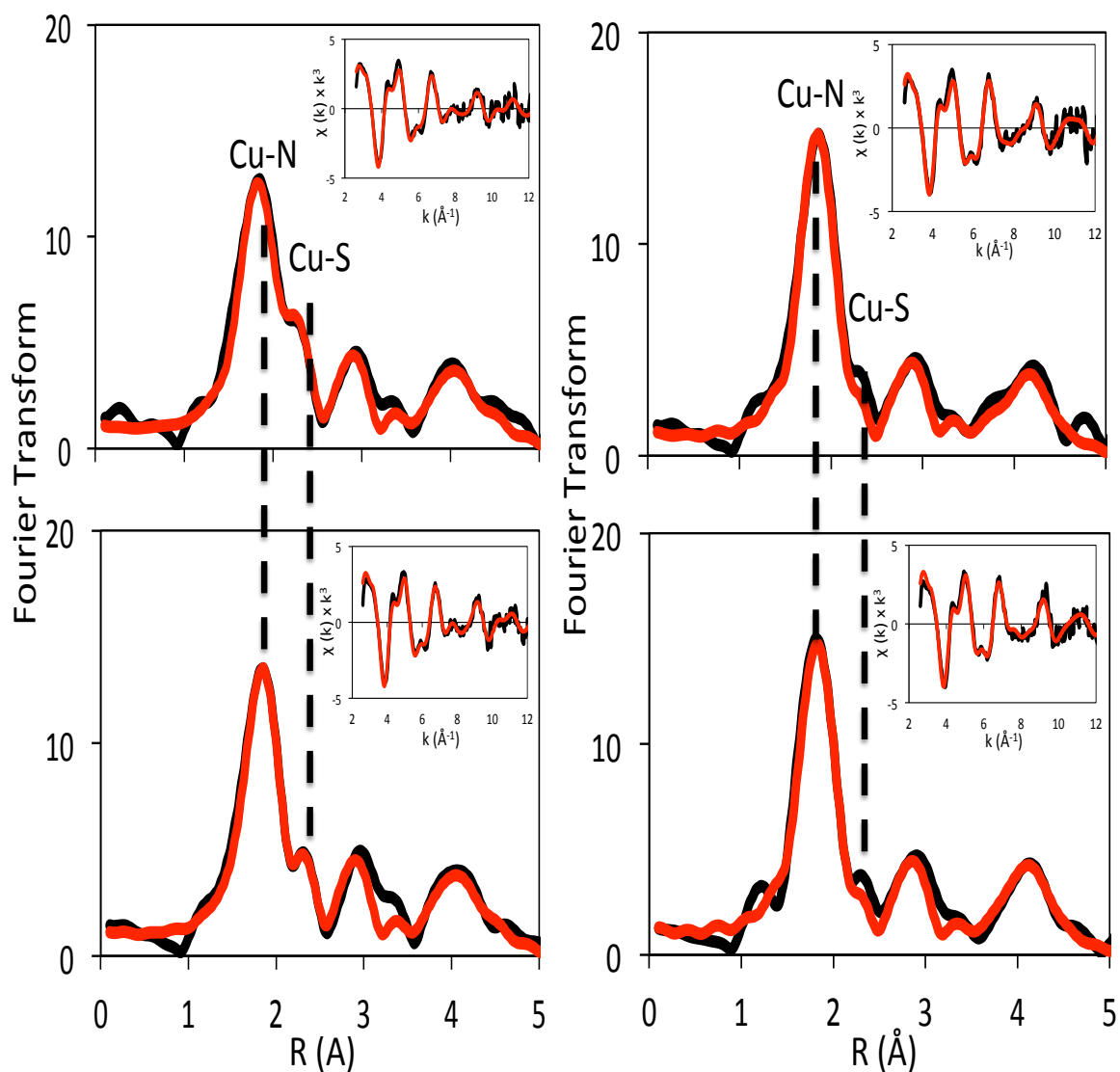
**Figure 5.8.** *pH-dependent (insets) and Fourier transforms of HM Loop variants M2,4I (left) and M3,4I (right), Cu (I) 1:1. Black traces are experimental data and red traces are simulated data. The top panel represents data collected at pH 8.0 and the bottom panel is data collected at pH 3.5.*

closely resembles the SeM labeled HM Loop-like coordination with the edge feature characteristic of coordination number (Figure 5.10). All other mutations again resemble a 2-coordinate like environment, as bond lengths are also good indicators of coordination number. However, upon careful examination of the FT spectra in Figure 5.9 (comparing the 6 double mutants at both high and low pH), almost all of the variants show some slight Cu-S scattering at about 2.2 Å, with insets focused on the Cu-S region between 2.0 and 2.5 Å.

Simulations of EXAFS data confirmed that a Cu-S(Met) interaction occurred consistently when the Met 3 ligand was present. For example, M1,2I, which contains Met 3 as well as Met 4, was simulated at pH 8.0 and pH 3.5 with 0.5 S(Met) and 0.2 S(Met), respectively (Figure 5.6 and Table 5.3). M1,4I as well as M2,4I both of which contain the Met3 ligand produced best fits corresponding to 0.5 S(Met) at both high and low pH (Figure 5.7 and Figure 5.8, respectively). Furthermore, the M2,3I variant showed interesting behavior, simulating 0.1 S(Met) at pH 8.0 and increasing the coordination number to 0.5 at pH 3.5 (Figure 5.7). This variant along with the M3,4I mutant, which also contains Met1 as a remaining residue, demonstrated only 0.2 S(Met) coordinates at either pH appearing to indicate a pH-dependent role for the Met 1 residue (Figure 5.8). Furthermore, there was very little indication that Met 4 participates in Cu-S(Met) coordination since Met 2 and Met 4 (or M1,3I variant) showed no signs of coordinating S(Met) at either pH (Figure 5.6 and Table 5.3). Overall these data suggest a highly variable, yet critical role for the methionine residues of the HM Loop where Met 3 and possibly Met 1 are important in copper binding.
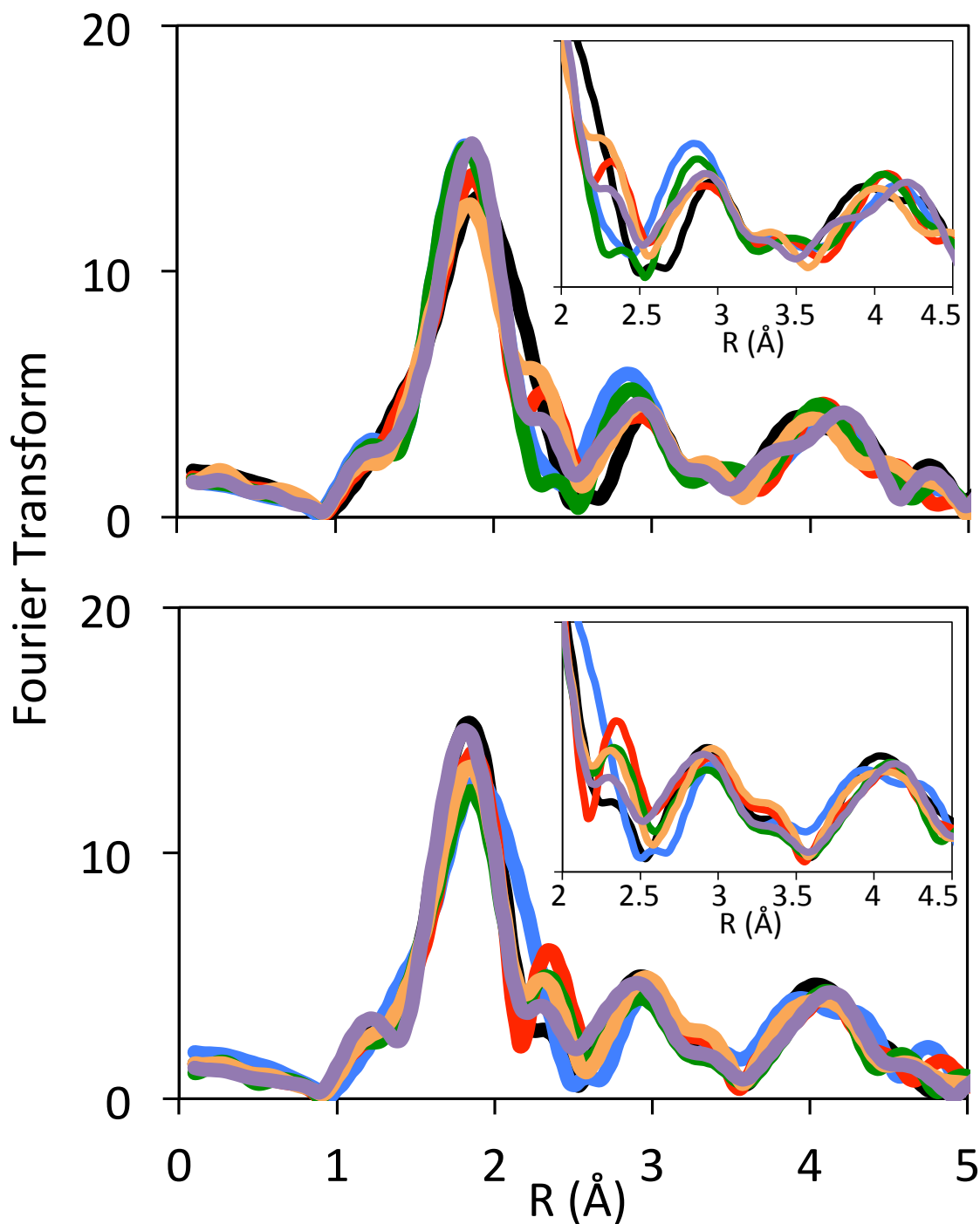
**Figure 5.9**. *XAS data comparing the Fourier transforms of ascorbate-reduced HM Loop double Met mutants at pH 8.0 above and pH 3.5 below. The insets shows an expanded view of the Cu-S region of the transform. Black (M1,2I); Blue (M1,3I); Red (M1,4I); Green (M2,3I); Orange (M2,4I); Purple (M3,4I).*
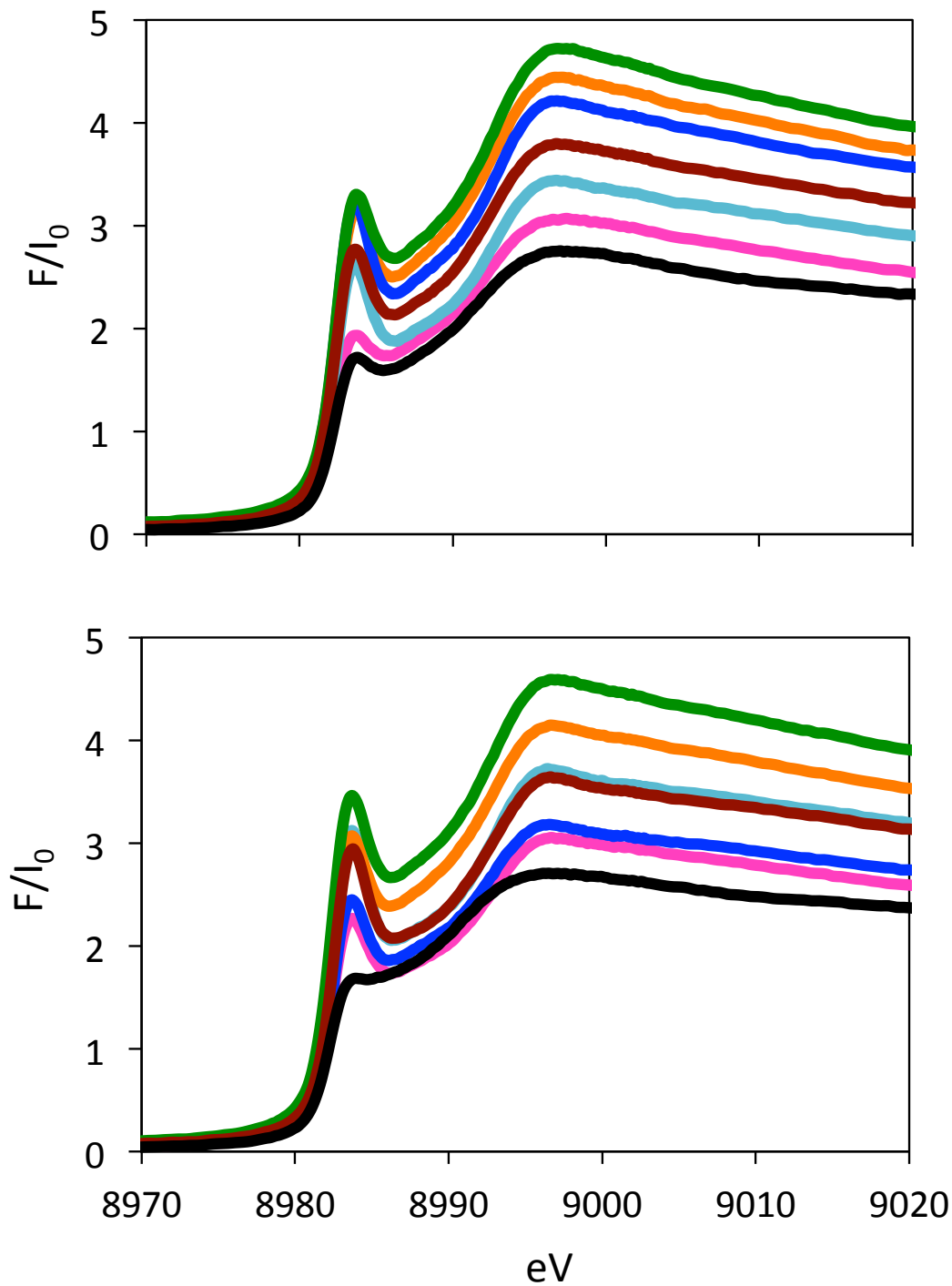
***Figure 5.10.*** *Comparison of absorption edges for SeM labeled HM Loop and double Met mutants at pH 8.0 (above) and pH 3.5 (below). Black (SeM labeled HM Loop); Pink (M1,2I); Teal (M1,3I); Orange (M1,4I); Blue (M2,3I); Green (M2,4I); Maroon (M3,4I).*

## 5.2.5 PH-DEPENDENT CHARACTERIZATION OF CU (I) BOUND TO SELENIUM LABELED HM LOOP VARIANT M2,4I AT THE CU AND SE K-EDGE

In order to study Met 1 and Met 3 coordination in more detail, the HM Loop variant M2,4I was SeM labeled and characterized via XAS at both the Cu and Se K-edge. Selenium substitution is capable of providing a more resolved Cu (I)-Met peak, with bond distances approximately 2.4 Å compared to Cu (I)-(S)Met, which can sometimes appear as a shoulder from the Cu-N(His) peak. In addition, selenium is a heavier atom than sulfur and produces a stronger Cu-Met EXAFS signal. Comparison of the pH-dependent EXAFS (insets) and Fourier transforms of selenium labeled HM Loop variant M2,4I at both the Cu (left) and Se K-edge (right) are observed in Figure 5.11 (Table 5.3). EXAFS simulations suggest that 0.5 Se(Met) bind Cu (I) at both pH 8.0 and pH 3.5, which validate the results found for the unlabeled variant.

Further Se K-edge data of the SeM labeled M2,4I variant concluded sub stoichiometric binding of the Se(Met) residues with 0.3 Cu per Se(Met), corresponding to a maximum of 0.6 Se(Met) bound at both pH's (Figure 5.11 and Table 5.3). The Debye-Waller (DW, a consequence from thermal motion and static disorder from the interacting atoms) in the SeM labeled M2,4I experiments were fitted at 0.016 Å$^2$, while the unlabeled samples have a DW of 0.012 and 0.015 Å$^2$ at pH 8.0 and pH 3.5, respectively. The Debye-Waller factors for the mutants as well as the SeM labeled HM Loop appear to be quite large suggesting an active, highly dynamic species  (Table 5.1). Albeit the DW factors are similar for the SeM labeled HM Loop and SeM labeled M2,4I variant, two Met residues were still found to be insufficient and could not complement the 3-coordinate His$_2$Met structure observed
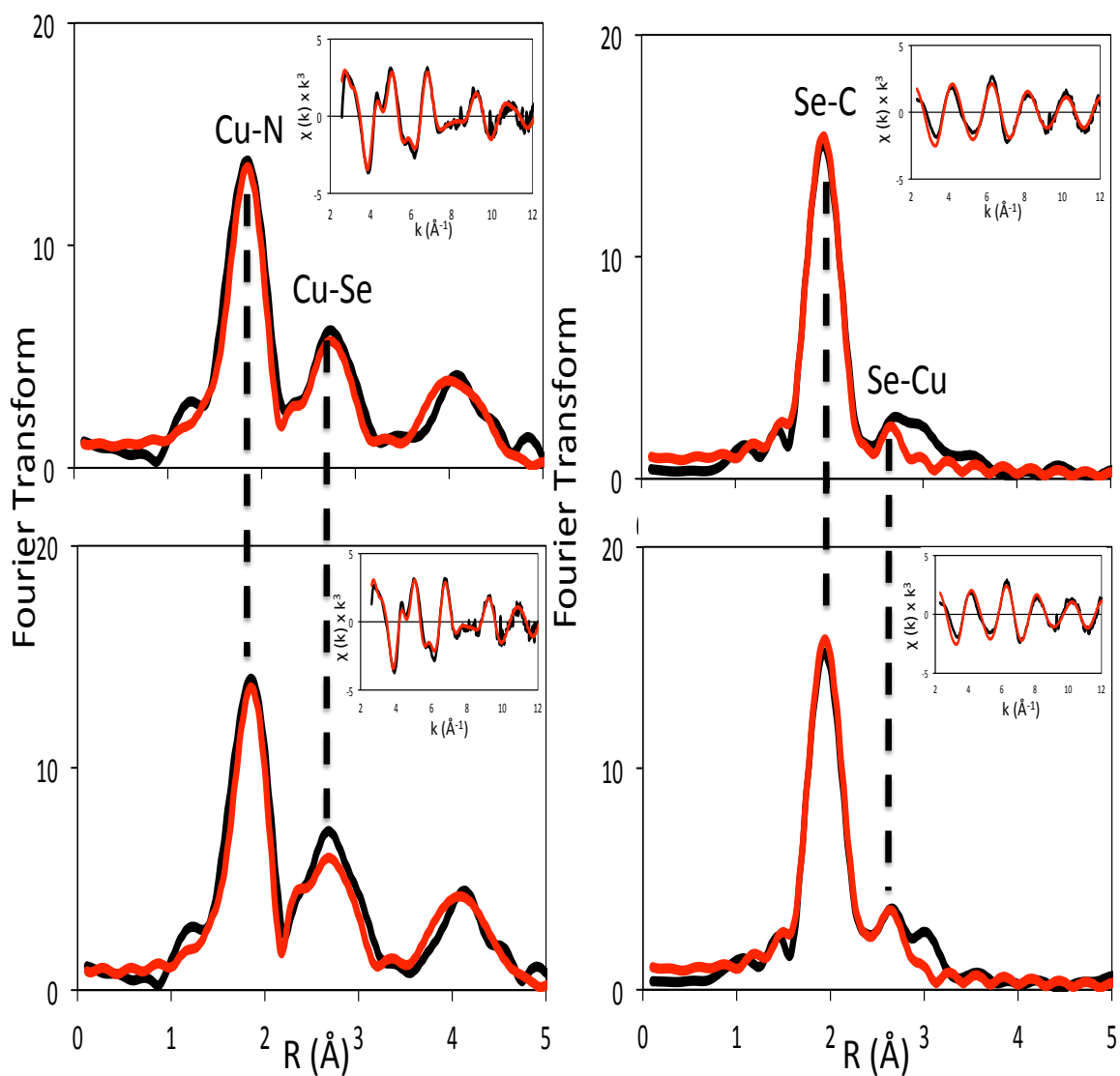
***Figure 5.11.*** *pH-dependent (insets) and Fourier transforms of SeM labeled M2,4I HM Loop at the Cu K-edge (left) and Se K-edge (right), Cu (I) 1:1. Black traces are experimental data and red traces are simulated data. The top panel represents data collected at pH 8.0 and the bottom panel is data collected at pH 3.5.*

in WT.

## 5.3 DISCUSSION

Despite significant progress trying to identify the S(Met) residue coordinating copper in the HM Loop, the mechanism of copper release remains poorly understood. Maturation of the secretory pathway employs sophisticated strategies to sort and process proteins, possibly exploiting vesicular pH for regulation (Paroutis, Touret, and Grinstein 2004; Vishwanatha et al. 2014; Williamson et al. 2013), Copper proteins are highly regulated and generally metalated by chaperones, (Kim, Nevitt, and Thiele 2008; Lutsenko, Bhattacharjee, and Hubbard 2010) yet PHM, DβM and TYR are suggested to be metalated within secretory vesicles without the need for a specific metallochaperone. Indeed, evidence from colocation studies (Setty et al. 2008; Prigge et al. 2000; El Meskini et al. 2003; Petris, Strausak, and Mercer 2000) implicates ATPases as the copper donor. However, the environment of the lumen of these vesicles is not the same for all cuproproteins, particularly with respect to pH (Marshansky 2007) and yet mixed His-Met environments appear again in these systems (Hess, Klinman, and Blackburn 2010) suggestive of a functional significance (Rosenzweig and Sazinsky 2006). For example, TYR resides in specialized lysosomes termed melanosomes with close to neutral pH. Current ideas suggest that the pH of melanosomes is also highly variable, and may be a factor in determining the differences in pigmentation between different racial and ethnic populations (Ancans et al. 2001; Smith et al. 2004). For PHM, the activity maximum of purified PHMcc (catalytic core) is ~5.5 (Bauman, Jaron, et al. 2006)

126

which corresponds to the pH of its secretory vesicles. However, the pH optimum of the intact PAM-1 integral membrane protein containing PHM, PAL and the transmembrane domains together with associated linker peptides is one pH unit lower at 4.5 (Perkins et al. 1990). On the other hand, the presence of the granule associated factor SPAM shifts the pH optimum into the neutral pH range suggesting that protein interactions within the vesicle can perturb the effect of pH on active conformations (Hu et al. 2006). It is not yet known under what conditions copper is inserted into the cuproteins, but one may speculate that transport must likewise be able to respond to the varying conditions of pH. The conformational mobility of the Cu (I) complexes of the ATP7A lumenal loop may provide a mechanism for satisfying this requirement.

A feature of chaperone-partner interactions is the tendency for the chaperones to mimic the coordination chemistry of their partners (Pufahl et al. 1997; Field, Luk, and Culotta 2002). Recently we showed that the HHM motif present at the electron transfer H-center of PHM is involved in novel pH and copper-dependent conformational dynamics (Bauman, Jaron, et al. 2006; Bauman et al. 2011; Kline, Mayfield, and Blackburn 2013). The enzyme was found to undergo structural reorganization in the pH range of 8.0 to 3.5 in which a sulfur ligand (assigned to Met109) bound to copper in place of one of the histidines, abrogating catalytic function. This chemistry provided validation of predictions from model chemistry that His-Met motifs could be important as pH-triggered conformational switches (Haas et al. 2011; Rubino et al. 2011). In the present study we asked the question whether its putative donor (the ATP7A lumenal loop) which contains

similar (yet more complex) HM elements, undergoes similar pH-dependent copper binding, providing a mechanism whereby ATP7A could tailor its transfer chemistry to the very different conditions required for different cuproprotein metallation.

In this work we used XAS to further examine the Cu (I) binding sites at 1:1 ratios and concluded that two distinct pH-dependent Cu (I) coordinated species were observed in the HM Loop of ATP7A (with or without SeM labeling), trading His ligands for Met as the pH was lowered (Figure 5.12, Table 5.1). At pH 8.0 copper adopted 3-coordinate $His_2Met$ complex, while at pH 3.5 a different 3-coordinate species occurs with 2 Met and 1 His. The HM Loop toggles between various His and Met ligands, favoring a higher degree of methionine coordination as the pH decreases to an extreme of 3.5. These data support our hypothesis that His and Met pairs are capable of responding to the strict control of a pH- triggered event for regulating structure-function aspects as observed previously in PHM, and may also provide important roles for metal transport in this pathway.

The XAS measurements at the Se edge validated conclusions derived from Cu edge data allowing precise measurement of the Se(Met)-Cu bond (Bagai et al. 2008; Chacon and Blackburn 2012). Figure 5.12 compares the FT spectra of HM Loop with and without selenium at pH 8.0 and 3.5 as well as the triple Met variants at pH 3.5. The increase in the (Se)Met-Cu peak around 2.2 to 2.4 Å is clearly seen in the data, but practically no Cu-Met coordination was observed for the triple Met variants. Therefore double Met mutants of the HM Loop were constructed and examined for Cu (I) binding in further hopes of identifying the Cu-(S)Met ligand that coordinates at pH 8.0. The double Met mutants were analyzed at both high and low pHs and
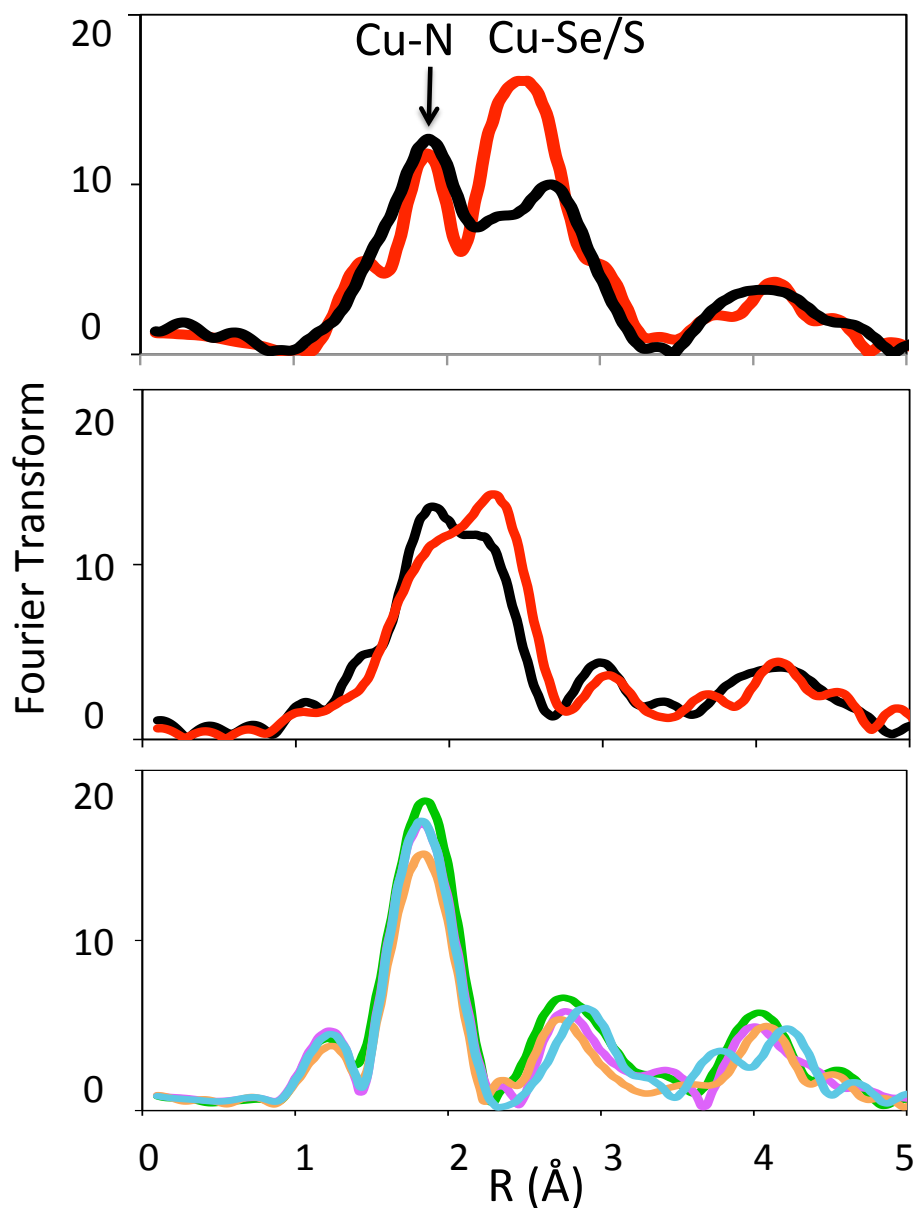
***Figure 5.12.*** *XAS data comparing the Fourier transforms of ascorbate-reduced HM Loop WT and triple Met variants at the Cu K-edge. Top panel compares SeM labeled HM Loop at pH 8.0 (black) and pH 3.5 (red). The middle panel compares HM Loop WT FT data at pH 8.0 (black) and pH 3.5 (red). The bottom figure compares SeM1, M2, M3, and M4 data at pH 3.5 representing the loss of Cu-Met coordination for all four triple mutants (green, purple, orange, and blue traces correspond to the triple met mutants respectively).*

demonstrated different behavior from the triple Met variants. EXAFS simulations of triple Met mutants determined that less than 0.2 S(Met) coordinated Cu (I) at low pH, whereas double Met mutants contained no more than 0.5 S(Met) bound to copper at either pH. In an attempt to further acquire and understand WT-like coordination, we chose to selenium label the M2,4I variant, given that when Met 3 and Met 1 are present, there is some Cu-S(Met) interaction. The M2,4I variant was characterized at both the Cu and Se K-edge and at both high and low pH's, but once again only produced a fractional amount of WT-like coordination.

The FT and EXAFS data of the HM Loop variants ultimately confirm that all four methionines in the HM Loop are important for ambiguously coordinating copper. Both triple and double methionine mutants were designed in the hopes of assigning the Cu (I)-Met residue, but overall failed to produce a full coordinating S(Met) ligand. The dramatic effect upon pH doesn't appear to take place upon mutating more than two methionine residues and may need at least 3 methionines in order to recruit copper coordination. Upon comparing the XAS data of all the mutants, we demonstrate that Met3 is insufficient on its own to bind and seems to recruit Met 1 and Met 2 differently, while Met1 appears to be pH-dependent, with increased coordination observed in the M2,3I variant at pH 3.5 (Figure 5.7 and Table 5.3). Met 2 and Met 4 seem to be less important with no binding observed at all in the M1,3I double mutant (Figure 5.6 and Table 5.3).

Spectroscopic evidence demonstrates that the His and Met residues in the donor ATP7A HM Loop and target cuproprotein, PHM have various pH-triggered metal coordination, but these transitions are perturbed by mutations. Therefore the

130

ability of cuproproteins to adopt different structures and conformations as a

function of pH, copper loading, and or redox potential may be the controlling factor

ensuring efficient copper acquisition and distribution. However, it is important to

emphasize the need for developing an activity assay for the HM Loop capable of

detecting actively transferable coordinating complexes. Transfer experiments have

shown to be informative for both Cu (I) and Cu (II) loaded HM Loop, where

approximately 2 copper atoms are able to transfer from the HM loop to the target

protein PHM (Otoikhian et al. 2012). Transfer experiments involving pH as a factor

will also be explored in future experiments.

| | $F^a$ | $N_o^b$ | $R(Å)^c$ | $DW(Å^2)$ | $N_o^b$ | $R(Å)^c$ | $DW(Å^2)$ | $N_o^b$ | $R(Å)^c$ | $DW(Å^2)$ | $-E_0$ |
|---|---|---|---|---|---|---|---|---|---|---|---|
| | | | Cu-N(His)[d] | | | Cu-S | | | | | |
| **HM Loop WT Cu Edge (S-Met)** | | | | | | | | | | | |
| Reduced pH 8.0 | 0.245 | 2.0 | 1.942 | 0.012 | 1.0 | 2.268 | 0.012 | | | | -1.7 |
| Reduced pH 3.5 | 0.288 | 1.0 | 1.912 | 0.008 | 2.0 | 2.251 | 0.021 | | | | 0.06 |
| **HM Loop WT Cu Edge (Se-Met)** | | | | | | | | | | | |
| | | | | | | | | | Cu-Se | | |
| Reduced pH 8.0 | 0.298 | 2.0 | 1.932 | 0.016 | | | | 1.0 | 2.433 | 0.018 | -1.8 |
| Reduced pH 3.5 | .300 | 1.0 | 1.944 | 0.003 | | | | 2.0 | 2.414 | 0.017 | -4.1 |
| **HM Loop WT Se Edge (Se-Met)** | | | | | | | | | | | |
| | | | Se-C | | | | | | Se-Cu[e] | | |
| Reduced pH 8.0 | 0.374 | 2.0 | 1.962 | 0.005 | | | | 0.2 (0.8) | 2.415 | 0.017 | -5.8 |
| Reduced pH 3.5 | 0.341 | 2.0 | 1.960 | 0.004 | | | | 0.5 (2.0) | 2.414 | 0.017 | -5.6 |

**Table 5.1.** *Fits obtained for Cu (I) HM Loop with and without SeM labeling at pH 8.0 and pH 3.5 for both the Cu and Se K-edges. [a]F is a least-squares fitting parameter defined as $F^2 = (1/N)\sum_{i=1}^{N} k^6(data - model)^2$. [b]Coordination numbers are generally considered accurate to ±25%. [c]In any one fit, the statistical error in bond lengths is ± 0.005 Å. However, when errors due to imperfect background subtraction, phase shift calculations, and noise in the data are compounded, the actual error is closer to ±0.02 Å. [d]Fits modeled histidine coordination by an imidazole ring, which included single and multiple scattering contributions from the second-shell (C2/C5) and third-shell (C3/N4) atoms, respectively. The Cu– N–Cx angles were as follows: Cu–N–C2, 126°; Cu–N–C3, –126°; Cu–N–N4, 163°; Cu–N–C5, –163°. [e]Samples were prepared at Cu to protein ratios of 1:1. Since there are 4 Met residues in the HM Loop sequence, such samples will have Se:Cu ratios of 4:1, with some of the Se-containing sites in the apo form. The values of the Se–Cu coordination numbers determined from EXAFS simulation at the Se edge have therefore been renormalized by multiplying the calculated Se:Cu shell occupancy by 4 and are in parenthesis. This process renders the Cu–Se and Se–Cu coordination numbers determined from the Cu and the Se edges comparable.*

| | F[a] | No[b] | R(Å)[c] | DW(Å²) | No[b] | R(Å)[c] | DW(Å²) | No[b] | R(Å)[c] | DW(Å²) | -E$_0$ |
|---|---|---|---|---|---|---|---|---|---|---|---|
| | | **Cu-N(His)[d]** | | | **Cu-S** | | | **Cu-Se[e]** | | | |
| **SeM1 HM Loop at pH 3.5** | | | | | | | | | | | |
| Reduced pH 3.5 | 0.322 | 2.0 | 1.877 | 0.007 | | | | 0.0 | | | -2.0 |
| **M2 HM Loop at pH 3.5** | | | | | | | | | | | |
| Reduced pH 3.5 | 0.354 | 2.0 | 1.872 | 0.008 | 0.1 | 2.372 | 0.009 | | | | -1.4 |
| **M3 HM Loop at pH 3.5** | | | | | | | | | | | |
| Reduced pH 3.5 | 0.324 | 2.0 | 1.881 | 0.011 | 0.1 | 2.300 | 0.008 | | | | -1.5 |
| **M4 HM Loop at pH 3.5** | | | | | | | | | | | |
| Reduced pH 3.5 | 0.320 | 2.0 | 1.869 | 0.009 | 0.0 | | | | | | -1.3 |

*Table 5.2. Fits obtained for Cu (I) Triple Met mutants of the HM Loop at pH 3.5. [a]F is a least-squares fitting parameter defined as $F^2 = (1/N)\sum_{i=1}^{N} k^6(data - model)^2$. [b]Coordination numbers are generally considered accurate to ±25%. [c]In any one fit, the statistical error in bond lengths is ± 0.005 Å. However, when errors due to imperfect background subtraction, phase shift calculations, and noise in the data are compounded, the actual error is closer to ±0.02 Å. [d]Fits modeled histidine coordination by an imidazole ring, which included single and multiple scattering contributions from the second-shell (C2/C5) and third-shell (C3/N4) atoms, respectively. The Cu– N–Cx angles were as follows: Cu–N–C2, 126°; Cu–N–C3, –126°; Cu–N–N4, 163°; Cu–N–C5, –163°. [e]Samples were prepared at Cu to protein ratios of 1:1.*

| | $F^a$ | $N_o^b$ | $R(Å)^c$ | $DW(Å^2)$ | $N_o^b$ | $R(Å)^c$ | $DW(Å^2)$ | $-E_0$ |
|---|---|---|---|---|---|---|---|---|
| | | | Cu-N(His)[d] | | | Cu-S | | |
| **M1,2I HM Loop (Met3,4)** | | | | | | | | |
| Reduced pH 8.0 | 0.331 | 2.0 | 1.927 | 0.013 | 0.5 | 2.234 | 0.010 | -1.4 |
| Reduced pH 3.5 | 0.270 | 2.0 | 1.898 | 0.011 | 0.2 | 2.244 | 0.008 | -1.6 |
| **M1,3I HM Loop (Met2,4)** | | | | | | | | |
| Reduced pH 8.0 | 0.266 | 2.0 | 1.899 | 0.011 | 0.0 | | | -2.1 |
| Reduced pH 3.5 | 0.273 | 2.0 | 1.883 | 0.010 | 0.0 | | | -2.5 |
| **M1,4I HM Loop (Met2,3)** | | | | | | | | |
| Reduced pH 8.0 | 0.238 | 2.0 | 1.911 | 0.012 | 0.5 | 2.279 | 0.014 | -2.0 |
| Reduced pH 3.5 | 0.244 | 2.0 | 1.908 | 0.011 | 0.5 | 2.299 | 0.008 | -2.5 |
| **M2,3I HM Loop (Met1,4)** | | | | | | | | |
| Reduced pH 8.0 | 0.276 | 2.0 | 1.896 | 0.012 | 0.1 | 2.221 | 0.008 | -1.7 |
| Reduced pH 3.5 | 0.299 | 2.0 | 1.900 | 0.015 | 0.5 | 2.279 | 0.014 | -1.6 |
| **M2,4I HM Loop (Met1,3)** | | | | | | | | |
| Reduced pH 8.0 | 0.269 | 2.0 | 1.911 | 0.014 | 0.5 | 2.264 | 0.012 | -1.8 |
| Reduced pH 3.5 | 0.239 | 2.0 | 1.902 | 0.013 | 0.5 | 2.275 | 0.015 | -1.9 |
| **M3,4I HM Loop (Met1,2)** | | | | | | | | |
| Reduced pH 8.0 | 0.234 | 2.0 | 1.906 | 0.010 | 0.2 | 2.249 | 0.008 | -1.7 |
| Reduced pH 3.5 | 0.239 | 2.0 | 1.881 | 0.011 | 0.2 | 2.245 | 0.008 | -2.1 |
| | | | Cu-N(His)[d] | | | Cu-S | | |
| **M2,4I HM Loop Cu Edge (Se-Met 1,3)** | | | | | | | | |
| Reduced pH 8.0 | 0.273 | 2.0 | 1.899 | 0.013 | 0.5 | 2.406 | 0.016 | -3.3 |
| Reduced pH 3.5 | 0.258 | 2.0 | 1.892 | 0.012 | 0.5 | 2.400 | 0.016 | -1.7 |
| | | | Se-C | | | Se-Cu[e] | | |
| **M2,4I HM Loop Se Edge (Se-Met 1,3)** | | | | | | | | |
| Reduced pH 8.0 | 0.327 | 2.0 | 1.959 | 0.005 | 0.3 (0.6) | 2.422 | 0.016 | -5.5 |
| *Reduced pH 3.5* | *0.310* | *2.0* | *1.959* | *0.005* | *0.3 (0.6)* | *2.400* | *0.016* | *-5.4* |

***Table 5.3.*** *Fits obtained for Cu (I) HM Loop with and without SeM labeling at pH 8.0 and pH 3.5 for both the Cu and Se K-edges. [a]F is a least-squares fitting parameter defined as $F^2 = (1/N)\sum_{i=1}^{N} k^6(data - model)^2$. [b]Coordination numbers are generally considered accurate to ±25%. [c]In any one fit, the statistical error in bond lengths is ± 0.005 Å. However, when errors due to imperfect background subtraction, phase shift calculations, and noise in the data are compounded, the actual error is closer to ±0.02 Å. [d]Fits modeled histidine coordination by an imidazole ring, which included single and multiple scattering contributions from the second-shell (C2/C5) and third-shell (C3/N4) atoms, respectively. The Cu– N–Cx angles were as follows: Cu–N–C2, 126°; Cu–N–C3, –126°; Cu–N–N4, 163°; Cu–N–C5, –163°. [e]Samples were prepared at Cu to*

*protein ratios of 1:1. Since there are 2 Met residues in the HM Loop sequence, such samples will have Se:Cu ratios of 2:1, with some of the Se-containing sites in the apo form. The values of the Se–Cu coordination numbers determined from EXAFS simulation at the Se edge have therefore been renormalized by multiplying the calculated Se:Cu shell occupancy by 2 and are in parenthesis. This process renders the Cu–Se and Se–Cu coordination numbers determined from the Cu and the Se edges comparable.*

# CHAPTER 6

# CONCLUSION AND FUTURE STUDIES

## 6.1 HIS AND MET CONTRIBUTION TO FUNCTION IN PHM

In PHM, the histidine and methionine residues provide two unique mononuclear copper centers that function cohesively across an 11 Å solvent filled gap. Both centers perform redox cycling in order to hydroxylate glycine-extended substrates for essential biological function. The two copper centers are critical for catalytic function, whereby substrate binding triggers oxygen to bind at the catalytic CuM center bound by two histidines (242 and 244) and a methionine (314), while the CuH center bound by three histidines (107, 108, and 172) is required to donate electrons to complete the reaction. A combination of spectroscopic and kinetic studies were used for a variety of His and Met PHM variants in order to try and understand their individual roles and examine the means by which substrate influences the chemistry.

Fourier transform infrared (FTIR) spectroscopy is an exquisitely sensitive marker for coordination and provides the only spectroscopic evidence for substrate activation observed for PHM WT. In this study we further probed the carbonyl assignments exploring the CO reactivity for PHM WT and variants. We have determined that upon carbonylation (i) a major CO band at 2092 cm$^{-1}$ and a second minor CO band at 2063 cm$^{-1}$ are observed in the absence of peptide substrate Ac-YVG; (ii) the presence of peptide substrate amplifies the minor CO band and

partially inter-converts with the CO band at 2092 cm$^{-1}$; (iii) the substrate induced CO band is associated with a second conformer at CuM; and (iv) the CuH-site mutants eliminate the substrate induced CO band together with catalytic activity. These data provide evidence that meticulous structural mobility of CuH and the catalytic CuM center are required for the two CO species to exist at CuM, one of which is induced in the presence of peptide substrate, with the implication that this represents the conformation that allows binding and activation of O$_2$.

PHM WT has a maximum catalytic activity at pH 5.8 and undergoes loss of activity at lower pHs due to a protonation event with a pK$_A$ of 4.6. Low pH also causes a unique structural transition in which an additional S ligand coordinates to copper with an identical pK$_A$, manifested by a large increase in Cu−S intensity via X-ray absorption spectroscopy. Bauman *et al.,* 2011 tentatively assigned the new Cu−S interaction to binding of M109 at the CuH-site (part of an HHM conserved motif common to all but one member of the monooxygenase family). Here we followed up on these findings via studies on the catalytic activity, pH-activity profiles, and spectroscopic (electron paramagnetic resonance, XAS, and Fourier transform infrared) properties of a number of H-site variants, including H107A, H108A, H172A, and M109I. Our results established that M109 is indeed the coordinating ligand and confirmed the prediction that the low pH structural transition with associated loss of activity is abrogated when the M109 thioether is absent. The histidine mutants showed more complex behavior, but the almost complete lack of activity in all three variants coupled with only minor differences in their spectroscopic properties suggested that unique structural elements at H are again

critical for functionality. Furthermore, the catalytic activity in PHM is dramatically influenced by the His and Met coordination chemistry at both copper centers, demonstrating an important need to communicate with each other.

## 6.2    HIS AND MET RESIDUES IN THE HM LOOP OF ATP7A

The data from cuproteins, such as PHM and DβM suggest a general utility for the His and Met residues as a copper- and pH-dependent conformational switch. In fact, these cuproteins mature in the secretory pathway where changes in vesicle pH are employed for sorting and post-translational processing. In previous work we have suggested that metallation of the cuproteins is achieved by spatial colocation of partner proteins in their specific organelles or vesicles and that the lumenal loop of sequence located between TM helices 1 and 2 of the ATPase, containing five histidines and four methionines acts as an organelle-specific chaperone for metallation. The hypothesis posits that the pH of the vesicle regulates copper ligation and loop conformation via a mechanism that involves His to Met ligand switching induced by histidine protonation.  Results described in this thesis demonstrated an effect of pH on the HM loop copper coordination via X-ray absorption spectroscopy (XAS), and showed via selenium substitution of the Met residues that the HM loop undergoes similar conformational switching to that found earlier for its partner PHM. Attempts to try and identify a unique S(Met) ligand that coordinated copper failed, but included XAS experiments using double and triple Met mutants (some) with and without seleno-methionine labeling at both high and low pH. As with PHM, the HM Loop contains His/Met residues that influence copper

138

coordination and seem to all be critical for coordinating copper properly.

Furthermore, the His Met residues in the HM Loop provide a template for building a

flexible, pH-sensitive transfer site whose structure and function can be regulated to

accommodate the different active site structural elements and pH environments of

its partner proteins in the absence of specific chaperones. However, this emphasizes

the importance of further developing an activity assay in order to detect active

coordination, with a similar approach needed to study the transfer kinetics of

copper between the HM Loop and target cuproteins.

## 6.3    FUTURE STUDIES

### 6.3.1  FTIR SPECTROSCOPY OF DEUTERATED PEPTIDE SUBSTRATE

In Chapter 3, we used FTIR spectroscopy to show that addition of CO to PHM

WT results in two CO stretching frequencies at the CuM center, a major CO band and

a minor CO band that is amplified in the presence of substrate.  The presence of

substrate Ac-YVG decreases the major CO band slightly while dramatically

increasing the intensity of the minor CO band that we suggest is a catalytically active

form of the enzyme. Interestingly, the identity of the substrate was found to affect

the CO stretching frequency of the minor CO band with no affect on the stretching

frequency of the major CO band. We hypothesize that the observed difference in CO

stretching frequencies represents a change in the H-bonded network that is

required for substrate triggering, but whether the change involves a reorientation of

the solvent or reorganization of the CO towards the substrate pocket in the presence

139

and absence of substrate is unknown. In order to interpret and assign the origin of the minor, "substrate inducible" CO band, we will compare the IR spectra of PHM WT with peptide substrate in the presence of deuterated water ($D_2O$), as well as with and without deuterated peptide substrate hippuric acid.

Deuterium is a heavier atom than hydrogen and will cause direct bonds to absorb at lower stretching frequencies. The change in C—O stretching region may not be as dramatic, but should still downshift slightly. It's possible that neither one of these experiments depict a downshift in the CO stretching frequencies. Therefore we would be left to consider that a reorganization of the electronics at CuM result in the minor CO band that can be amplified in the presence of peptide substrate. The results of these studies will help us identify the electronic effects at the CuM due to substrate binding and will allow us further insight into elucidating the overall catalytic mechanism relating to the nature of reactive intermediates and electron transfer pathways.

## 6.3.2 PH-DEPENDENT CHARACTERIZATION OF CU (I) BOUND TO SINGLE MET MUTANTS OF THE HM LOOP OF ATP7A

We will investigate the hypothesis that multiple Met residues are critical for inducing flexible copper binding sites in the HM Loop that are subsequently used for trafficking copper. Triple and double Met mutants in the HM Loop failed to provide full Cu-(S)Met coordination via XAS at either of the two extreme pHs tested, so our final experiments will include making and characterizing the coordination chemistry single Met mutants at both pH 8.0 and pH 3.5. We expect to observe a

fully coordinating S atom at either high or low pH, and hope to identify the Met residue that additionally coordinates at low pH. The single Met mutants of the HM Loop will help confirm the importance of the Met 3 coordination identified in Chapter 5. We hypothesize that the His and Met residues in the HM Loop of ATP7A act as a copper chaperone to PHM and/or DβM.

# LITERATURE CITED

Abad, E., J. B. Rommel, and J. Kaestner. 2014. 'Reaction Mechanism of the Bicopper Enzyme Peptidylglycine-alpha-Hydroxylating Monooxygenase', *J Biol Chem*.

Aboelella, N. W., B. F. Gherman, L. M. Hill, J. T. York, N. Holm, V. G. Young, Jr., C. J. Cramer, and W. B. Tolman. 2006. 'Effects of thioether substituents on the $O_2$ reactivity of β-diketiminate-Cu(I) complexes: probing the role of the methionine ligand in copper monooxygenases', *J. Am. Chem. Soc.*, 128: 3445-58.

Alben, J. O., P. P. Moh, F. G. Fiamingo, and R.A. Altschuld. 1981. 'Cytochromeoxidase (a3) heme and copper observed by low- temperature Fourier transform infrared spectroscopy of the CO complex', *Proc. Natl. Acad. Sci. U.S.A.*, 78: 234-37.

Alben, James O., and Lei Yen Fager. 1972. 'Infrared studies of azide bound to myoglobin and hemoglobin. Temperature dependence of ionicity', *Biochem.*, 11: 842-47.

Aller, S. G., and V. M. Unger. 2006. 'Projection structure of the human copper transporter CTR1 at 6-A resolution reveals a compact trimer with a novel channel-like architecture', *Proc. Natl. Acad. Sci. U.S.A.*, 103: 3627-32.

Ancans, J., D. J. Tobin, M. J. Hoogduijn, N. P. Smit, K. Wakamatsu, and A. J. Thody. 2001. 'Melanosomal pH controls rate of melanogenesis, eumelanin/phaeomelanin ratio and melanosome maturation in melanocytes and melanoma cells', *Exp Cell Res*, 268: 26-35.

Andersson, M., D. Mattle, O. Sitsel, T. Klymchuk, A. M. Nielsen, L. B. Moller, S. H. White, P. Nissen, and P. Gourdon. 2014. 'Copper-transporting p-type ATPases use a unique ion-release pathway', *Nat. Struct. Mol. Biol.*, 21: 43-8.

Atkinson, L. E., P. McVeigh, M. J. Kimber, N. J. Marks, B. A. Eipper, R. E. Mains, T. A. Day, and A. G. Maule. 2010. 'A PAL for Schistosoma mansoni PHM', *Mol Biochem Parasitol*, 173: 97-106.

Bagai, I., C. Rensing, N.J. Blackburn, and M. M. McEvoy. 2008. 'Direct metal transfer between periplasmic proteins identifies a bacterial copper chaperone', *Biochemistry*, 47: 11408-14.

Banci, L., I. Bertini, F. Cantini, C. Massagni, M. Migliardi, and A. Rosato. 2009. 'An NMR study of the interaction of the N-terminal cytoplasmic tail of the Wilson disease protein with copper(I)-HAH1', *J. Biol. Chem.*, 284: 9354-60.

Banci, L., I. Bertini, F. Cantini, A. C. Rosenzweig, and L. A Yatsunyk|. 2008. 'Metal binding domains 3 and 4 of the Wilson disease protein: Solution structure and interaction with the copper(I) chaperone HAH1', *Biochem.*, 47: 7423-29.

Banci, Lucia, Ivano Bertini, Fiorenza Cramaro, Rebecca Del Conte, and Maria Silvia Viezzoli. 2002. 'The solution structure of reduced dimeric copper zinc superoxide dismutase', *European J. of Biochem.*, 269: 1905-15.

Barnes, N., R. Tsivkovskii, N. Tsivkovskaia, and S. Lutsenko. 2005. 'The copper-transporting ATPases, Menkes and Wilson disease proteins, have distinct roles in adult and developing cerebellum', *J. Biol. Chem.*, 280: 9640-45.

Barry, A. N., A. Otoikhian, S. Bhatt, U. Shinde, R. Tsivkovskii, N. J. Blackburn, and S. Lutsenko. 2011. 'The lumenal loop Met672-Pro707 of copper-transporting ATPase ATP7A binds metals and facilitates copper release from the intramembrane sites', *J. Biol. Chem.*, 286: 26585-94.

Bauman, A. T., B. A. Broers, C. D. Kline, and N. J. Blackburn. 2011. 'A copper-methionine interaction controls the pH-dependent activation of peptidylglycine monooxygenase', *Biochem.*, 50: 10819-28.

Bauman, A. T., S. Jaron, E. T. Yukl, J. R. Burchfiel, and N. J. Blackburn. 2006. 'pH dependence of peptidylglycine monooxygenase. Mechanistic implications of Cu-methionine binding dynamics', *Biochem.*, 45: 11140-50.

Bauman, A. T., M. Ralle, and N. J. Blackburn. 2007. 'Large scale production of the copper enzyme peptidylglycine monooxygenase using an automated bioreactor', *Protein Expr. Purif.*, 51: 34-8.

Bauman, A. T., E. T. Yukl, K. Alkevich, A. L. McCormack, and N. J. Blackburn. 2006. 'The hydrogen peroxide reactivity of Peptidylglycine Monooxygenase supports a Cu(II)-superoxo catalytic intermediate', *J. Biol. Chem.*, 281: 4190-8.

Berg, Jeremy M., John L. Tymoczko, and Lubert Stryer. 2002. *Biochemistry* (W.H Freeman).

Bertini, I, C Luchinat, and R Monnanni. 1985. 'Evidence of the breaking of the copper-imidazolate bridge in copper/cobalt-substituted superoxide dismutase upon reduction of the Cu(II) centers', *J. AM. CHEM. SOC.*, 107: 2178–79.

Bertini, Ivano, Harry B. Gray, Edward I. Stiefel, and Joan Selverstone Valentine. 2007. *Biological inorganic chemistry structure and reactivity* (University Science Book).

Binsted, N., and S.S. Hasnain. 1996. 'State of the art analysis of whole X-ray absorption spectra', *J. Synchrotron Rad.*, 3: 185-96.

Blackburn, N. J., T. M. Pettingill, K. S. Seagraves, and R. T. Shigeta. 1990. 'Characterization of a carbon monoxide complex of reduced dopamine hydroxylase', *J. Biol. Chem.*, 265: 15383-86.

Blackburn, N. J., F. C. Rhames, M. Ralle, and S. Jaron. 2000. 'Major changes in copper coordination accompany reduction of peptidylglycine monooxygenase: Implications for electron transfer and the catalytic mechanism', *JBIC Journal of Biological Inorganic Chemistry*, 5: 341-53.

Blackburn, N. J., N. Yan, and S. Lutsenko. 2014. *Binding Transport and Storage of Metal Ions in Biological Cells* (Royal Society of Chemistry ).

Blackburn, Ninian J., SamarS. Hasnainll, Trudie M. Pettingillg, and RichardW. Strange. 1991. 'Copper & extended X-ray absorption fine structure studies of oxidized and reduced dopamin hydroxylase. Confirmation of a sulfur ligand to copper(I) in the reduced enzyme', *J. Biol. Chem.*, 226: 23120-2312.

Blackburn, NJ, SS Hasnain, N Binsted, GP Diakun, CD Garner, and PF Knowles. 1984. 'An extended X-ray absorption fine structure study of bovine erythrocyte superoxide dismutase in aqueous solution. Direct evidence for three-coordinate Cu(I) in the reduced enzyme', *Biochem.*, 219.

Blackburn, NJ, RW Strange, A Farooq, MS Haka, and KD Karlin. 1988. 'X-ray absorption studies of three- coordinate dicopper(I) complexes and their dioxygen adducts', *J. AM. CHEM. SOC.*, 110: 4263– 72.

Boswell, J. S., B. J. Reedy, R. Kulathila, D. Merkler, and N. J. Blackburn. 1996. 'Structural investigations on the coordination environment of the active-site copper centers of recombinant bifunctional peptidylglycine amidating enzyme', *Biochem.*, 35: 12241-50.

Cardenas, D. J., J. M. Cuerva, M. Alias, E. Bunuel, and A. G. Campana. 2011. 'Water-based hydrogen-atom wires as mediators in long-range proton-coupled electron transfer in enzymes: a new twist on water reactivity', *Chemistry*, 17: 8318-23.

Chacon, K. N., and N. J. Blackburn. 2012. 'Stable Cu(II) and Cu(I) mononuclear intermediates in the assembly of the CuA center of *Thermus thermophilus* cytochrome oxidase', *J. AM. CHEM. SOC.*, 134: 16401-12.

Chauhan, S., C. D. Kline, M. Mayfield, and N. J. Blackburn. 2014. 'Binding of copper and silver to single-site variants of peptidylglycine monooxygenase reveals the structure and chemistry of the individual metal centers', *Biochem.*, 53: 1069-80.

Chen, P. , J. Bell, B. A. Eipper, and E. I. Solomon. 2004. 'Oxygen activation by the noncoupled binuclear copper site in peptidylglycine hydroxylating monooxygenase. Spectroscopic definition of the resting sites and the putative Cu(II)M-OOH intermediate', *Biochem.*, 43: 5735-47.

Chen, P., D. E. Root, C. Campochiaro, K. Fujisawa, and E. I. Solomon. 2003. 'Spectroscopic and electronic structure studies of the diamagnetic side-on CuII-superoxo complex Cu(O2)[HB(3-R-5-iPrpz)3]: antiferromagnetic coupling versus covalent delocalization', *J. AM. CHEM. SOC.*, 125: 466-74.

Chen, P., and E. I. Solomon. 2004a. 'O2 activation by binuclear Cu sites: noncoupled versus exchange coupled reaction mechanisms', *Proc. Natl. Acad. Sci. U.S.A.*, 101: 13105-10.

———. 2004b. 'Oxygen activation by the noncoupled binuclear copper site in Peptidylglycine Hydroxylating Monooxygenase. Reaction mechanism and role of the noncoupled nature of the active site', *J. AM. CHEM. SOC.*, 126: 4991-5000.

Chufa´n, E. E., S. T. Prigge, X. Siebert, B. A. Eipper, R. E. Mains, and L. M. Amzel. 2010. 'Differential reactivity between two copper sites in peptidylglycine hydroxylating monooxygenase', *J. AM. CHEM. SOC.*, 132: 15565–72.

Citek, C, CT Lyons, EC Wasinger, and TD Stack. 2012. 'Self-assembly of the oxy-tyrosinase core and the fundamental components of phenolic hydroxylation', *Nat. Chem.*, 4: 317–22.

Crespo, Alejandro, Marcelo A. Mart´, Adrian E. Roitberg, L. Mario Amzel, and Dar´ıo A. Estrin. 2006. 'The catalytic mechanism of peptidylglycine hydroxylating monooxygenase investigated by computer simulation', *J. AM. CHEM. SOC.*, 128: 12817-28.

Culotta, Valeria Cizewski, Leo W. J. Klomp, Jeffrey Strain, Ruby Leah B. Casareno, Bernhard Krems, and Jonathan D. Gitlin. 1997. 'The copper chaperone for superoxide dismutase', *J. Biol. Chem.*, 272: 23469-72.

Dancis, A., D.S. Yuan, D. Haile, C. Askwith, D. Eide, C. Moehle, J. Kaplan, and R.D. Klausner. 1994. 'Molecular characterization of a copper transport protein in S. cerevisiae: An unexpected role for copper in iron transport', *Cell*, 76: 393-402.

De Feo, C. J., S. G. Aller, G. S. Siluvai, N. J. Blackburn, and V. M. Unger. 2009. 'Three-dimensional structure of the human copper transporter hCTR1', *Proc. Natl. Acad. Sci. U.S.A.*, 106: 4237-42.

De, M., G. D. Ciccotosto, R. E. Mains, and B. A. Eipper. 2007. 'Trafficking of a secretory granule membrane protein is sensitive to copper', *J. Biol. Chem.*, 282: 23362-71.

Deen, Henk van der, and Henk Hoving. 1979. 'An infrared study of carbon monoxide complexes of hemocyanins. Evidence for the structure of the CO-binding site from vibrational analysis', *Biophys. Chem.*, 9: 169-79.

Dey, A., Y. Peng, W. E. Broderick, B. Hedman, K. O. Hodgson, J. B. Broderick, and E. I. Solomon. 2011. 'S K-edge XAS and DFT calculations on SAM dependent pyruvate formate-lyase activating enzyme: nature of interaction between the Fe4S4 cluster and SAM and its role in reactivity', *J. AM. CHEM. SOC.*, 133: 18656-62.

DiDonato, M., H. Hsu, S. Narindrasorasak, L. Que, and B. Sarkar. 2000. 'Copper-induced conformational changes in the N-terminal domain of the Wilson disease copper-transporting ATPase', *Biochem.*, 39: 1890-96.

Eipper, B. A., S. L. Milgram, E. J. Husten, H. Yun, and R. E. Mains. 1993. 'Peptidylglycine amidating monooxygenase: A multifunctional protein with catalytic, processing, and routing domain', *Protein Science*, 2: 489-97.

Eipper, B. A., A. S. W. Quon, R. E. Mains, J. S Boswel, and N. J. Blackburn. 1995. 'The catalytic core of peptidylglycine hydroxylating monooxygenase: Investigation by site-directed mutagenesis, Cu X-ray absorption spectroscopy, and electron paramagnetic resonance', *Biochem.*, 34: 2857-65.

El Meskini, R., V. C. Culotta, R. E. Mains, and B. A. Eipper. 2003. 'Supplying copper to the cuproenzyme Peptidylglycine alpha-Amidating Monooxygenase', *J. Biol. Chem.*, 278: 12278-84.

Evans, J. P., K. Ahn, and J. P. Klinman. 2003. 'Evidence that dioxygen and substrate activation are tightly coupled in dopamine beta-monooxygenase. Implications for the reactive oxygen species', *J. Biol. Chem.*, 278: 49691-8.

Evans, J. P., N. J. Blackburn, and J. P. Klinman. 2006. 'The catalytic role of the copper ligand H172 of peptidylglycine hydroxylating monooxygenase: A kinetic study of the H172A mutant', *Biochem.*, 45: 15419-29.

Fager, Lei Yen, and James O. Alben. 1972. 'Structure of the carbon monoxide binding site of hemocyanins studied by Fourier transform infrared spectroscopy', *Biochem.*, 11: 4786-92.

Field, Lori Sturtz, Edward Luk, and Valeria Cizewski Culotta. 2002. 'Copper chaperones: Personal escorts for metal ions', *J. Bioenergetics and Biomembranes*, 34: 373-79.

Francisco, W. A., M. K. Knapp, N. J. Blackburn, and J. P. Klinman. 2002a. 'Hydrogen tunneling in peptidylglycine hydroxylating monooxygenase', *J. AM. CHEM. SOC.*, 124: 8194-95.

Francisco, W.A., M.J. Knapp, N.J. Blackburn, and J.P. Klinman. 2002b. 'Hydrogen tunneling in peptidylglycine $\alpha$-hydroxylating monooxygenase', *J. Am. Chem. Soc.*, 124: 8194 - 95.

Francisco, Wilson A., David J. Merkler, Ninian J. Blackburn, and Judith P. Klinman. 1998. 'Kinetic mechanism and intrinsic isotope effects for the peptidylglycine amidating enzyme reaction', *Biochem.*, 37: 8244-52.

Fujisawa, Kiyoshi, Masako Tanaka, Yoshihiko Moro-oka, and Nobumasa Kitajima. 1994. 'A monomeric side-on superoxocopper(II) complex: $Cu(O_2)(HB(3\text{-}tBu\text{-}5\text{-} iPrpz)_3)$', *J. Am. Chem. Soc.*, 116: 12079-80.

George, G. N. 1995. 'EXAFSPAK ', *Stanford Synchrotron Radiation Laboratory , Menlo Park, CA.*

George, G. N., and I.J. Pickering. 2000. 'Exafspak', *Stanford Synchrotron Radiation Laboratory*.

Gerdemann, C, C Eicken, and B. Krebs. 2002. 'The crystal structure of catechol oxidase: new insight into the function of type-3 copper protein', *Acc. Chem. Res.*, 35: 183–91.

Ginsbach, J. W., R. L. Peterson, R. E. Cowley, K. D. Karlin, and E. I. Solomon. 2013. 'Correlation of the electronic and geometric structures in mononuclear Copper(II) superoxide complexes', *Inorg. Chem.*, 52: 12872-4.

Gourdon, P., X. Y. Liu, T. Skjorringe, J. P. Morth, L. B. Moller, B. P. Pedersen, and P. Nissen. 2011. 'Crystal structure of a copper-transporting PIB-type ATPase', *Nature*, 475: 59-64.

Gupta, A., and S. Lutsenko. 2009. 'Human copper transporters: mechanism, role in human diseases and therapeutic potential', *Future Med. Chem.*, 1: 1125-42.

Gurman, S. J., N. Binsted, and I. Ross. 1984. 'A rapid, exact curved-wave theory for EXAFS calculations', *J. Phys. C: Solid State Phys.*, 17: 143-51.

———. 1986. 'A rapid, exact, curved-wave theory for EXAFS calculations. II. The multiple-scattering contributions', *J. Phys. C: Solid State Phys.*, 19: 1845-61.

Guss, J. M., P. R. Harrowell, M. Murata, V. A. Norris, and H. C. Freeman. 1986. 'Crystal structure analyses of reduced Cu(I) poplar plastocyanin at six pH values', *J. Mol. Biol.*, 192: 361–87.

Haas, K. L., A. B. Putterman, D. R. White, D. J. Thiele, and K. J. Franz. 2011. 'Model peptides provide new insights into the role of histidine residues as potential ligands in human cellular copper acquisition via Ctr1', *J. AM. CHEM. SOC.*, 133: 4427-37.

Harrison, Mark D., Christopher E. Jones, and Charles T. Dmeron. 1999. 'Copper chaperons: function, structure, and copper-binding properties', *JBIC Journal of Biological Inorganic Chemistry*, 4: 145-53.

Hatori, Y., E. Majima, T. Tsuda, and C. Toyoshima. 2007. 'Domain organization and movements in heavy metal ion pumps: papain digestion of CopA, a Cu-transporting ATPase', *J. Biol. Chem.*, 282: 25213-21.

Hess, C. R., J. P. Klinman, and N. J. Blackburn. 2010. 'The copper centers of tyramine beta-monooxygenase and its catalytic-site methionine variants: an X-ray absorption study', *JBIC Journal of Biological Inorganic Chemistry*, 15: 1195-207.

Hess, C. R., M. M. McGuirl, and J. P. Klinman. 2008. 'Mechanism of the insect enzyme, tyramine beta-monooxygenase, reveals differences from the mammalian enzyme, dopamine beta-monooxygenase', *J Biol Chem*, 283: 3042-9.

Hess, C. R., Z. Wu, A. Ng, E. E. Gray, M. A. McGuirl, and J. P. Klinman. 2008. 'Hydroxylase activity of Met471Cys tyramine β-monooxygenase', *J. Am. Chem. Soc.*, 130: 11939-44.

Himes, R. A., G. Y. Park, A. N. Barry, N. J. Blackburn, and K. D. Karlin. 2007. 'Synthesis and X-ray absorption spectroscopy structural studies of Cu(I) complexes of histidyl-histidine peptides: The predominance of linear 2-coordinate geometry', *J. AM. CHEM. SOC.*, 129: 5352-53.

Himes, R. A., G. Y. Park, G. S. Siluvai, N. J. Blackburn, and K. D. Karlin. 2008. 'Structural studies of copper(I) complexes of amyloid-beta peptide fragments: formation of two-coordinate bis(histidine) complexes', *Angew. Chem. Int. Ed.*, 47: 9084-7.

Horton, R. M., Z. L. Cai, S. N. Ho, and L. R. Pease. 1990. 'Gene splicing by overlap extension: tailor-made genes using the polymerase chain reaction', *Biotechniques*, 8: 528-35.

Hu, J., R. Fu, K. Nishimura, L. Zhang, H. X. Zhou, D. D. Busath, V. Vijayvergiya, and T. A. Cross. 2006. 'Histidines, heart of the hydrogen ion channel from influenza A virus: toward an understanding of conductance and proton selectivity', *Proc. Natl. Acad. Sci. U.S.A.*, 103: 6865-70.

Husten, E. Jean, and Betty A. Eipper. 1991. 'The membrane-bound bifunctional peptidylglycine α-amidating monooxygenase protein. Exploration of its domain structure through limited proteolysis', *J. Biol. Chem.*, 266: 17004-10.

Jaron, S., and N. J. Blackburn. 1999. 'Does superoxide channel between the copper centers in peptidylglycine monooxygenase? A new mechanism based on carbon monoxide reactivity', *Biochem.*, 38: 15086-96.

Jaron, S., R. E. Mains, B. A. Eipper, and N. J. Blackburn. 2002. 'The catalytic role of the copper ligand H172 of peptidylglycine hydroxylating monooxygenase (PHM): A spectroscopic study of the H172A mutant', *Biochem.*, 41: 13274-82.

Jaron, Shulamit, and Ninian J. Blackburn. 2001. 'Characterization of a half-apo derivative of peptidylglycine monooxygenase. Insight into the reactivity of each active site copper', *Biochem.*, 40: 6867-75.

Kaplan, J. H., and S. Lutsenko. 2009. 'Copper transport in mammalian cells: special care for a metal with special needs', *J. Biol. Chem.*, 284: 25461-5.

Kim, B. E., T. Nevitt, and D. J. Thiele. 2008. 'Mechanisms for copper acquisition, distribution and regulation', *Nat. Chem. Biol.*, 4: 176-85.

Kim, S., J. Y. Lee, R. E. Cowley, J. W. Ginsbach, M. A. Siegler, E. I. Solomon, and K. D. Karlin. 2015. 'A N3S(thioether)-ligated Cu(II)-superoxo with enhanced reactivity', *J. AM. CHEM. SOC.*, 137: 2796-9.

Kline, C. D., M. Mayfield, and N. J. Blackburn. 2013. 'HHM motif at the CuH-site of peptidylglycine monooxygenase is a pH-dependent conformational switch', *Biochem.*, 52: 2586-96.

Klinman, J. P. 2006a. 'The copper-enzyme family of dopamine beta-monooxygenase and peptidylglycine alpha-hydroxylating monooxygenase: resolving the chemical pathway for substrate hydroxylation', *J. Biol. Chem.*, 281: 3013-6.

———. 2006b. 'The role of tunneling in enzyme catalysis of C-H activation', *Biochim. Biophys. Acta.*, 1757: 981-7.

———. 2015. 'Dynamically achieved active site precision in enzyme catalysis', *Acc Chem Res*, 48: 449-56.

Klomp, A.E.M, J.A Juijn, L.T.M. Van Der Gun, I.E.T. Van Den Berg, R. Berger, and L.W.J. Klomp. 2003. 'The N-terminus of the human copper transporter 1 (hCTR1) is localized extracellularly, and interacts with itself', *Biochem.*, 370: 881–89

Kolhekar, A. S., H. T. Keutmann, R. E. Mains, A. S. W. Quon, and B. A. Eipper. 1997. 'Peptidylglycine hydroxylating monooxygenase: Active site residues, disulfide linkages, and a two-domain model of the catalytic core', *Biochem.*, 36: 10901-09.

Kolhekar, Aparna S., Marie S. Roberts, Ning Jiang, Richard C. Johnson, Richard E. Mains, Betty A. Eipper, and Paul H. Taghert. 1997. 'Neuropeptide amidation in *Drosophila*: Separate genes encode the two enzymes catalyzing amidation', *J. Neurosci.*, 17: 1363-76.

Kunishita, A., M. Z. Ertem, Y. Okubo, T. Tano, H. Sugimoto, K. Ohkubo, N. Fujieda, S. Fukuzumi, C. J. Cramer, and S. Itoh. 2012. 'Active site models for the Cu(A) site of peptidylglycine alpha-hydroxylating monooxygenase and dopamine beta-monooxygenase', *Inorg. Chem.*, 51: 9465-80.

Kunishita, A., M. Kubo, H. Sugimoto, T. Ogura, K. Sato, T. Takui, and S. Itoh. 2009. 'Mononuclear Copper(II)-Superoxo Complexes that Mimic the Structure and Reactivity of the Active Centers of PHM and DbetaM', *J. Am. Chem. Soc.*, 131: 2788-89.

Lanci, M. P., V. V. Smirnov, C. J. Cramer, E. V. Gauchenova, J. Sundermeyer, and J. P. Roth. 2007. 'Isotopic probing of molecular oxygen activation at copper(I) sites', *J. AM. CHEM. SOC.*, 129: 14697-709.

Lee, D. H., L. Q. Hatcher, M. A. Vance, R. Sarangi, A. E. Milligan, A. A. Sarjeant, C. D. Incarvito, A. L. Rheingold, K. O. Hodgson, B. Hedman, E. I. Solomon, and K. D. Karlin. 2007. 'Copper(I) complex $O_2$-reactivity with a $N_3S$ thioether ligand: a copper-dioxygen adduct including sulfur ligation, ligand oxygenation, and comparisons with all nitrogen ligand analogues', *Inorg. Chem.*, 46: 6056-68.

Lee, Y., G. Y. Park, H. R. Lucas, P. L. Vajda, K. Kamaraj, M. A. Vance, A. E. Milligan, J. S. Woertink, M. A. Siegler, A. A. Narducci Sarjeant, L. N. Zakharov, A. L. Rheingold, E. I. Solomon, and K. D. Karlin. 2009. 'Copper(I)/O2 chemistry with imidazole containing tripodal tetradentate ligands leading to mu-1,2-peroxo-dicopper(II) species', *Inorg. Chem.*, 48: 11297-309.

Lee, Yunho, Dong-Heon Lee, Amy A. Narducci Sarjeant, Lev N. Zakharov, Arnold L. Rheingold, and Kenneth D. Karlin. 2006. 'Thioether sulfur oxygenation from

O2 or H2O2 reactivity of copper complexes with tridentate N2Sthioether ligands', *Inorg. Chem.*, 45: 10098-107.

Lewis, Elizabeth A., and William B. Tolman. 2004. 'Reactivity of dioxygen–copper systems', *Chem. Rev*, 104: 1047–76.

Li, C., M. J. Banfield, and C. Dennison. 2007. 'Engineering copper sites in proteins: Loops confer native structures and properties to chimeric cupredoxins', *J. AM. CHEM. SOC.*, 129: 709–18.

Li, C., K. Sato, S. Monari, I. Salard, M. Sola, M. J. Banfield, and C. Dennison. 2011. 'Metal-binding loop length is a determinant of the pKa of a histidine ligand at a type 1 copper site', *Inorg. Chem.*, 50: 482-8.

Lin, Su-Ju, and Valeria Cizewski Culotta. 1995. 'The *ATX1* gene of *Saccharomyces cerevisiae* encodes metal homeostasis factor that protects cells against oxygen toxicity', *Proc. Natl. Acad. Sci. U.S.A.*, 92: 3784-88.

Lutsenko, S. 2010. 'Human copper homeostasis: a network of interconnected pathways', *Curr. Opin. Chem. Biol.*, 14: 211-7.

Lutsenko, S., N. L. Barnes, M. Y. Bartee, and O. Y. Dmitriev. 2007. 'Function and regulation of human copper-transporting ATPases', *Physiol. Rev.*, 87: 1011–46.

Lutsenko, S., A. Bhattacharjee, and A. L. Hubbard. 2010. 'Copper handling machinery of the brain', *Metallomics*, 2: 596-608.

Lutsenko, S., A. Gupta, J. L. Burkhead, and V. Zuzel. 2008. 'Cellular multitasking: the dual role of human Cu-ATPases in cofactor delivery and intracellular copper balance', *Arch. Biochem. Biophys.*, 476: 22-32.

Lutsenko, S., E. S. LeShane, and U. Shinde. 2007. 'Biochemical basis of regulation of human copper-transporting ATPases', *Arch. Biochem. Biophys.*, 463: 134-48.

Magnus, KA , B Hazes, H Ton-That, C Bonaventura, J Bonaventura, and WGJ. Hol. 1994. 'Crystallographic analysis of oxygenated and deoxygenated states of arthropod hemocyanin shows unusual differences', *Proteins Struct. Funct. Genet.*, 19: 302–09.

Maiti, D. , H. C. Fry, J. S. Woertink, M. A. Vance, E. I. Solomon, and K. D. Karlin. 2007. 'A 1:1 Copper-Dioxygen Adduct is an End-on Bound Superoxo Copper(II) Complex which Undergoes Oxygenation Reactions with Phenols', *J. AM. CHEM. SOC.*, 129: 264-65.

Marshansky, V. 2007. 'The V-ATPase a2-subunit as a putative endosomal pH-sensor', *Biochem. Soc. Trans.*, 35: 1092-99.

Maryon, E. B., S. A. Molloy, K. Ivy, H. Yu, and J. H. Kaplan. 2013. 'Rate and regulation of copper transport by human copper transporter 1 (hCTR1)', *J. Biol. Chem.*, 288: 18035-46.

Matoba, Y, T Kumagai, A Yamamoto, H Yoshitsu, and M Sugiyama. 2006a. 'Crystallographic evidence that the dinuclear copper center of tyrosinase is flexible during catalysis. ', *J. Biol. Chem*, 281: 8981– 90.

Matoba, Y., T. Kumagai, A. Yamamoto, H. Yoshitsu, and M. Sugiyama. 2006b. 'Crystallographic evidence that the dinuclear copper center of tyrosinase is flexible during catalysis', *J. Biol. Chem.*, 281: 8981-90.

McIntyre, N. R., E. W. Lowe, J. L. Belof, M. Ivkovic, J. Shafer, B. Space, and D. J. Merkler. 2010. 'Evidence for substrate preorganization in the peptidylglycine

amidating monooxygenase reaction describing the contribution of ground state structure to hydrogen tunneling', *J. AM. CHEM. SOC.*, 132: 16393–402.

Nakamoto, Kazuo. 1986. *Infrared and Raman Spectra of Inorganic and Coordination Compounds* (John Wiley & Sons).

Osborne, R. L., H. Zhu, A. T. Iavarone, N. J. Blackburn, and J. P. Klinman. 2013. 'Interdomain long-range electron transfer becomes rate-limiting in the Y216A variant of tyramine beta-monooxygenase', *Biochem.*, 52: 1179-91.

Otoikhian, A., A. N. Barry, M. Mayfield, M. Nilges, Y. Huang, S. Lutsenko, and N. J. Blackburn. 2012. 'Lumenal loop M672-P707 of the Menkes protein (ATP7A) transfers copper to peptidylglycine monooxygenase', *J. AM. CHEM. SOC.*, 134: 10458-68.

Oyarce, A. M., T. C. Steveson, L. Jin, and B. A. Eipper. 2001. 'Dopamine beta-monooxygenase signal/anchor sequence alters trafficking of peptidylglycine alpha-hydroxylating monooxygenase', *J. Biol. Chem.*, 276: 33265-72.

Padilla-Benavides, T., C. J. McCann, and J. M. Arguello. 2013. 'The mechanism of Cu transport ATPases: interaction with Cu chaperones and the role of transient metal-binding sites', *J. Biol. Chem.*, 288: 69-78.

Park, G. Y., J. Y. Lee, R. A. Himes, G. S. Thomas, N. J. Blackburn, and K. D. Karlin. 2014. 'Copper-peptide complex structure and reactivity when found in conserved his-xaa-his sequences', *J. AM. CHEM. SOC.*, 136: 12532-5.

Paroutis, P., N. Touret, and S. Grinstein. 2004. 'The pH of the secretory pathway: Measurement, determinants, and regulation', *Physiology (Bethesda)*, 19: 207-15.

Pasquali, M., and C. Floriani. 1984. *Cu(I)-carbon monoxide chemistry: recent advances and perspectives* (Adenine Press: New York).

Perkins, S. N., E. J. Husten, R. E. Mains, and B. A. Eipper. 1990. 'pH-dependent stimulation of peptidylglycine amidating monooxygenase activity by a granule-associated factor', *Endocrinology*, 127: 2771-78.

Perrone, L., E. Mothes, M. Vignes, A. Mockel, C. Figueroa, M. C. Miquel, M. L. Maddelein, and P. Faller. 2010. 'Copper transfer from Cu-Abeta to human serum albumin inhibits aggregation, radical production and reduces Abeta toxicity', *Chem. Biochem*, 11: 110-8.

Peterson, R. L., J. W. Ginsbach, R. E. Cowley, M. F. Qayyum, R. A. Himes, M. A. Siegler, C. D. Moore, B. Hedman, K. O. Hodgson, S. Fukuzumi, E. I. Solomon, and K. D. Karlin. 2013. 'Stepwise protonation and electron-transfer reduction of a primary copper-dioxygen adduct', *J. AM. CHEM. SOC.*, 135: 16454-57.

Peterson, R. L., R. A. Himes, H. Kotani, T. Suenobu, L. Tian, M. A. Siegler, E. I. Solomon, S. Fukuzumi, and K. D. Karlin. 2011. 'Cupric superoxo-mediated intermolecular C-H activation chemistry', *J. AM. CHEM. SOC.*, 133: 1702-5.

Petris, Michael J., Daniel Strausak, and Julian F.B. Mercer. 2000. 'The Menkes copper transporter is required for the activation of Tyrosinase', *Human Molecular Genetics*, 9: 2845-51.

Pettingill, T. M., R. W. Strange, and N. J. Blackburn. 1990. 'Carbonmonoxy dopamine hydroxylase: Structural characterization by FTIR, fluorescence and XAS spectroscopy', *J. Biol. Chem.*, 266: 16996–7003.

Pickering, IJ, GN George, CT Dameron, B Kurz, DR Winge, and IG Dance. 1993. 'X-ray absorption spectroscopy of cuprous-thiolate clusters in proteins and model systems', *J. AM. CHEM. SOC.*, 115: 9498–505.

Pope, C. R., A. G. Flores, J. H. Kaplan, and V. M. Unger. 2012. 'Structure and function of copper uptake transporters', *Curr .Top. Membr.*, 69: 97-112.

Prigge, S. T., B. A. Eipper, R. E. Mains, and L. M. Amzel. 2004. 'Dioxygen binds end-on to mononuclear copper in a precatalytic enzyme complex', *Science*, 304: 864-7.

Prigge, S. T., A. S.  Kolhekar, B. A. Eipper, R. E. Mains, and L. M. Amzel. 1999. 'Substrate-mediated electron transfer in peptidylglycine $\alpha$-hydroxylating monooxygenase', *Nat. Struct. Bio.*, 6: 976-83.

Prigge, S. T., R. E. Mains, B. A. Eipper, and L. M. Amzel. 2000. 'New insights into copper monooxygenases and peptide amidation: structure, mechanism and function', *Cell Mol. Life Sci.*, 57: 1236–59.

Prigge, Sean T., Aparna S. Kolhekar, Betty A. Eipper, Richard E. Mains, and L. Mario Amzel. 1997. 'Amidation of bioactive peptides: The structure of peptidylglycine alpha- hydroxylating monooxygenase', *Science*, 278: 1300-05.

Prohaska, Joseph R., and Anna A. Gybina. 2004. 'Intracellular Copper Transport in Mammals', *J. Nutrition*, 134: 1003–06.

Pufahl, R. A., C. P. Singer, K. L.  Peariso, S.-J.  Lin, P. J.  Schmidt, C. J. Fahrni, V.C. Culotta, J. E.  Penner-Hahn, and T. V.  O'Halloran. 1997. 'Metal ion chaperone function of the soluble Cu(I) receptor Atx1', *Science*, 278: 853-56.

Puig, S., J. Lee, M. Lau, and D. J. Thiele. 2002. 'Biochemical and genetic analyses of yeast and human high affinity copper transporters suggest a conserved mechanism for copper uptake', *J. Biol. Chem.*, 277: 26021-30.

Puustinen, A., J. A. Bailey, D. R. B., S. L. Mecklenburg, M. Wikstrom, and W. H. Woodruff. 1997. 'Fourier transform infrared evidence for connectivity between CuB and glutamic acid 286 in cytochrome bo3 from *escherichia coli*', *Biochem.*, 36: 13195-200.

Qin, Zhenyu, Shinichi Itoh, Viktoria Jeney, Masuko Ushio-Fukai, and Tohru Fukai. 2006. 'Essential role for the Menkes ATPase in activation of extracellular superoxide dismutase: implication for vascular oxidative stress', *J. Fed. Am. Soc. Exp. Biol.*, 20: 334-3366.

Que, Lawrence 2000. *Physical methods in bioinorganic chemistry: spectroscopy and magnetism* (University Science Books).

Ralle, M., M.J. Cooper, S. Lutsenko, and N. J. Blackburn. 1998. 'The Menkes disease protein binds copper via novel 2-coordinate Cu(I)-cysteinates in the N-terminal domain', *J. AM. CHEM. SOC.*, 120: 13525-26.

Ralle, M., S. Lutsenko, and N. J. Blackburn. 2003. 'X-ray absorption spectroscopy of the copper chaperone HAH1 reveals a linear two-coordinate Cu(I) center capable of adduct formation with exogenous thiols and phosphines', *J. Biol. Chem.*, 278: 23163-70.

Reedy, Brian J., and Ninian J. Blackburn. 1994. 'Preparation and characterization of half-apo dopamine-hydroxylase by selective removal of CuA. Identification of

a sulfur ligand at the dioxygen binding site by EXAFS and FTIR spectroscopy', *J. AM. CHEM. SOC.*, 116: 1924-31.

Rosenzweig, A. C., and M. H. Sazinsky. 2006. 'Structural insights into dioxygen-activating copper enzymes', *Curr Opin Struct Biol*, 16: 729-35.

Rubino, J. T., M. P. Chenkin, M. Keller, P. Riggs-Gelasco, and K. J. Franz. 2011. 'A comparison of methionine, histidine and cysteine in copper(I)-binding peptides reveals differences relevant to copper uptake by organisms in diverse environments', *Metallomics*, 3: 61-73.

Rubino, J. T., and K. J. Franz. 2012. 'Coordination chemistry of copper proteins: how nature handles a toxic cargo for essential function', *Inorg. Biochem.*, 107: 129-43.

Rudzka, K., D. M. Moreno, B. Eipper, R. Mains, D. A. Estrin, and L. M. Amzel. 2013. 'Coordination of peroxide to the Cu(M) center of peptidylglycine alpha-hydroxylating monooxygenase (PHM): structural and computational study', *JBIC Journal of Biological Inorganic Chemistry*, 18: 223-32.

Sanyal, Indrajit, Richard W. Strange, Ninian J. Blackburn, and Kenneth D. Karlin. 1991. 'Formation of a copper-dioxygen complex (Cu2-02) using simple imidazole ligands', *J. AM. CHEM. SOC.*, 113: 4692-93.

Schatz, M., V. Raab, S.P. Foxon, G. Brehm, S. Schneider, M. Reiher, M.C. Holthausen, J. Sundermeyer, and A. Schindler. 2004. 'Combined spectroscopic and theoretical evidence for a persistent end-on copper superoxo complex', *Angew. Chem*, 43: 4360-63.

Schushan, M., A. Bhattacharjee, N. Ben-Tal, and S. Lutsenko. 2012. 'A structural model of the copper ATPase ATP7B to facilitate analysis of Wilson disease-causing mutations and studies of the transport mechanism', *Metallomics*, 4: 669-78.

Sendovski, M., M. Kanteev, V. S. Ben-Yosef, N. Adir, and A. Fishman. 2011. 'First structures of an active bacterial tyrosinase reveal copper plasticity', *J Mol Biol*, 405: 227-37.

Setty, S. R., D. Tenza, E. V. Sviderskaya, D. C. Bennett, G. Raposo, and M. S. Marks. 2008. 'Cell-specific ATP7A transport sustains copper-dependent tyrosinase activity in melanosomes', *Nature*, 454: 1142-46.

Siebert, X., B. A. Eipper, R. E. Mains, S. T. Prigge, N. J. Blackburn, and L. M. Amzel. 2005. 'The catalytic copper of Peptidylglycine alpha-Hydroxylating Monooxygenase also plays a critical structural role', *J. Biophys.*, 89: 3312-9.

Smith, D. R., D. T. Spaulding, H. M. Glenn, and B. B. Fuller. 2004. 'The relationship between Na(+)/H(+) exchanger expression and tyrosinase activity in human melanocytes', *Exp Cell Res*, 298: 521-34.

Steveson, T. C., G. D. Ciccotosto, X. M. Ma, G. P. Mueller, R. E. Mains, and B. A. Eipper. 2003. 'Menkes protein contributes to the function of peptidylglycine alpha-amidating monooxygenase', *Endocrinology*, 144: 188-200.

Strange, R. W., N. J. Blackburn, P.F. Knowles, and S.S Hasnain. 1987. 'X-ray absorption spectroscopy of metal-histidine coordination in metalloproteins. Exact simulation of the EXAFS of tetrakis(imidazole)copper(II) nitrate and other copper-imidazole complexes by the use of a multiple-scattering treatment', *J. AM. CHEM. SOC.*, 109: 7157-62.

Tano, T., Y. Okubo, A. Kunishita, M. Kubo, H. Sugimoto, N. Fujieda, T. Ogura, and S. Itoh. 2013. 'Redox properties of a mononuclear copper(II)-superoxide complex', *Inorg. Chem.*, 52: 10431-7.

Urbañski, Norbert K., and Andrzej Berêsewicz. 2000. 'Generation of ·OH initiated by interaction of Fe2+ and Cu+ with dioxygen; comparison with the Fenton chemistry', *Acta Biochimica Polonica*, 47: 951–62.

Vishwanatha, K., N. Back, R. E. Mains, and B. A. Eipper. 2014. 'A histidine-rich linker region in peptidylglycine alpha-amidating monooxygenase has the properties of a pH-sensor', *J. Biol. Chem.*, 289: 12404-20.

Walker, J. M., R. Tsivkovskii, and S. Lutsenko. 2002. 'Metallochaperone Atox1 transfers copper to the NH2-terminal domain of the Wilson's disease protein and regulates its catalytic activity', *J. Biol. Chem.*, 277: 27953-59.

Williamson, D. M., J. Elferich, P. Ramakrishnan, G. Thomas, and U. Shinde. 2013. 'The mechanism by which a propeptide-encoded pH sensor regulates spatiotemporal activation of furin', *J. Biol. Chem.*, 288: 19154-65.

Woertink, J. S., L. Tian, D. Maiti, H. R. Lucas, R. A. Himes, K. D. Karlin, F. Neese, C. Wurtele, M. C. Holthausen, E. Bill, J. Sundermeyer, S. Schindler, and E. I. Solomon. 2010. 'Spectroscopic and computational studies of an end-on bound superoxo-Cu(II) complex: geometric and electronic factors that determine the ground state', *Inorg Chem*, 49: 9450-9.

## BIOGRAPHICAL SKETCH

Chelsey Dawn Kline was born on February 8, 1987 in Fresno, California. In 2009, she received B.S. degree in Molecular and Cellular Biology with a minor in Spanish from Pacific University, Oregon. In the winter of 2010, she began her graduate studies in the Institute of Environmental Health at Oregon Health and Science University.

**Publications:**

Chauhan, S., **Kline, C.D.**, Mayfield, M., Blackburn N.J. Single-Site Variants of Peptidylglycine Monooxygenase (PHM) Reveal the Structure and Chemistry of the Individual Copper Centers. *Biochemistry*. 2014 Feb;53(6):1069-80.

**Kline, C.D.**, Mayfield, M., Blackburn N.J. The HHM Motif at the CuH-site of Peptidylglycine Monooxygenase is a pH-Dependent Conformational Switch. *Biochemistry*. 2013;52(15):2586–2596.

Bauman, A., Broers, B., **Kline, C.D.,** Blackburn, N. A Role for H-site Conformational Change in the pH-   Dependent Activation of Peptidylglycine Monooxygenase. *Biochemistry*. 2011;50(50):10819-28.

Boitz, J.M., Yates, P.A., **Kline, C.**, Gaur, U., Wilson, M.E., Ullman, B., Roberts, S.C. 2008. *Leishmania donovani* Ornithine Decarboxylase is Indispensable for Parasite Survival in Mammalian Host. *Infect. Immun*. 2009;77(2):756-63.

Roberts, S.C., **Kline, C.**, Liu, W., Ullman, B. Generating knock-in parasites: Integration of an ornithine decarboxylase transgene into its chromosomal locus in *Leishmania donovani. Exp. Parasitol*. 2011;128(2):166-169.